THE UNIVERSITY
of LIVERPOOL

Antenna Diversity for Hand-portable Radio at 450MHz

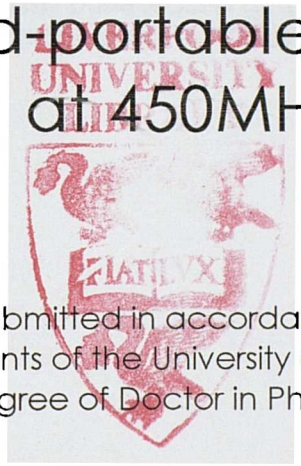

Thesis submitted in accordance with the requirements of the University of Liverpool for the degree of Doctor in Philosophy by

Paul Simon Holt Leather

May 1996

To my parents John and Barbara
and others whom I love dearly.

Est brevitate opus, ut cı ·at sı ıentia

Hı ace

Antenna Diversity for Hand-portable Radio at 450MHz

Paul S.H. Leather

It has been shown that the classical field autocorrelation model, which has become established and accepted for use in base station antenna diversity calculations, is an inadequate tool for the prediction of the signal correlation associated with closely spaced antennas found in hand-portable radios. An alternative modelling method was thus developed in conjunction with an analysis of the relationship between field, signal and antenna correlation.

Using this new modelling method and a simple parallel dipole configuration, it was shown through simulation that antenna correlation is not only a function of the antenna separation but also of the angular distribution of the incoming plane waves and the impedances in which the antennas are terminated. For small horizontal antenna separations, lower levels of antenna correlation are predicted using the new analysis technique than with the established field autocorrelation model. This is due to the mutual coupling of the antennas affecting their combined radiation pattern and is achieved at the expense of reduced antenna radiation efficiency. The antenna correlation may be further reduced or optimized through the termination of the antennas in matched impedance loads.

The results of the simulation were confirmed through an experimental programme comprised of line-of-sight, partial line-of-sight and non-line-of-sight measurement routes. In addition to spatial diversity experiments, the results of investigations made using dipole-cum-loop antennas, helical and patch antennas, a split-feed antenna and a two-piece handset configuration were presented. The so-called comparative antenna diversity gain was developed in order that performance comparisons could be made between handsets by relating the diversity gain of any particular handset to a common reference standard. For received signals that follow the Rayleigh distribution, diversity gain figures in the range of 2.5dB to 13.3dB were obtained at the 1% probability level for the handsets considered in this investigation.

Acknowledgements

Collaborative projects that embody the skills, resources and motivation of both academia and industry, are perhaps the optimum form of university-based research. The Engineering and Physical Sciences Research Council are thus to be applauded for their management of the Collaborative Awards in Science and Engineering (CASE) programme.

This CASE project was supported by Philips Electronics (UK) Ltd. for whom the author wishes to express his greatest praise for realizing their responsibility to university research. Similar accolades are offered to Dr. A.M.D. Turkmani and Dr. S.R. Saunders for their inceptive activities from which this study was born.

Implicit with such research work as this, are the many unnamed people without whom things would not have happened. Gratitude is thus extended to the administrative, secretarial and technical staff of both the University of Liverpool, Philips Research Laboratories (PRL) Redhill and Philips Private Mobile Radio (PMR) Cambridge. Particular thanks are extended to: Mr. D.G. Lewis, Mrs. B.F. Lussey, Miss A.A. McMurray and Mr. R. Smith of the Department of Electrical Engineering and Electronics; Mr. R. Hill, Mr. D. Stanton and Mr. M. Goodwin of PRL, Redhill; and Mr. R. Burton of Philips PMR, Cambridge.

It is the author's belief that the success of a project is directly proportional to the understanding that exists between the relevant parties—especially that of the student and supervisor or supervisors. To this end, the utmost respect is given to Dr. P.J. Massey and Prof. J.D. Parsons for playing their roles as industrial and academic supervisor respectively.

Research students should not undervalue the succour of their colleagues and contemporaries. The author therefore wishes to avow his appreciation to Mr. Y.H. Chung, Mr. J.G. Davies, Dr. U.S. Goni, Dr. K.P. Murray, Mr. M. Nakhkash, Mr. S. Naruniranat and Dr. C. Nche.

In addition to the many aforementioned people, there are a few whose association with this project was less directly apparent. Although their names are not listed here, their help, encouragement and support is whole-heartedly acknowledged by the author.

Contents

1
Introduction

Mobile radio, especially in the industrialized nations of the world, has become common place through the increased availability of affordable and reliable communication systems. The variety of radio systems in use and the purposes for which they were designed are considerable. Common to all of these systems, and indeed to any future method of radio communication, is the propagation channel. The channel not only provides the mechanism by which energy propagates from the transmit antenna to receive antenna, but also accounts for many of the problems and limitations that besiege mobile radio systems.

In the mobile radio channel, energy rarely travels between the transmit antenna and receive antenna by way of only one path. Such "multi-path" propagation accounts for variations in the received signal when either end of the communication link moves. The variations in signal strength are often severe and under such conditions the received signal is said to be "fading". Techniques have been developed over the years to safeguard against such effects and are used in a variety of radio communication equipment to improve both the system performance and service quality.

Diversity reception is a specific technique for combating fading whereby the energy delivered to a receiver is increased by either selecting or combining the energy from individual transmission paths or branches. Ideally, the branch signals should be uncorrelated and of equal mean power. This may be achieved in a variety of ways by either man-made or natural methods. Antenna diversity may be placed into this latter category where the source of fading—the multipath nature of the channel itself—is exploited through the implementation of diversity antennas.

Extensive antenna diversity investigations at the base station, including both theoretical studies and experimental measurements, have been reported in the literature. Much attention has also been devoted to mobile vehicle-borne equipment. In both cases, the distances by which antennas may be separated is constrained only by the relatively large dimensions of either the base station or the vehicle upon which the antennas are mounted. At very high frequencies and above, these distances are typically of the order of at least several wavelengths. Under such conditions, a simple field autocorrelation model may be used to

predict the cross-correlation between the signals produced by the receive antennas whether they be horizontally or vertically spaced.

Hand-portable radio presents a considerably more challenging set of problems as the dimensions of a radio handset are perhaps less than one wavelength. The application of the simple field autocorrelation model would suggest that it is therefore not possible to place antennas at sub-wavelength separations and still obtain significantly decorrelated signals for use in a diversity receiver. Experimental investigations have, however, indicated that this is not so.

The work contained within this thesis is an investigation of antenna diversity for hand-portable radio (that is, mobile radio equipment that is designed for hand-held operation). This subject is of particular importance to Philips Electronics who supported the work through the Engineering and Physical Sciences Research Council (EPSRC) Collaborative Award in Science and Engineering (CASE) programme. The thesis is arranged as follows:

In Chapter 2, a review of the multipath channel and some of the models used to predict its effect upon radio waves and signals is presented. This serves as an introduction to the concept of fading. Attention is then devoted to techniques for reducing fading such as diversity and in particular, the numerous forms of antenna diversity. A comparison of hand-held antenna diversity experiments is given which illustrates the need to investigate some of the parameters associated with closely spaced antennas. Chapter 3 consists of such an investigation where the antenna driving point impedance, radiation efficiency and correlation of two dipole antennas is considered. A method of antenna correlation analysis is developed in this chapter and is combined with other antenna parameters to produce a figure of merit called diversity gain. Appendix A should be read in conjunction with Chapter 3 as it contains a thorough examination of the relationship between antenna, field and signal correlation. The effect of varying the spatial distribution of the incoming field energy upon the antenna correlation is studied. It is shown that the cross-correlation of the signals produced by a pair of receiving antennas is not only a function of their separation but also of the field in which they reside and the impedances in which they are terminated. Field distributions that are representative of the mobile radio propagation channel are thus used to show that significant antenna decorrelation may be obtained from closely spaced dipoles contrary to the predictions arising from simple field autocorrelation models. Furthermore, it is demonstrated that by terminating the antennas in matched impedances, the diversity gain for a given antenna arrangement may be optimized.

A two-branch antenna correlation measuring receiver design is presented in Chapter 4. The architecture of this receiver was designed to employ inexpensive local oscillators and yet maintain relative phase tracking between branches. Combined with vector or quadrature demodulation, this design enabled the complex signal cross-correlation between branches to be determined in the absence of phase synchronization between the source transmitter and the receiver. The measuring receiver and its associated data recording equipment were fully portable, self-contained and battery powered. Chapter 4 also contains a description of the six experimental handsets that were designed for both specific antenna diversity investigations and as practical prototypes for Philips.

In conjunction with the measuring receiver equipment, the six experimental handsets were used to perform a series of measurements within the precinct of the University of Liverpool. A set of "measurement routes" was chosen within the precinct to include environments where the distribution of the received signal envelope followed either a Rayleigh distribution or some other, non-Rayleigh distribution. Such signal distributions were obtained for line of sight (LOS), non-LOS and partial LOS routes Details of the experimental procedure and the data analysis methods used are given in Chapter 5.

Chapter 6 presents the results of the experimental investigation in three distinct sections. Firstly, the characteristics of each measurement route are presented in terms of the cumulative distribution function of the received signal and the ratio of the vertically and horizontally polarized electric fields. Secondly, the results of a specific experiment designed to validate the theoretical study of Chapter 3 is given. The results produced are contrasted with those predicted using the simple field autocorrelation model introduced in Chapter 2. The relationship between the complex correlation and the envelope correlation is also presented to illustrate the effect of the environment upon this parameter. To preserve commonality with later comparisons, the diversity gain produced from individual antenna separations is calculated relative to a reference set of data. In the third section of the chapter, candidate antenna-cum-handset designs are compared in terms of the following measures: branch mean signal level; inter-branch cross-correlation; and a relative figure of merit diversity gain. This last parameter enables the suitability of a particular antenna cum handset configuration to be assessed against a common reference.

The final chapter summarises the results of the work and discusses several proposals for future studies that have arisen out of this research.

2
Background

2.1 Introduction

The phenomenon of multipath propagation is responsible for many of the deleterious effects that can severely affect mobile radio communication. This phenomenon is introduced in this chapter in conjunction with some of the models that have been developed to predict the behaviour of radio waves and signals in multipath environments. An example of the effect of fading at ultra-high frequencies is presented.

Diversity is one of the techniques that may be used to combat fading. Antenna diversity is a specific form of diversity which may be further subdivided into spatial, pattern and polarization diversity. Each of these categories are described in Sections 2.4.1 to 2.4.3.

The results of many antenna diversity experiments may be found in the open literature. A comparison of some of the experiments performed for hand-held radio applications is given in Section 2.5.

The Trans-European Trunked Radio System (TETRA) is mentioned in Section 2.6 where particular detail is given to the application of diversity.

2.2 Multipath Propagation

In mobile radio communication it is very rare for the energy sent by a transmitter to arrive at the receiver having travelled by only one path. Buildings, trees and other obstacles produce reflected and scattered waves that produce the "multipath" condition [1]. Waves thus arrive at the receiver from many different directions having propagated over different distances and hence having different time delays. These waves combine vectorially at the receive antenna to give a resultant signal that is either large or small depending whether the waves combine constructively or destructively. A moving receiver operating in such an environment is said to be experiencing a fading signal.

The rate at which the signal fades is a function of the speed of the mobile and the frequency of transmission. Fading is essentially a spatial effect but can be considered as temporal when the mobile is moving through the fading environment. The rapid fluctuation of the signal produced by the local multipath is termed fast-fading and should be distinguished from the longer-term variation in the mean level which is known as slow-fading. Over relatively short distances (a few tens of wavelengths), the amplitude of the fast-fading signal often has a Rayleigh probability density function and is sometimes called a Rayleigh-fading signal.

Fast fading can produce fades that are frequently 20dB below the mean level whilst deeper fades, in excess of 30dB below the mean, are less frequent but not uncommon. The average duration of a fade is a function of the depth of the fade as well as the frequency of transmission and the speed of the mobile. Deep fades are, on average, very short when the mobile is travelling quickly through a multipath environment. At 450MHz for example (a frequency typically used for private mobile radio), a hand-portable radio carried by a person walking briskly at 5mph ($2.2ms^{-1}$) would experience 20dB fades whose spatial duration was on average 22mm. If this person were to stop walking the stationary receiver could be "sitting" in a fade of 30dB below the local mean signal level and reception could become impaired.

2.3 Review of Models

In this section, some of the mathematical models that have been developed to predict the behaviour of radio waves and signals in multipath environments are summarised. The common features of these models are presented in Section 2.3.4.

2.3.1 Ossanna

The earliest interference model, due to Ossanna [2], considers the interference of waves incident and reflected from flat sided randomly-positioned buildings. Whilst Ossanna's theoretical and measured power spectra show good agreement within the spectral limits for certain suburban areas, the model is limited by a restricted range of incidence angles and assumes the existence of a direct path between the mobile and the base station. The model is therefore constrained in its application and unsuitable for urban environments where the direct path is often obscured by buildings or other obstructions.

2.3.2 Gilbert, Clarke and Gans

Gilbert's scattering model [3] was extended and made popular by Clarke [4]. The model assumes that randomly phased horizontally-travelling waves, of arbitrary azimuth angle, are incident on the receiving antenna. It is therefore a two-dimensional model and restricted in its usage. It is appropriate to mention that Gans [5] derived similar solutions to those presented by Clarke by considering the propagation environment from a power spectrum point of view.

2.3.3 Aulin, Parsons and Turkmani

Aulin [6] modified Clarke's model and considered waves arriving from all directions thus creating a three-, rather than two-dimensional model. To simplify the analytical solution of his three-dimensional model Aulin chose elevational distribution functions that, while providing the mathematical elegance he sought, were somewhat unrealistic. Although Aulin had introduced a powerful and improved model, he failed to exploit it fully because he did not use it to investigate variations in the vertical direction.

Parsons and Turkmani [7,8] improved upon this by considering realistic wave arrival distributions. They thus refined Aulin's model and demonstrated the mechanism of vertical spatial antenna diversity.

Experimental measurements performed by Ebine [9], Lee [10] and Yamada [11] confirm the suitability of the above three-dimensional model.

2.3.4 Idealized Models

In all of the above models, the conversion of propagating wave energy from the free-space to the guided wave environment is idealized, as neither the manner of transformation nor the effect of the antenna upon the field it is sensing is considered. While such effects may reasonably be ignored for a single wire antenna, the situation is somewhat complicated by the presence of a second antenna. The experimental results of Section 2.5 show that ignorance of the antennas' effects, especially when they are closely spaced[1], yields misleading correlation coefficients.

[1] Closely spaced antennas are categorised by major axis separations of sub-wavelength distances.

2.4 Diversity Combining

Jakes [12] states that diversity combining experiments were first reported in 1927. The diversity method requires that a number of transmission paths carry the same information but have independent fading statistics. For best results, the difference in mean signal level between the paths should be small. When properly combined, the resultant signal produced from these transmission paths has greatly reduced fading characteristics and the reliability of transmission is improved.

It should be noted that diversity is a method of improving communication quality by increasing the amount of signal energy delivered to a receiver. Elaborate modulation schemes and complex coding algorithms are only of benefit when the received signal contains sufficient energy for these techniques to take effect. Modulation and coding may therefore be thought of as "high-end" communication improvements as they only provide enhanced system performance when the received signal is sufficiently strong. Diversity should therefore be considered as a "low-end" communication improvement for it not only improves the reliability of transmission for low signal energy levels (that is in the region of fading) but also provides less improvement when the signal energy is stronger. Diversity, modulation and coding, as techniques for improving signal reliability are thus complementary.

System designers can either rely on the natural properties of the radio propagation channel or employ some form of transmit diversity; for example, frequency diversity or time diversity [1,13] in order to obtain independent transmission paths at the receiver. Transmit diversity techniques will not be examined here. In passing, it is worth noting that other methods such as frequency hopping [14] and adaptive retransmission [15] are sometimes engaged to reduce the signal impairments experienced by portable radio telephones; these too are excluded from discussion.

Natural methods for obtaining independent transmission paths at the receiver usually employ two or more receive antennas. The signals produced by the antennas should have similar mean levels and be reasonably decorrelated [16]. Various forms of antenna diversity will be outlined in the following sections.

2.4.1 Spatial Diversity

The normalized autocovariance function (or autocorrelation function) of the envelope of the E_z field component in an isotropically scattered field is shown by Clarke [4] to follow:

$$\rho_{\delta|E_z|} \cong J_0^2(k\xi) \qquad (2\text{-}1)$$

where $J_0(\ )$ is the zero-order Bessel function of the first kind, $k = 2\pi/\lambda$ is the free-space phase constant and ξ is the distance away from 0 in the x-direction. This quantity is also the normalized correlation coefficient of the signal envelopes at the terminals of two vertical monopole antennas ξ apart in an isotropically scattered field. At 456MHz, the value of ξ required to obtain an autocorrelation function value of 0.7 is 82mm. The first zero crossing of this function occurs at 250mm. As stated in Section 2.3.4, Clarke's model is a field autocorrelation model. It is subsequently demonstrated in Chapter 3 that such a model is unsuited for the calculation of the cross-correlation of the signals received by two closely spaced dipoles since the model neither considers the effect of the antennas on the field in which they reside nor the coupling between them.

Vaughan [17] examines the effect of mutual coupling between closely spaced monopoles and shows how it serves to improve the decorrelation of signals. The analysis considers parallel monopoles that reside in the same plane (horizontal spatial diversity (HSD)). Vaughan's experimental work using similar antennas supports his theoretical findings. In Section 2.5, a comparison of the experimental work of Adachi [18], Tsunekawa [19] and Yamada [20,21] is presented. Their findings also show that lower correlation coefficients are obtained when antennas are closely spaced than predicted by Clarke's field autocorrelation model.

The mutual coupling between an antenna pair is a function of the impedance connected to those antennas. This effect is particularly noticeable when there is strong mutual coupling between the antennas; that is, when they are closely spaced. Vaughan considers the termination impedance of the antennas and shows how it may be adjusted to obtain even lower levels of correlation.

It should be noted that the effect of antenna radiation efficiency is not considered by either Vaughan or in any of the other published papers that the author has seen. This short coming in the analysis of antenna correlation is addressed in Chapter 3.

Vertical spatial diversity (VSD) uses antennas perpendicularly spaced along their vertical axis to provide independent transmission paths. Because the distribution of wave arrival in elevation is related to the height of the receive antenna, the spacing required for reasonable decorrelation ($\rho_e \leq 0.7$) is less for antennas nearer to the ground [9]. Ebine [9] reports that the spacing required for vehicle mounted antennas, 1.5m above the ground, is about 0.3λ whilst 30λ separation is needed to achieve the same decorrelation for antennas 156m above the ground. In existing cellular radio systems, vehicle mounted VSD antennas are sometimes used whilst HSD antennas are more common at the base station.

2.4.2 Pattern Diversity

Lee's experiments [10] at 836MHz have demonstrated that the angular probability distribution function (PDF) of wave arrival in the azimuth plane along a given route is non-uniform. In the same paper, Lee compares the theoretical results of two sets of calculations: one set assumes that the angular PDF of azimuthal wave arrival is uniform whereas the other set assumes a non-uniform PDF. The error produced by incorrectly assuming that the PDF is uniform has little effect on the first order statistical properties of the received signal (such as its mean value and cumulative probability distribution) but its second order statistical properties (such as its level crossing rate and correlation function) will be substantially in error. Whilst it can be anticipated that certain routes experience non-uniform angle of arrival PDF's, the ensemble average PDF, averaged over many routes, will be uniform. The angle of arrival of incoming waves in a multipath environment is thus assumed to be evenly distributed in azimuth [8]. This would seem obvious for vehicle mounted antennas but may not necessarily be true for hand-held radios where the antennas are often shielded in one direction by the user's head, hand or body.

The signals produced by a moving directional antenna, pointing in a given direction, will have different fading characteristics from the signals produced by a similar antenna pointing in a different direction. Antennas can thus be arranged to receive signals from a given direction thereby producing the required independent transmission paths necessary

for diversity combining. The antennas can either rely on their individual radiation patterns to provide independent branches or similar directional antennas can point in different directions. This latter case is often termed angle diversity.

Pattern diversity has been implemented using active window antennas in motor vehicles to improve the reception of FM domestic broadcast radio [23]. A circular array of sectored pattern antennas can be used to achieve even greater reduction in fading through the optimum combining of all antenna ports [24]. It is expected that such systems, or "smart antennas", will form part of new base station installations for cellular radio as they improve the overall signal-to-interference-plus-noise ratio as well as reducing fading [25].

For a simple pattern diversity scheme consisting of two antennas, Yamada [11] states that a pattern difference (in this case the front-to-back ratio) in excess of 10dB is required to produce correlation coefficients less than 0.6. Yamada adds that spatial diversity is more effective than pattern diversity as a phase difference of 60 degrees or more achieves the same value of ρ_e. Antenna spatial diversity and antenna pattern diversity may be combined to achieve improved signal decorrelation.

2.4.3 Polarization Diversity

The simple description of multipath propagation presented in Section 2.2 may now be extended to embrace the idea that the signals arriving at the receiver not only experience different path lengths but, by the effects of reflection and refraction, also endure depolarization. The amount of depolarization is related to the propagation environment; for example, a dense urban environment, containing many scatterers, will produce more depolarization than an open rural environment.

The cross-polar ratio (XPR) is often used as a measure of depolarization in a given environment. Base station transmit antennas are normally vertically polarized allowing the specific definition $XPR = P_V / P_H$ where P_V and P_H are the average received powers of the vertical (co-polar) and horizontal (cross-polar) components [26]. Kozono [27] and Kuboyama [28] use a similar definition but refer to the ratio as the cross-polar discrimination (CPD). Cox [29] defines cross-polarization coupling (XPOL) as $XPOL = E_X / E_T$ where E_T is the average or median field magnitude of the

polarization aligned with the transmitted polarization and E_X is the average (or median) field magnitude of the polarization orthogonal (crossed) to E_T. This latter definition is the reciprocal of those mentioncd above and will not be used.

Table 2-1: Comparison of cross-polar coupling ratio (XPR) measurements reported by various workers in different locations.

Reported by	Location	Frequency (MHz)	Environment	XPR (dB)
Lemieux [30]	Ottawa, Canada	915	University, In-building	≤|2|
Vaughan [31]	Frejlev, Denmark	463	Suburban Urban	12.0 7.0
Kozono [27]	Tokyo, Japan	920	Metropolitan	5-6
Kuboyama [28]	Tokyo, Japan	920	Car antenna/rural Car antenna/urban Handset antenna/rural Handset antenna/urban	11.6 6.5 11.7 5.1
Taga [26]	Tokyo, Japan	900	Metropolitan area	5.1
Bergmann [32]	New Jersey, U.S.A.	816	Crawford Hill non-LOS Crawford Hill line-of-sight	~0 10-20
Cox [29]	New Jersey, U.S.A.	800	Outside houses Insides houses Crawford Hill lab. Holmdel lab.	4.1 2.6 -0.2 -2.1
Lee [33]	New Jersey, U.S.A.	836	Holmdel area V_{TX}-H_{RX} H_{TX}-V_{RX}	 4.0-8.0 4.5-8.5
Hashimoto [34]	Southampton, U.K.	905	University, In-building	~10

Measurements of the XPR using various methods have been made in North America, Denmark, Japan and the United Kingdom. Table 2-1 summarises the results of these investigations. The table has been produced using the workers' definition of environment and no attempt has been made to harmonize such definitions between countries. Caution should thus be taken when comparing Japanese metropolitan results with Danish urban results for example.

The use of polarization diversity antennas in hand-held radio applications is attractive because not only is the spacing required between antennas of less importance than in spatial diversity (allowing more compact designs) but the effects of random handset orientation are also reduced [35].

2.5 Comparison of Japanese Workers' Experimental Results

Many antenna diversity investigations, including both base station and mobile station experiments, are reported in the open literature. The majority of published work in the latter category (vehicle-borne and hand-portable studies), originates from the communication laboratories of the Nippon Telegraph and Telephone Public Corporation, Japan (NTT). A short selection of NTT's published findings, spanning thirteen years, are compared in this section using Fig. 2-1. The figure also shows Clarke's field autocorrelation function [4] and Yamada's coupling function [21] for comparison.

The details of each experiment are summarised under the sub-heading of the first named author in the following subsections.

2.5.1 Adachi

Adachi's 880MHz experiments [18] were made using vehicle mounted vertical quarter-wavelength whip antennas. The height of the van roof is not given but the base station antenna height and distance from transmitter to (mobile) receiver are reported as 160m and 3km respectively. Measurements were made in an industrial environment around a closed circuit using vehicular antenna separations of 0.09λ to 2.00λ. The encircled-A symbol denotes Adachi's results in Fig. 2-1.

2.5.2 Tsunekawa

Tsunekawa [19] performed portable equipment experiments using a carrier frequency of 800MHz for both over-the-shoulder and hand-held receivers equipped with planar inverted-F antennas (PIFA's). The rectangular urban measurement course was located 1.3km from the base station. Results are presented for a hand-held unit whose height was varied from 0.3λ to 0.6λ and with antenna separations of 0.05λ to 0.18λ and for an over-the-shoulder unit with (base mounted) antenna spacings of 0.5λ and 0.6λ. The encircled-T symbol denotes Tsunekawa's results in Fig. 2-1.

2.5.3 Yamada 1

Yamada [20] conducted hand-held equipment experiments using an 800MHz carrier frequency for combinations of top-mounted whip antennas and built-in PIFA's. Neither details of the whip antenna length nor the experimental method are given. Results are presented for whip-to-built-in antenna separations of 0.07λ and whip-to-whip antenna separations of 0.09λ and 0.19λ. The encircled-Y symbol denotes Yamada's results in Fig. 2-1.

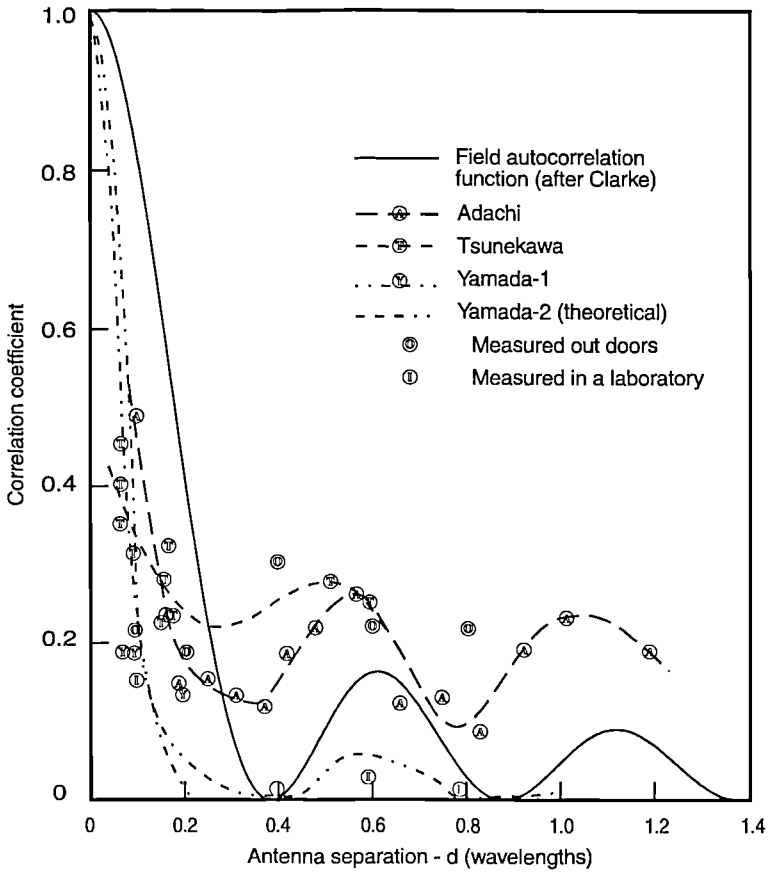

Figure 2-1: Antenna correlation versus antenna separation: a comparison of Japanese workers' experimental results.

2.5.4 Yamada 2

In the second of Yamada's papers referenced in this section, results are presented for both indoor and outdoor experiments [21]. Once again, the experimental detail is lacking. The outdoor experiments were conducted in various urban Tokyo areas using vehicle mounted whip antennas whose separation was varied from 0.1λ to 0.8λ. These

results are denoted with the encircled-O symbol in Fig. 2-1. The indoor experiments were made in a laboratory where Yamada reports the propagation condition to be "idealized", a term referenced to Taga's 1991 paper published in Japanese [36]. An earlier paper by Taga [37] describes a method of laboratory experiment where the transmitter and receiver antennas are both placed midway between the floor and the ceiling. Taga argues that such an arrangement provides vertically and horizontally polarized waves whose average incoming direction is horizontal since equal reflection is provided in elevation from both the floor and the ceiling. These results are denoted with the encircled-I symbol in Fig. 2-1.

In his theoretical analysis, Yamada considers the mutual coupling between the antennas and uses the implied phase shift thereof to model the correlation coefficient as a function of separation. This function is plotted in Fig. 2-1 over a single wavelength.

2.5.5 Summary

All the sets of experimental results are at variance with the theoretical predictions for correlation in the absence of antenna mutual coupling, which are exemplified by the theoretical curve for Clarke's model [4] in Fig 2-1. Yamada's theoretical approximation which models mutual coupling by modifying the phase shifts of the antenna elements comes closest to resembling an experimental data set. An alternative method of antenna correlation analysis is presented in Chapter 3.

2.6 Diversity and TETRA

The Trans-European Trunked Radio (TETRA) system is a digital time division multiple access (TDMA) system that is intended for private mobile radio (PMR) and public access mobile radio (PAMR). Standardization of TETRA is currently being completed by the European Telecommunications Standards Institute (ETSI). Table 2-2 summarizes the TETRA system and shows the Global System for Mobile Communications (GSM) for comparison [38].

The use of diversity combining in TETRA mobile stations is particularly attractive for the reasons described in the following sub-sections.

Table 2-2: Comparison of the GSM and TETRA communication systems.

FEATURE	GSM	TETRA
Technology	digital TDMA	digital TDMA
Frequency	900MHz	400MHz[2]
Effective bandwidth per voice channel	25kHz, 12.5kHz with ½ rate codec	6.25kHz
Call set-up times	<10s	<1s
Data facilities	yes	yes
Group calls	no (except via conference call facility)	yes
Direct Mode	no	under development
Wide area communications	yes	possible
Maximum speed	250km/h	200km/h
Hand-over	yes	yes
Roaming	yes	yes
Authentication and encryption	yes	under development
Status	available	standardization near-complete

2.6.1 High Speed Mobile Operation

Diversity combining can yield significant performance improvements when the fading rate is high as experienced by vehicle-borne receivers travelling at speed. Spatially separated antennas are relatively easy to accommodate on vehicles and diversity combining is an attractive alternative to receiver equalization where channel tracking at high fading rates increases the complexity of the equalizer.

In hilly terrain environments, hand-portable radios, although travelling at much lower speeds, can experience higher delay spreads where the use of an equalizer may be more appropriate. Diversity combining and equalization thus offer complementary advantages.

Saunders [39] has shown that for the specified sensitivity limit of 2% bit error rate (BER), a system improvement or diversity gain of 8dB in the TU50 (typical urban, mobile speed of 50 kmh^{-1}) environment can be expected. This can be translated into a range improvement of 1.6 or a coverage improvement of 2.5 using the fourth power law. For the HT200 environment (hilly terrain, mobile speed of 200 kmh^{-1}), Saunders reports a diversity gain of 10dB for the same 2% BER. A basic differential demodulator cannot achieve the required performance in so-called simulcast or quasi-synchronous transmission environments (QS200). Saunders has shown that two branch maximal ratio diversity combining exceeds the specified performance limits in QS200 scenarios by 7dB.

[2] Most likely continental frequency.

2.6.2 Low Speed Mobiles

Hand-held or low speed vehicle-borne receivers are likely to experience fades of extended duration where it is possible for the signal to fall 40dB below the local average. The coverage area under such conditions will be severely reduced if some form of diversity is not implemented.

2.6.3 Link Budget Imbalance

The link budget calculations for both mobile station to base station and hand portable to base station show an imbalance in the uplink (e.g. HH→BS) direction [40]). Diversity employed at the base station can remove this imbalance. This study is primarily concerned with hand-portable radio operation and no further mention of diversity implementation at base stations will be made.

2.7 References

1. PARSONS, J.D., and GARDINER, J.G., 1989, "Mobile Communication Systems", Blackie and Son Limited, (John Wiley & Sons Inc.), New York, USA, pp189-243

2. OSSANNA, J.F., 1964, "A Model For Mobile Radio Fading Due to Building Reflections: Theoretical and Experimental Fading Waveform Spectra", Bell Sys. Tech. J., Vol. 43, No. 6, pp2935-2971.

3. GILBERT, E.N., 1965, "Energy Reception for Mobile Radio", Bell Sys. Tech. J., Vol. 44, No. 8, pp1779-1803.

4. CLARKE, R.H., 1968, "A Statistical Theory of Mobile-Radio Reception", Bell Sys. Tech. J., Vol. 47, No. 6, pp957-1000.

5. GANS, M.J., 1972, "A Power-Spectral Theory of Propagation in the Mobile-Radio Environment", IEEE Trans. Veh. Tech., Vol. VT-21, No. 1, pp27-38.

6. AULIN, T., 1979, "A Modified Model for the Fading Signal at a Mobile Radio Channel", IEEE Trans. on Vehicular Tech., Vol. VT-28, No. 3, pp182-203.

7. PARSONS, J.D., and TURKMANI, A.M.D., 1991, "Characterisation of mobile radio signals: model description", IEE Proc.-I, Vol. 138, No. 6, pp549-556.

8. TURKMANI, A.M.D. and PARSONS, J.D., 1991, "Characterisation of mobile radio signals: base station crosscorrelation", IEE Proc.-I, Vol. 138, No. 6, pp557-565.

9. EBINE, Y., TAKAHASHI, T., and YAMADA, Y., 1991, "A Study of Vertical Space Diversity for a Land Mobile Radio", Electron. and Comms. in Japan Pt. I, Vol. 74, No. 10, pp68-76.

10. LEE, W.C.-Y., and BRANDT, R.H., 1973, "The Elevation Angle of Mobile Radio Signal Arrival", IEEE Trans. Comms., Vol. COM-21, No. 11, pp1194-1197.

11. YAMADA, Y., EBINE, Y., and KAKAJIMA, N., 1987, "Base Station / Vehicular Antenna Design Techniques Employed in High-Capacity Land Mobile Communications System", NTT Rev. of the Electric. Comms. Lab., Vol. 35, No.2, ppll5-121.

12. JAKES, W.C., 1974, "Microwave Mobile Communications", IEEE Inc. Press (1993), New York, USA, p310.

13. SAUNDERS, S.R., 1994, "Base station transmit diversity for improving service quality for low speed mobiles", *Unpublished Work*, Philips Telecom—PMR, Cambridge, UK.

14. CHANG, L.F., and PORTER, P.T., 1989, "Performance Comparison of Antenna Diversity and Slow Frequency Hopping for the TDMA Portable Radio Channel", IEEE Trans. on Veh. Tech., Vol. VT-38, No. 4, pp222-229.

15. COX, D.C., 1983, "Time Division Adaptive Retransmission for Reducing Signal Impairments in Portable Radiotelephones", IEEE Trans. on Veh. Tech., Vol. VT-32, No. 3, pp230-238.

16. BRENNAN, D.G., 1959, "Linear Diversity Combining Techniques", Proc. IRE, 47, pp1075-1102.

17. VAUGHAN, R.G., and SCOTT, N.L., 1993, "Closely spaced monopoles for mobile communications", Radio Science, Vol. 28, No. 6, pp1259-1266.

18. ADACHI, F., HATTORI, T., HIRADE, K., and KAMATA, T., 1978, "A Periodic Switching Diversity Technique for a Digital FM Land Mobile Radio", IEEE Trans. on Veh. Tech., Vol. VT-74, No. 4, pp2ll-219.

19. TSUNEKAWA, K. 1989, "Diversity Antennas for Portable Telephones", Proc. 39th IEEE Veh. Tech. Conf., San Francisco, USA, pp50-56.

20. YAMADA, Y., EBINE, Y. and TSUNEKAWA, K., 1991, "Base and Mobile Station Antennas for Land Mobile Radio Systems", IEICE Trans., Vol. E 74, No. 6, pp1547-1555.

21. YAMADA, Y., KAGOSHIMA, K., and TSUNEKAWA, K., 1991, "Diversity Antennas for Base and Mobile Stations in Land Mobile Communication Systems", IEICE Trans., Vol. E 74, No. 10, pp3202-3209.

22. LEE, W.C.-Y, 1973, "Finding the Approximate Angular Probability Density Function of Wave Arrival by Using a Directional Antenna", IEEE Trans. on Ants. and Prop., Vol. AP-21, No. 3, pp328-334.

23. LINDENMEIER, H.K., 1989, "Antennas on Land Vehicles for Improved Communications", NATO AGARD-LS-165, pp7-1 to 7-19.

24. BARRET, M. and ARNOTT, R., 1994, "Adaptive antennas for mobile communications", IEE Electron. and Comms. Eng. J., Vol. 6, No.4, pp203-214.

25. *Editorial*, 1994, "DCS1800 now gets active across Europe - Northern Telecom Smart Antenna", Microwave Engineering Europe, pp11-14.

26. TAGA, T., 1991, "Analysis of Correlation Characteristics of Antenna Diversity in Land Mobile Radio Environments", Electron. and Comms. in Japan Pt. 1, Vol. 74, No. 8, pp101-115.

27. KOZONO, S., TSURUHARA, T., and SAKAMOTO, M., 1984, "Base Station Polarization Diversity for Mobile Radio", IEEE Trans. on Veh. Tech., Vol. VT-33, No.4, pp30l-306.

28. KUBOYAMA, H., TANAKA, Y., SATO, K., FUJIMOTO, K., HIRASAWA, K., 1990, "Experimental Results with Mobile Antennas Having Cross-Polarization Components in Urban and Rural Areas", IEEE Trans. on Veh. Tech., Vol. VT-39, No. 2, ppl50-160.

29. COX, D.C, MURRAY, R.R., ARNOLD, H.W., NORRIS, A.W., and WAZOWICZ, M.F., 1986, "Cross-Polarization Coupling Measured for 8OOMHz radio Transmission in and around Houses and Large Buildings", IEEE Trans. on Ants. and Prop., Vol. AP-34, No. 1, pp83-87.

30. LEMIEUX, J-F, EL-TANANY, M.S., and HAFEZ, H.M., 1991, "Experimental Evaluation of Space/Frequency/Polarization Diversity in the Indoor Wireless Channel", IEEE Trans. on Veh. Tech., Vol. VT-40, No.3, pp569-574.

31. VAUGHAN, R.G., 1990, "Polarization Diversity in Mobile Communications", IEEE Trans. on Veh. Tech., Vol. VT-39, No, 3, pp177-186.

32. BERGMANN, S.A., and ARNOLD, H.W, 1986, "Polarisation Diversity in Portable Communications Environment", Electron. Lett., Vol. 22, No. 11, pp609-6l0.

33. LEE. W.C.-Y, and YEH, Y.S., 1972, "Polarization Diversity System for Mobile Radio", IEEE Trans. on Comms., Vol. COM-20, No. 5, pp912-923.

34. HASHIMOTO, K., CHIA, S.T.S. and STEELE, R., 1988, "Utilization of Polarisation Diversity and Antenna Directivity to Combat Co-channel Interference for Indoor Cordless Telephony", IEE Coll. on 'Propagation Factors and Interference Modelling for Mobile Radio Systems', Dig. No. 123, pp7/1-7/6.

35. COX, D.C, 1983, "Antenna Diversity Performance in Mitigating the Effects of Portable Radio Telephone Orientation and Multipath Propagation", IEEE Trans. on Comms., Vol. COM-31, No. 5, pp620-628.

36. TAGA, T., 1991, "Characteristics of space diversity branches using parallel dipole antennas in mobile radio communications", Tech. Grp. of IEICE Japan, AP 91-17. (*Japanese language*)

37. TAGA, T., TSUNODA, K., and IMAHORI, H., 1989, "Correlation Properties of Antenna Diversity in Indoor Mobile Communication Environments", Proc. 39th IEEE Veh. Tech. Conf., Vol. 2, San Francisco, USA, pp446-451.

38. WEBB, W.T, and SHENTON, R.D., 1994, "Pan-European railway communications: where PMR and cellular meet", IEE Electron. Comms. Eng. J., Vol. 6, No.4, pp195-202.

39. SAUNDERS, S.R., 1994, "The Potential for Diversity in DPMR", TETRA Work-package 3, Issue 1, Philips Telecom-PMR (Company Confidential). Cambridge, UK.

40. SAUNDERS, S.R., 1993, "Diversity: Initial Study", TETRA Work-package 3, Euroglue (Company Confidential), Mägenwil, Switzerland.

3
Antenna Diversity from Two Closely Spaced Dipoles

3.1 Introduction

This chapter presents a parametric investigation of two closely spaced dipole antennas paying particular attention to their cross-correlation and radiation efficiency. It is shown that Clarke's simple planar scattering model [1] and Aulin's extended three-dimensional model [2], neither of which consider the effect of antenna coupling, are inadequate tools for calculating the cross-correlation between two closely spaced antennas.

The concept of diversity gain and its specific application in the use of antenna correlation analysis is also presented. This quantity is used to provide a figure of merit for assessing the system performance improvement that may be expected from the use of certain antenna configurations and signal combining techniques.

A description of antenna correlation and its relationship to field and signal correlation is given in Appendix A.

3.2 Investigation Method

To describe the parametric investigation procedure, it is perhaps appropriate to introduce the parameters considered and explain how they are calculated.

3.2.1 Antenna Correlation

The coordinate system geometry is shown in Fig. 3-1. Figure 3-2 shows the two dipoles situated in free-space. Each of the dipole arms is a 0.001λ diameter perfectly conducting rod which is cut to a resonant length of 0.2375λ. The dipoles are parallel to the z-axis and are situated a distance d apart along the x-axis.

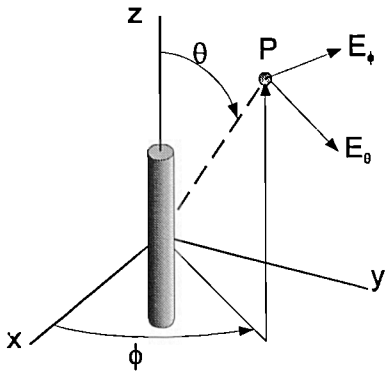

Figure 3-1: Coordinate system geometry and dipole orientation.

The Principle of Superposition is applied to the calculation of the correlation between the antennas shown in Fig. 3-2. In configuration 1 (Fig. 3-2a), the first dipole is fed and the second dipole is terminated. These roles are swapped in configuration 2 (Fig. 3-2b) where the second dipole is fed and the first dipole is terminated. The terminated or undriven antenna is subsequently called the parasitic antenna.

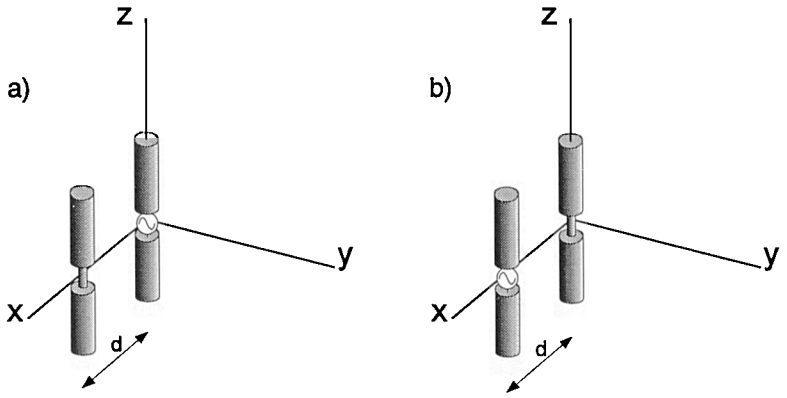

Figure 3-2: Antenna configuration showing driven and terminated half-wave dipoles in free space. In a) dipole-a is driven whilst dipole-b is terminated. These roles are swapped in b).

To calculate the antenna correlation between these configurations, the radiation patterns for each of the antenna configurations must be known. The antenna correlation ρ_a^2 is computed from the formula (see Section A.3 of Appendix A):

$$\rho_a^2 = \frac{\left| \iint_\Omega \left(E_{1\theta} E_{2\theta}^* P_\theta + E_{1\phi} E_{2\phi}^* P_\phi \right) e^{jk\mathbf{d}\bullet\mathbf{a}_r} d\Omega \right|^2}{\iint_\Omega \left(E_{1\theta} E_{1\theta}^* P_\theta + E_{1\phi} E_{1\phi}^* P_\phi \right) d\Omega \iint_\Omega \left(E_{2\theta} E_{2\theta}^* P_\theta + E_{2\phi} E_{2\phi}^* P_\phi \right) d\Omega} \qquad (3\text{-}1)$$

where $\{E_{1\theta}, E_{1\phi}\}$ are the radiation fields of configuration 1, $\{E_{2\theta}, E_{2\phi}\}$ are the radiation fields of configuration 2, $P_\theta(\theta,\phi)$ and $P_\phi(\theta,\phi)$ are weighting functions that describe the power distribution of the incoming θ and ϕ waves, and $\iint_\Omega \ldots d\Omega$ denotes integration over all angles.[1]

As the origins of the two configurations are identical, the origin displacement vector $\mathbf{d} \equiv 0$. Also for dipoles that are parallel to the z-axis, $E_\phi = 0$. Therefore eqn. (3-1) reduces to:

$$\rho_a^2 = \frac{\left| \iint_\Omega E_{1\theta} E_{2\theta}^* P_\theta d\Omega \right|^2}{\iint_\Omega \left(E_{1\theta} E_{1\theta}^* P_\theta\right) d\Omega \iint_\Omega \left(E_{2\theta} E_{2\theta}^* P_\theta\right) d\Omega} \qquad (3\text{-}2)$$

3.2.2 Radiation Efficiency

The antenna radiation efficiency, η_{rad}, of an antenna configuration is defined as:

$$\eta_{rad} = \frac{P_{rad}}{P_{in}} = \frac{R_{rad}}{R_{rad} + R_{loss}} \qquad (3\text{-}3)$$

Where P_{rad} is the power radiated by the antenna, P_{in} is the power delivered to its driving point, R_{rad} is the radiation resistance and R_{loss} is the loss resistance [3, p257].

3.2.3 Diversity Gain

The improvements available from the various diversity techniques may be expressed in different ways. Most of the theoretical results have been obtained for the case when the branches[2] have signals with independent Rayleigh-fading envelopes and equal mean SNR [4]. Brennan [5] extended this general case and investigated the effect of both inter-branch cross-correlation and inter-branch mean signal level difference.

Diversity gain may therefore be defined in general terms as the ratio of the average signal to noise ratio (SNR) measured at the output of a particular diversity system to the average signal

[1] See Section A.3 of Appendix A for further details.

[2] A branch represents a unique input signal. This may be provided by the same information being transmitted at a different time or frequency, or, as in this application, the same temporal information being received by two antennas.

to noise ratio measured at one of its inputs[3] providing that both the input and output signal to noise ratios are measured at the same level.[4] This quantity is often expressed in decibels.

In this investigation, diversity gain is a function of both the antenna correlation and the radiation efficiency which in turn are functions of both the antenna separation and the value of termination connected to the parasitic antenna. Diversity gain may therefore be represented as a surface in three-dimensional space, where the vertical axis represents diversity gain, and the horizontal axes represent antenna correlation and radiation efficiency.

3.2.3.1 Production of diversity gain surfaces

Because the calculation of diversity gain using analytical equations is too complex in the context of this study, it must be computed numerically. The process used to produce the diversity gain surfaces is described in this section. Figure 3-3 should be viewed in conjunction with the description. The process is implemented in software using MATLAB [6].

3.2.3.1.1 Description of simulation blocks

Complex Signal Generator (a). Two sequences of complex data are generated at block (a) using a Classical[5] fading generator. These sequences are both of length 0.1 million and represent fading data sampled at a rate of 100Hz using a carrier frequency of 456MHz and a mobile speed of 5mph. Cumulative distribution plots of the data show it to be Rayleigh distributed. The two sequences are correlated by the given complex correlation input variable, ρ. Both sequences have a mean level of 0dB.

Variable Attenuation (b). The complex fading signal sequences are now attenuated by an amount directly proportional to the radiation efficiency using eqn. (3-4) where η_{rad} is the percentage radiation efficiency of the receive antenna and α is the corresponding signal attenuation expressed in decibels. The attenuation is ideal in that it adds neither phase nor noise.

$$\alpha = 10\log_{10}(\eta_{rad}) \qquad (3\text{-}4)$$

[3]The choice of input is arbitrary. A pessimistic measure is however, often made through the selection of the strongest signal.

[4]The level at which the measurement is taken is often a percentage cumulative probability.

[5]An infinite impulse response filter with a classical Doppler fading spectrum is applied to a Gaussian distributed data sequence of unity variance to yield the required complex fading data. This method is computationally more efficient than the multi-oscillator fading simulator presented by Jakes [7].

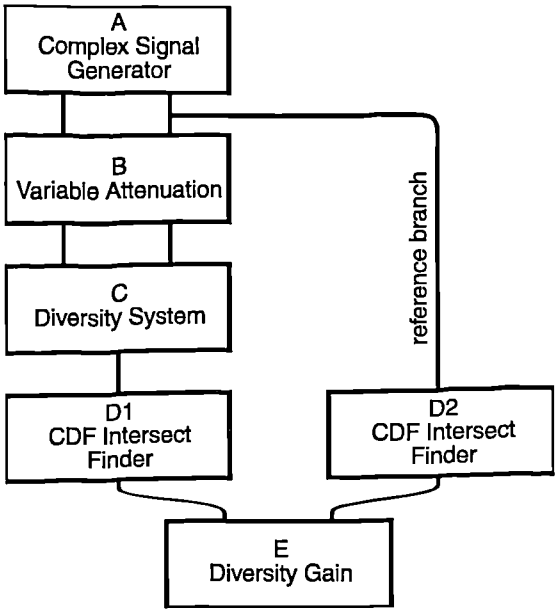

Figure 3-3: Flow chart illustrating the calculation of diversity gain.

Diversity System (c). It is assumed that the two signals have equal noise power which allows them to be combined using each of the following methods:

Selection Diversity. Selection diversity is perhaps the most simple form of diversity to implement. The output of such a system is simply equal to the strongest signal fed into it, that is:

$$v(t)_{sel} = \begin{matrix} v_1(t) & v_1(t) \geq v_2(t) \\ v_2(t) & v_1(t) < v_2(t) \end{matrix} \qquad (3\text{-}5)$$

Equal Gain Combining. For both equal gain and maximal ratio pre-detection combining, the signals must first be co-phased. This is a simple procedure to implement in software. Equal gain combiners use a summing unit to add together the signals fed to it, that is:

$$v_{egc}(t) = \frac{v_1(t) + v_2(t)}{\sqrt{2}} \qquad (3\text{-}6)$$

Maximal Ratio Combining. Equal gain combining has the disadvantage that weak signals, whose signal to noise ratio is relatively low, are weighted in exactly the same way as strong signals whose signal to noise ratio is relatively higher. For weak signals this can actually

result in more noise power being added than signal power. For low signal levels, selection diversity can thus yield greater diversity gains than equal gain combining. Maximal ratio combining however, weights each signal in accordance to its signal voltage to noise power ratio and therefore yields the highest diversity gain of the three methods listed for all signal levels. Maximal ratio combining may be implemented in software using the following equation:

$$v_{mrc}(t) = \sqrt{v_1^2(t) + v_2^2(t)} \qquad (3\text{-}7)$$

Cumulative Distribution Function Intersect Finder (d). The cumulative distribution function of the newly combined signal is produced in block (d1) and should be visualised as a plot on probability graph paper where the axes are percentage probability and mean signal to noise power ratio (SNR). From this function (or graph) the value of signal to noise for a given cumulative probability level is found using linear interpolation. A similar process is applied to the reference branch in block (d2).

Diversity Gain (e). The diversity gain, expressed in decibels, is calculated in accordance with the definition presented in Section 3.2.3.

Complete Procedure. Diversity gains are calculated in the way described above for each combination of branch-to-branch correlation and branch attenuation. These latter parameters are typically stepped from 0 to 1 in increments of 0.1 and from -30 to 0dB in 2dB steps.

3.2.4 Matched Terminations

This section explains how the value of the termination required to match the port of the parasitic antenna is calculated. Consider the twin dipole configuration as a two-port network. Then the impedances seen at each of the ports are:

$$Z_{1in} = \frac{V_1}{I_1} = Z_{11} + Z_{12}\frac{I_2}{I_1} \qquad (3\text{-}8)$$

$$Z_{2in} = \frac{V_2}{I_2} = Z_{22} + Z_{21}\frac{I_1}{I_2} \qquad (3\text{-}9)$$

where Z_{1in} and Z_{2in} are the input impedances of the ports, V_1 and I_1 are the voltage and current associated with antenna 1's port, V_2 and I_2 are the voltage and current associated

with antenna 2's port, and $Z_{11};Z_{12};Z_{21};Z_{22}$ are the coefficients of the two port impedance matrix. For two identical antennas the two port network is symmetric; $Z_{11} = Z_{22} = Z_s$ and $Z_{12} = Z_{21} = Z_m$, and eqs.3-8 and 3-9 become:

$$Z_{1in} = \frac{V_1}{I_1} = Z_s + Z_m \frac{I_2}{I_1} \quad (3\text{-}10)$$

$$Z_{2in} = \frac{V_2}{I_2} = Z_s + Z_m \frac{I_1}{I_2} \quad (3\text{-}11)$$

If port 2 is terminated with an impedance Z_b, then:

$$Z_b = -\frac{V_2}{I_2} \quad (3\text{-}12)$$

Substituting eqn. (3-12) and eqn. (3-11) into eqn. (3-10) gives:

$$Z_{1in} = Z_s - \frac{Z_m^2}{Z_b + Z_s} \quad (3\text{-}13)$$

As the antennas are identical, if port 1 is matched, then $Z_{1in} = Z_b$. Substituting this in eqn. (3-13) gives:

$$Z_b = \sqrt{Z_s^2 - Z_m^2} \quad (3\text{-}14)$$

To determine the values of Z_s and Z_m the two dipoles are driven with equal amplitude sources. If the sources are in-phase:

$$Z_{1in(in-phase)} = Z_s + Z_m \quad (3\text{-}15)$$

If the sources are in anti-phase:

$$Z_{1in(anti-phase)} = Z_s - Z_m \quad (3\text{-}16)$$

Rearranging gives:

$$Z_s = \frac{Z_{1in(in-phase)} + Z_{1in(anti-phase)}}{2} \quad (3\text{-}17)$$

$$Z_m = \frac{Z_{1in(in-phase)} - Z_{1in(anti-phase)}}{2} \quad (3\text{-}18)$$

3.2.5 Computation Method

The computation is divided into three parts as follows:

Antenna Current Distributions. The antenna current distributions were computed using the publicly available Moment Method [8] computer package, NEC2[6] compiled under FORTRAN. Appropriate segmentation schemes and NEC modelling techniques were observed in accordance with the methods presented by Murray [9].

Antenna Radiation Patterns. The radiation computation method described by Massey [10] was extended so as to take the antenna current distributions and compute the antenna correlation using eqn. (3-2). *Mathematica* [11] was used for this computation.

Diversity Gain. The diversity gain was calculated from the previously computed surfaces of diversity gain (see Section 3.2.3.1) by mapping the values of antenna correlation and radiation efficiency calculated above. This process was implemented in MATLAB.

3.3 Results

This section is organised as follows:

- Section 3.3.1 describes the effects of varying the elevational distribution of incoming waves.
- Section 3.3.2 describes the effects of varying the azimuthal distribution of incoming waves.
- Section 3.3.3 describes the effects of changing the resistance of the parasitic antenna's termination.
- Complex impedance terminations are considered in Section 3.3.4.

[6]NEC is a Method of Moments computer program for the analysis of the electromagnetic response of arbitrary structures to excitation by either voltage sources or plane waves.

- The results of Sections 3.3.3 and 3.3.4 suggest that the use of matched terminations generally leads to a very good decorrelation and efficiency performance. Section 3.3.5 describes this special case.

- The reasons for many of the properties described in Sections 3.3.1 to 3.3.4 can be seen with the help of plots of the radiation patterns and of the integrand of the antenna correlation integral. Section 3.3.6 describes the integrand plots and explains how they illustrate the correlation behaviour.

- Section 3.3.7 discusses what consequences the results described in sections 3.3.1 to 3.3.5 have for the gains achievable using selection, equal gain and maximal ratio combining.

3.3.1 Varying the Elevational Coverage

Figures 3-5 to 3-8 shows plots of antenna correlation against antenna separation and the resistive impedance terminating the parasitic dipole. The four plots vary in the elevation range of integration used in calculating the antenna correlation. The plots are very similar, showing that the range of elevation angles used does not significantly affect the antenna correlation.

3.3.2 Varying the Azimuthal Coverage

Figures 3-9 and 3-10 show two plots of antenna correlation against antenna separation and parasitic dipole resistive termination. One uses an azimuthal range of $\phi = 0 \rightarrow 180°$, and the other only considers the $-x$ facing hemisphere, with $\phi = 90 \rightarrow 270°$. The plots are very different, showing that the range of integration in azimuth can be very significant.

3.3.3 Resistive Terminations to the Parasitic Antenna

Figure 3-11 shows how the antenna correlation varies with dipole separation for the parasitic dipole when:

1. Shorted;

2. Terminated with a 71Ω resistance (this resistance would match an isolated dipole); and

3. Terminated with a 1MΩ resistance (this is effectively an open circuit).

The 1MΩ curve is very similar to the autocorrelation of the E_z field component, that is the classical J_0^2 Bessel function as determined by Clarke's model [1]. This is because the parasitic antenna is effectively open circuit and therefore prevented from resonating. The correlation calculated between the driven antenna and the non-resonating parasitic antenna is the autocorrelation of the E_z field component.

With the parasitic dipole in terminated 71Ω, the correlation is generally much lower. For d>0.1λ, this suggests that the coupling between the driven and parasitic antennas is strong and results in an asymmetric radiation pattern. As the direction of the asymmetric pattern varies according to which antenna is driven the antenna correlation is much lower.

When the parasitic dipole is short circuited, the correlation is generally higher than when terminated in a resistance of 71Ω and therefore suggests that it is not appropriately terminated. It does not therefore couple as strongly and the pattern is less directional. An exception to this occurs at around d=0.05λ. Here the dipoles are so close that the actual matching termination value of the parasitic antenna is very different to the 71Ω isolated d >> 1λ limit. The parasitic antenna couples strongly and the whole arrangement is superdirective. Unfortunately, the finite loss resistance of a practical antenna would reduce the radiation efficiency and therefore this arrangement is not of practical use [3, p455]. This is described in more detail in Section 3.3.6.4.

It should be noted that the two dimensional field autocorrelation model presented by Clarke [1] and Aulin's modified version of it [2]—neither of which consider the effect that a probe detecting a field has upon the field itself—are unsuited for the purpose of antenna correlation analysis when sub-wavelength antenna separations are employed except when the parasitic antenna is terminated in such high values of resistance as to make it superfluous.

In addition to the 0, 71 and 1000000Ω terminations, a variety of other termination values were investigated. The results for these are summarised in Fig. 3-12.

3.3.4 Complex Impedance Terminations to the Parasitic Antenna

The antenna correlation and radiation efficiency were calculated using combinations of:

1. $d = 0.01$ to 1.0λ in 0.01λ steps; and

2. Approximately logarithmically distributed values of R and X (the termination of the parasitic dipole $Z = R + jX$) as listed below:

   - R = 0, 1.0, 2.15, 4.65, 10.0, 21.5, 46.5, 71.0, 100.0Ω

   - X = -500, -100, -50, -10, -5, 0, 1, 5, 10, 50, 100, 500Ω

This gave 11,700 values of antenna correlation and radiation efficiency. To display these results, efficiency and correlation was plotted against R and X for a number of values of dipole separation distance d. Figures 3-13 to 3-18 show these:

- Plots of efficiency against R and X are shown in Figs. 3-13 and 3-14.

- Plots of correlation against R and X are shown in Figs. 3-15 and 3-16.

- The efficiency and correlation verses R and X data is plotted together in the surface plots shown in Figs. 3-17 and 3-18 where the efficiency is represented by the height of the surface and the correlation is represented by the colour of the surface.

The reader may either use Figs. 3-13 to 3-16 or Figs. 3-17 and 3-18.

At the extreme values of X, the parasitic dipole is effectively so decoupled that it does not resonate—but, more importantly, the current induced in it is very small. Therefore each fed dipole radiates effectively in isolation. This keeps the radiation efficiency high because, essentially, only the driven antenna is in circuit. As the radiation pattern of an isolated dipole is omnidirectional in the azimuth plane, the correlation is very high for small separations. However, for $d>0.2\lambda$, the individually radiating dipoles are separated sufficiently for the spatial diversity effect to ensure that the correlation is kept low, regardless of the loading employed.

At very small separations, (and when X is not at an extreme), the radiation efficiency is reduced. This is due to the currents in the parasitic antenna travelling out of phase with the currents in the driven antenna. The broadside radiation is reduced because the two dipoles are acting like the twin wires of a balanced line. The radiation is particularly suppressed for X=10Ω. Here the parasitic antenna is close to resonance and so has the maximum current flowing which balances out more of the radiation contribution of the current flowing on the driven antenna.

At $d \sim 0.03\lambda$ to 0.04λ, the correlation is lower at the region of low radiation efficiency than elsewhere. This is because of the twin dipoles acting in a superdirective manner as explained in Section 3.3.3 [3, p455] [12]. For $d \sim 0.03\lambda$ to 0.08λ, the reactance at which the twin dipoles become superdirective drops with increasing separation, so that at for instance, d=0.05λ, the superdirective condition is X~0Ω, which is the situation described in Section 3.3.3.

Above $d \sim 0.20\lambda$, the antennas are so well separated that:

- Spatial diversity ensures that the correlation is low regardless of the parasitic antenna's termination.
- Any current on the parasitic antenna is so far away from the current on the driven antenna that it cannot cancel out its radiation. Therefore the twin dipoles radiate well regardless of whether the parasitic antenna is resonating and the radiation efficiency is always high.

3.3.5 Matching the Parasitic Dipole

The value of complex matching termination for the parasitic dipole for varying dipole separation was determined using the method described in Section 3.2.4. In this case, the input impedance of the fed dipole equals the termination of the parasitic dipole, and is shown in Fig. 3-19.

Figure 3-20 shows the efficiency and the correlation achieved. The correlation is low almost everywhere. It only approaches 1 for very small antenna separations, and there the radiation efficiency is not high enough for practical configurations.

3.3.6 Radiation Patterns and Antenna Correlation Integrand Plots

To investigate the characteristics of certain antenna configurations further, radiation patterns and antenna correlation integrand plots were produced. The application of these visualization methods to antenna correlation analysis and the formula used for generating a correlation integrand plot is given in Section 3.3.6.1.

The specific antenna configurations investigated include: examples of high correlation (Section 3.3.6.2); wide antenna spacing (Section 3.3.6.3); superdirectivity (Section 3.3.6.4); and the effects of azimuth and elevation coverage restrictions (Section 3.3.6.5).

3.3.6.1 What is plotted

In this section radiation patterns are reviewed and a new concept of antenna correlation integrand plots is introduced. It is shown that radiation patterns of the two antenna configurations[7] together with the antenna correlation integrand plot, display the integrands of the three integrations in the antenna correlation formula eqn. (3-1).

3.3.6.1.1 Radiation patterns

Radiation patterns are plots of the power radiated from a transmitting antenna arrangement. The power radiated *in a given direction* $\Omega = (\theta, \phi)$, *is given by:*

$$P(\Omega) = E_\theta(\Omega)E_\theta^*(\Omega) + E_\phi(\Omega)E_\phi^*(\Omega) \qquad (3\text{-}19)$$

Note that eqn. (3-19) is similar to the integrands in the denominator of the antenna correlation formula of eqn. (3-1) with $P_\theta, P_\phi = 1$. In practice P_θ, P_ϕ is taken to be 1 over much of the range of $\Omega=(\theta, \phi)$. Therefore radiation patterns of 'dipole a' fed and 'dipole b' terminated with a load plot the integrand of $(E_{1\theta}E_{1\theta}^* + E_{1\phi}E_{1\phi}^*)$, and radiation patterns of 'dipole b' fed and 'dipole a' terminated with a load plot the integrand of $(E_{2\theta}E_{2\theta}^* + E_{2\phi}E_{2\phi}^*)$.

The radiation patterns in this chapter have been normalized so that:

$$\iint_\Omega P(\Omega)\, d\Omega = 4\pi \qquad (3\text{-}20)$$

With this normalization, if $P(\Omega) = 1$, then the power radiated in the Ω direction is the same as would be radiated from an isotropic antenna. So P represents the directivity relative to an isotropic antenna.

The radiation patterns have been shaded to show the phase of the electric far field on the surface of a sphere[8] which is centred at the origin of the coordinate system. The radius of the

[7] See Section 3.2.1 for the antenna configuration description.
[8] Often called the radiation sphere.

sphere, and hence the absolute value of the phase, is unimportant. What is important is the relative value of the phase across the surface of the sphere.

3.3.6.1.2 Antenna correlation integrand plots

Antenna correlation integrand plots are plots of the integrand in the numerator of the formula for antenna correlation (see eqn. (3-1)). The integrand is given by:

$$intgrnd = c_n(E_{1\theta}E_{2\theta}^{*}P_{\theta} + E_{1\phi}E_{2\phi}^{*}P_{\phi})e^{jk\mathbf{d}\bullet\mathbf{a}_r} \qquad (3\text{-}21)$$

where c_n is a normalization constant. The normalization constant for the plots in this chapter is set by demanding that:

$$\iint_{\Omega} |intgrnd| \, d\Omega = 4\pi \qquad (3\text{-}22)$$

Substituting this requirement into eqn. (3-21) gives:

$$c_n = \frac{4\pi}{\iint_{\Omega} \left| E_{1\theta}E_{2\theta}^{*}P_{\theta} + E_{1\phi}E_{2\phi}^{*}P_{\phi} \right| \, d\Omega} \qquad (3\text{-}23)$$

The antenna correlation integrand plots are similar to radiation plots, in that the integrand is a function of the (θ,ϕ) angle, and the magnitude of the integrand is represented by the distance from an origin. The phase of the integrand can be represented by shading the plot surface.

If $intgrnd(\theta,\phi)$ does not vary greatly, and its phase component is substantially in phase everywhere, then its average magnitude is approximately 1. However, if $intgrnd(\theta,\phi)$ cancels out substantially, its magnitudes are >>1. The amount of phase cancellation in the correlation integral is thus proportional to $|intgrnd|$. Examples of this are discussed below.

3.3.6.2 A high correlation example

An example of high correlation is with the antenna spacing d=0.01λ, and with a 100Ω resistance on the unfed antenna termination (Z=100Ω). Figure 3-22 shows the radiation patterns for when 'antenna a' is fed and 'antenna b' is terminated with 100Ω, when 'antenna b' is fed and 'antenna a' is terminated with 100Ω, and the correlation integrand plot. The radiation patterns are substantially doughnut shaped, with relatively uniform phases of approximately 180 degrees; that is, the phase fronts of the radiated waves are almost

spherical. The two radiation patterns give a doughnut shaped uniform phase correlation integrand plot. The uniform phase correlation integrand adds up to give a high value (~1) for the correlation.

Figure 3-21 shows the radiation patterns and correlation integrand plot when the 100Ω termination is replaced by a short circuit. The two radiation patterns have been distorted. However, the radiation field distortions are in opposite directions, and so the correlation integrand is still almost symmetrical and doughnut shaped. The radiation patterns retain uniform phase, and the correlation integrand thus has almost constant phase. Therefore $|intgrnd|$ sums in phase to give ρ~1.

3.3.6.3 An example of widely spaced antennas

As an example of widely spaced antennas consider d=1λ and Z=(100+j500)Ω. The radiation patterns and correlation integrand plot is shown in Fig. 3-28. The pattern for 'antenna a' fed is roughly doughnut shaped, with uniform phase. While the shape of the pattern for 'antenna b' fed is similar to that for 'antenna a' fed, its phase varies rapidly. This is because the phase centre is taken to lie at the centre of 'antenna a', while 'antenna b', which carries most of the current is 1λ away. This introduces a phase shift of $-2\pi d\sin(\theta)\cos(\phi)/\lambda$ for radiation due to currents flowing in 'antenna b' compared with radiation due to currents in 'antenna a'. The correlation integrand inherits this relative phase shift and there is substantial cancellation in the integration of the numerator of the antenna correlation formula. This is reflected in $|intgrnd|$ ~100 in the x-y plane.

Replacing the termination with a short circuit gives the patterns shown in Fig. 3-27. The passive antenna may now resonate creating a lobed radiation pattern. While the phase of the 'antenna a' fed radiation pattern is still fairly uniform, the phase of the 'antenna b' fed radiation pattern varies due to the displaced phase centre effect.

Figures 3-29 and 3-30 show the patterns for shorted passive antennas with d=2λ and d=5λ. With increasing separations, less current is excited into the passive antenna which results in less directional radiation patterns. However, the phase shift effect for the 'antenna b' fed pattern becomes more pronounced. Therefore there is even greater cancellation in the integration of the antenna correlation formula numerator, and $|intgrnd|$ becomes larger.

3.3.6.4 An example of superdirectivity

When d=0.05λ and Z=0Ω the antenna arrangement is superdirective. The radiation patterns and correlation integrand plots are shown in Fig. 3-23. The radiation patterns are directional with fairly uniform phase across the main lobes. Figure 3-24 shows a close up view of the back lobe of the radiation pattern when 'antenna a' is fed. The phase of the back lobe is also uniform, but 180 degrees different from the main lobe.

Combining the radiation patterns gives the correlation integrand shown. During integration the ±y directed lobes of the correlation integrand cancel with the ±x directed lobes to give a low correlation coefficient.

3.3.6.5 Varying the elevational and azimuthal coverage

The correlation integrand plots show why the correlation does not vary much with elevation coverage, but is very sensitive to azimuthal coverage (see Sections 3.3.1 and 3.3.2). For d<~1λ the phase of the correlation integrand depends only on the azimuthal angle ϕ, and the integrand's elevation dependency is $\sim\propto \sin^2(\theta)$. The radiation pattern plots show that this θ dependency is also true for the integrations in the denominator of eqn. (3-1). Therefore for d<~1λ, varying the elevation coverage does not change the final result of evaluating eqn. (3-1).

In cases where the radiation patterns and integrand varies with azimuthal angle ϕ, then varying the azimuthal coverage results in changes to ρ_a^2.

The d=2λ and d=5λ cases shown in Figs. 3-29 and 3-30 show significant variations in both the magnitude and phase of the integrand and radiation patterns with θ. Therefore for large spacings the elevation coverage does affect the antenna correlation.

3.3.7 Diversity Combination Methods

Figure 3-31 shows the contour plots of the diversity gain for selection diversity, equal gain and maximal ratio combining with the cumulative distribution function intersection finder set at 1% and 10% (see Section 3.2.3.1.1).

The six functions described in Fig. 3-31 could be applied to the twenty different plots shown in Figs. 3-17 and 3-18, to give 6x20=120 plots. However, most of these plots would not be

useful. The region of particular interest is where both the antenna correlation is small, and the radiation efficiency is large. Section 3.3.5 showed that a good rule of thumb for meeting these conditions was when the parasitic dipole port was matched. Figure 3-32 shows what happens when the data displayed in Fig. 3-20 is combined with the diversity gain functions plotted in Fig. 3-31. For all the cumulative distribution functions and combining schemes considered, positive diversity gain is evident for antenna spacings exceeding 0.03λ.

Figure 3-32 shows that for both cumulative distribution function levels, maximal ratio combining yields at least 0.6dB more diversity gain than equal gain combining, while equal gain combining yields at least 0.8dB more diversity gain than selection combining for all antenna separations greater than λ/10. For separations less than λ/10, the difference between the combining methods is small. For antenna spacings above 0.3λ, the improvement in diversity gain with increased antenna spacing is minimal.

3.3.8 Mutual Impedance

Antenna parameters are generally strongly inter-related. For example, the driving-point impedance of an antenna is a function of the currents that flow along it. Such antenna currents produce antenna radiation. The antenna driving-point impedance may therefore be viewed as an indication of the antenna's radiation performance.

The mutual impedance of a pair of antennas is a function of the antenna currents in both antennas and hence of their radiation patterns. To determine the accuracy of the antenna simulations in this chapter, the mutual impedance of side-by-side parallel antennas was calculated using eqn. (3-24) after Carter [13], where L is the length of the antennas, d is their separation and β is the phase constant. The antennas modelled by the following equation are infinitesimally thin.

$$Z_{21} = j30\int_0^L \left\{ \frac{\exp(-j\beta\sqrt{d^2+z^2})}{\sqrt{d^2+z^2}} + \frac{\exp[-j\beta\sqrt{d^2+(L-z)^2}]}{d^2+(L-z)^2} \right\} \sin(\beta z)\, dz \qquad (3\text{-}24)$$

The driving point impedance data computed using NEC was used in eqn. (3-18) to produce the computed mutual impedance, Z_m. This is plotted together with Z_{21} from eqn. (3-24) in Fig. 3-4. The displacement between the analytical and numerical values is due to the difference in thickness of the two sets of antennas. The general agreement suggests that the

values of antenna correlation based on the NEC generated current distributions, are accurate and reliable.

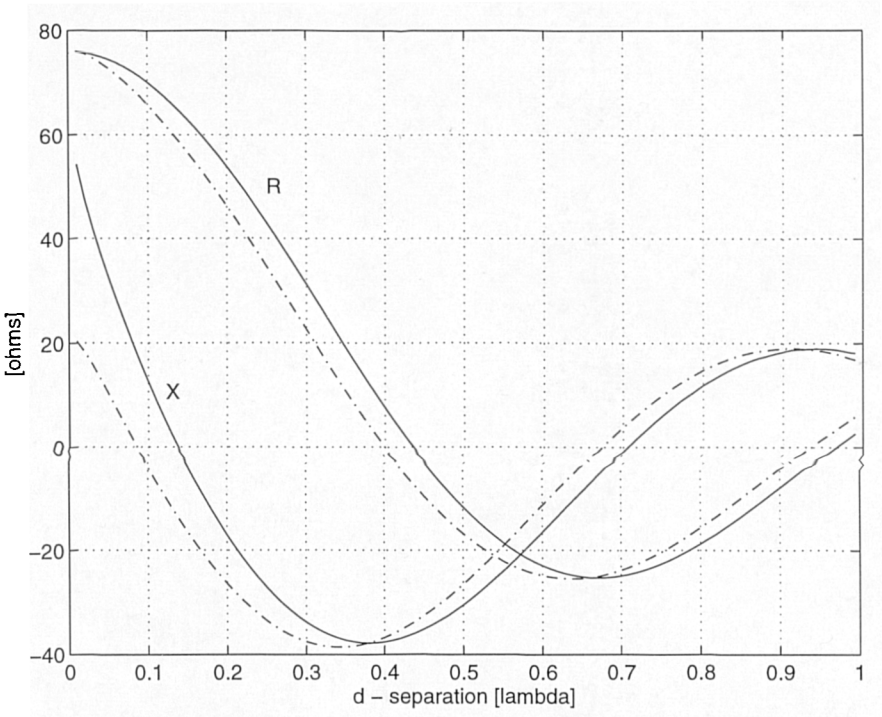

Figure 3-4: Curves of mutual resistance (R_m) and reactance (X_m) of two parallel side -by-side half-wave antennas as a function of the distance between them. The solid curves are for a theoretical infinitesimally thin antenna. The dashed curves are for the antenna used in the simulations with a length to diameter ratio of L/D=475.

3.4 Discussion

It has been shown that the far field radiation patterns of closely spaced antennas must be considered when calculating the cross-correlation between them. If the distribution of incoming waves is uniform in azimuth, then the correlation is affected only slightly when the distribution of elevational wave arrival is varied. However, varying the azimuthal distribution strongly affects correlation.

Significant decorrelation can be obtained by carefully selecting the value of termination resistance for the parasitic antenna. For close-in spacings this is achieved at the expense of reduced radiation efficiency. Using matched terminations for the parasitic antenna is usually a very good choice.

The effects of:

1. decorrelation;

2. any radiation efficiency reductions;

3. the signal selection or combination scheme used; and

4. the minimum acceptable signal to noise ratio

can be combined to give a figure of merit called *diversity gain.* This measures the performance improvement achievable using an antenna diversity scheme.

For all the signal selection and combining schemes investigated, there is an improvement in performance providing the antennas are spaced further than 0.03 wavelengths apart. Optimum performance gain (diversity gain) is approached for antenna spacings above 0.2 wavelengths. The performance gain approached is between 5dB and 7dB for signal to noise ratios measured at the 90% cumulative probability level, and between 10dB and 12dB for signal to noise ratios measured at the 99% cumulative probability level.[9]

[9]The x% cumulative probability level is the level which the signal to noise ratio exceeds for x% of the time.

3.5 References

1. CLARKE, R.H., 1968, "A Statistical Theory of Mobile-Radio Reception" Bell Sys. Tech. J, Vol. 47, No. 6, pp.957-1000.

2. AULIN, T., 1979, "A Modified Model for the Fading Signal at a Mobile Radio Channel" IEEE Trans. on Veh. Tech., Vol. VT-28, No. 3, pp182-203.

3. KRAUS, J.D., 1988, "Antennas", McGraw-Hill, Singapore (pages as listed in text).

4. PARSONS, J.D., and GARDINER, J.G., 1989, "Mobile Communication Systems", Blackie and Son Limited, (John Wiley & Sons Inc.), New York, USA, p196.

5. BRENNAN, D.G., 1959, "Linear Diversity Combining Techniques", Proc. IRE, 47, pp1075-1102.

6. MathWorks, 1991, "MATLAB: High Performance Numeric Computation Software", The MathWorks Inc., Massachusetts, USA.

7. JAKES, W.C., 1974, "Microwave Mobile Communications", IEEE Inc. (1993) New York, USA, p70.

8. BURKE, G.J., and POGGIO, A.J., 1981, "Numerical Electromagnetics Code Method of Moments", Tech. Doc. UCID-18834, Lawrence Livermore National Laboratory, California, USA.

9. MURRAY, K.P., 1993, "The Design of Antenna Systems on Complex Structures Using Characteristic Modes", Ph.D. Thesis, University of Liverpool, UK, pp7-37.

10. MASSEY, P.J., 1994, "Current based Antenna Radiation Computation and its application to Pager Antennas", Report No. 3465, Philips Research Laboratories, Redhill, UK.

11. WOLFRAM, S, 1991, "*Mathematica*: A System for Doing Mathematics by Computer", Addison-Wesley, Massachusetts, USA.

12. NEWMAN, E.H., RICHMOND, J.H., and WALTER, C.H., 1978, "Superdirective Receiving Arrays", IEEE Trans. on Ants. and Prop., Vol. AP-26, No. 5, pp629-635.

13. CARTER, P.S., 1932, "Circuit Relations in Radiating Systems and Applications to Antenna Problems", Proc. IRE, 20, pp1004-1041.

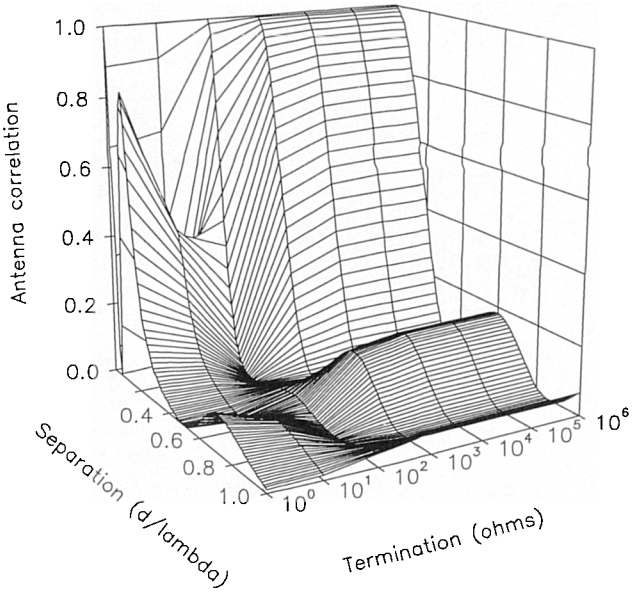

Figure 3-5: Antenna correlation as a function of antenna separation and termination resistance for incoming waves distributed uniformly from 0-360° in azimuth and at 90° in elevation.

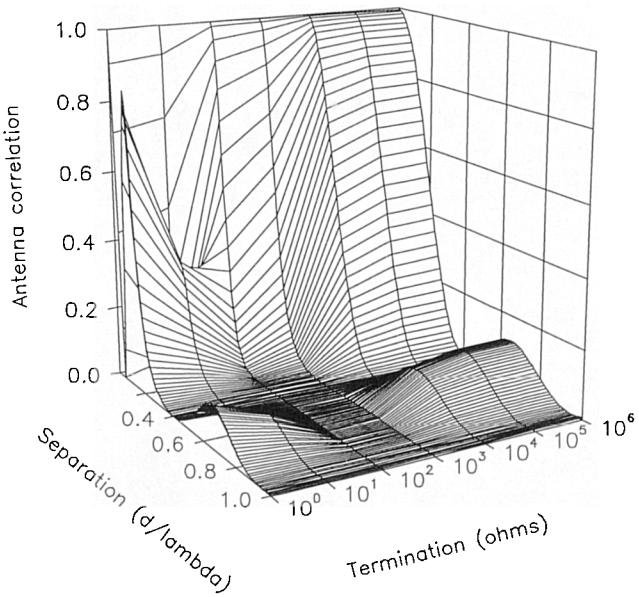

Figure 3-6: Antenna correlation as a function of antenna separation and termination resistance for incoming waves distributed uniformly from 0-360° in azimuth and from 0-180° in elevation.

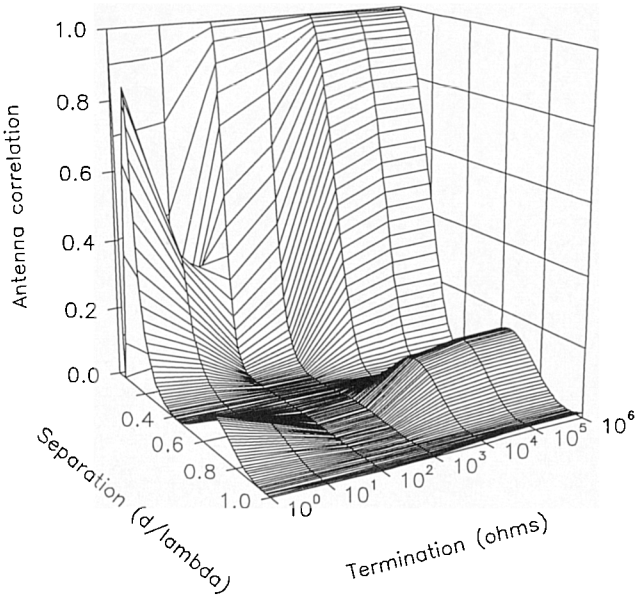

Figure 3-7: Antenna correlation as a function of antenna separation and termination resistance for incoming waves distributed uniformly from 0-360° in azimuth and from 45-90° in elevation.

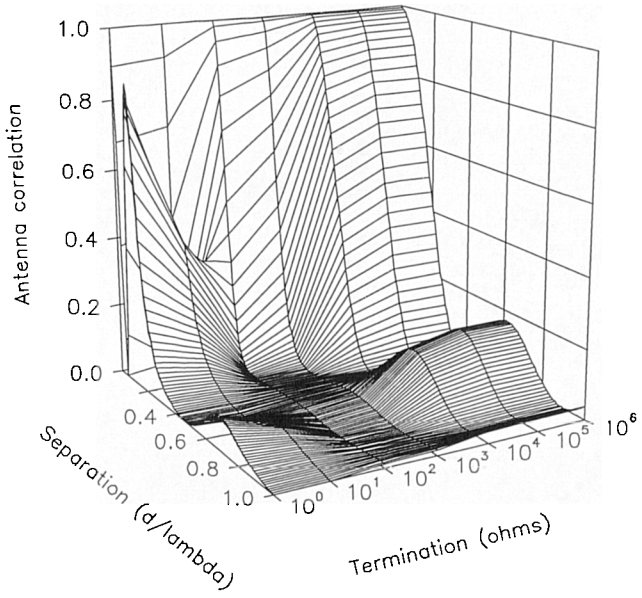

Figure 3-8: Antenna correlation as a function of antenna separation and termination resistance for incoming waves distributed uniformly from 0-360° in azimuth and from 65-115° in elevation.

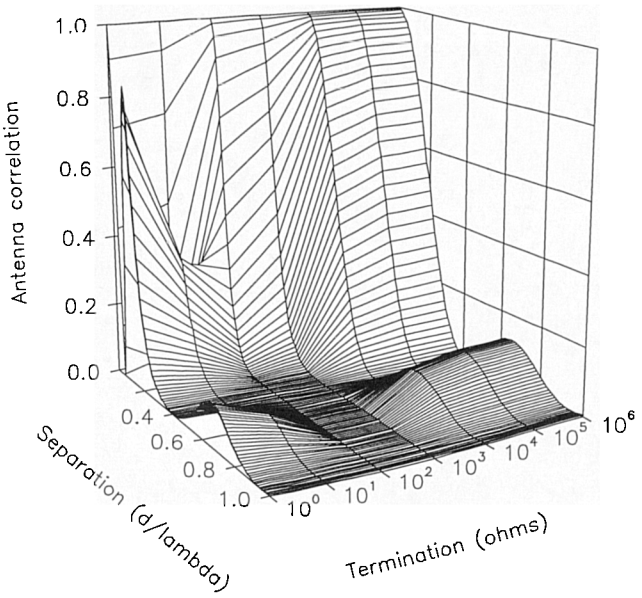

Figure 3-9: Antenna correlation as a function of antenna separation and termination resistance for incoming waves distributed uniformly from 0-180° in elevation and from 0-180° in azimuth.

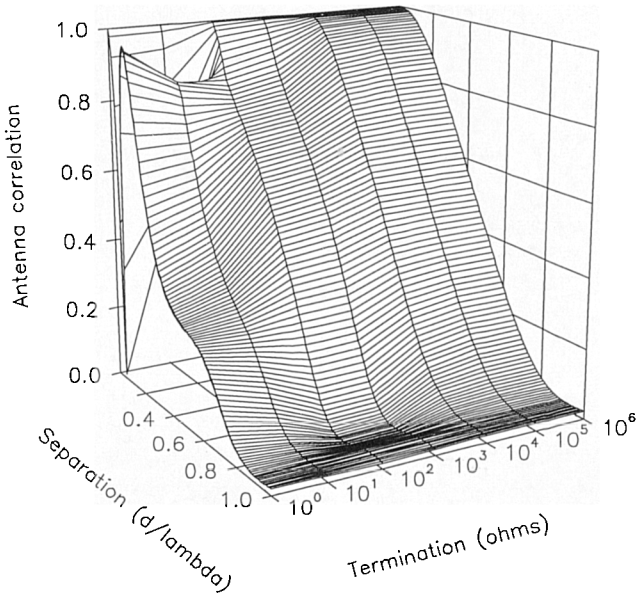

Figure 3-10: Antenna correlation as a function of antenna separation and termination resistance for incoming waves distributed uniformly from 0-180° in elevation and from 90-270° in azimuth.

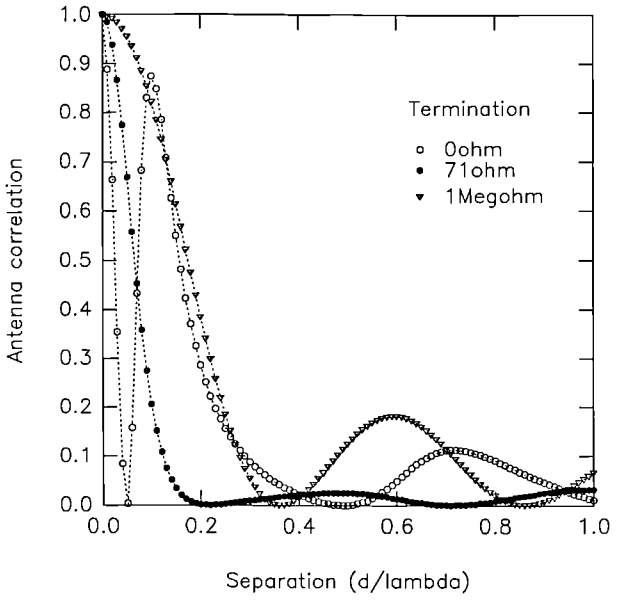

Figure 3-11: Antenna correlation as a function of antenna separation for three specific values of resistive termination. The incoming waves are uniformly distributed in spherical space.[11]

[11] Spherical space is used as shorthand to denote azimuth angles in the range of 0-360° and elevation angles in the range of 0-180°.

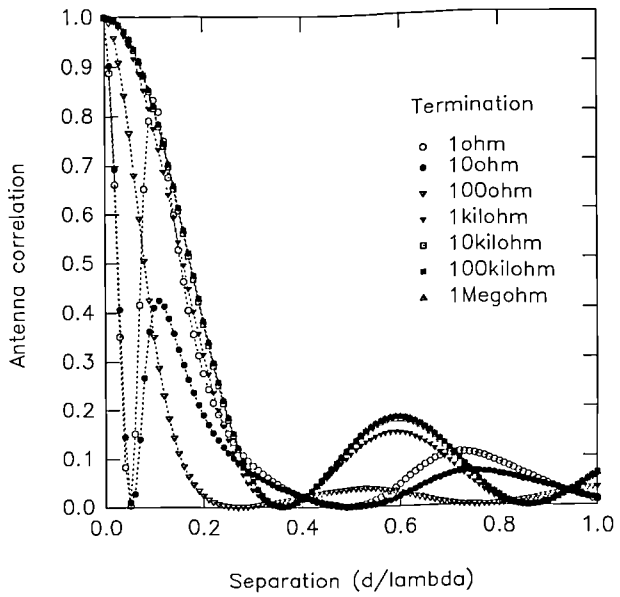

Figure 3-12a: Antenna correlation as a function of antenna separation for seven values of logarithmically spaced termination resistances. The incoming waves are uniformly distributed in spherical space.

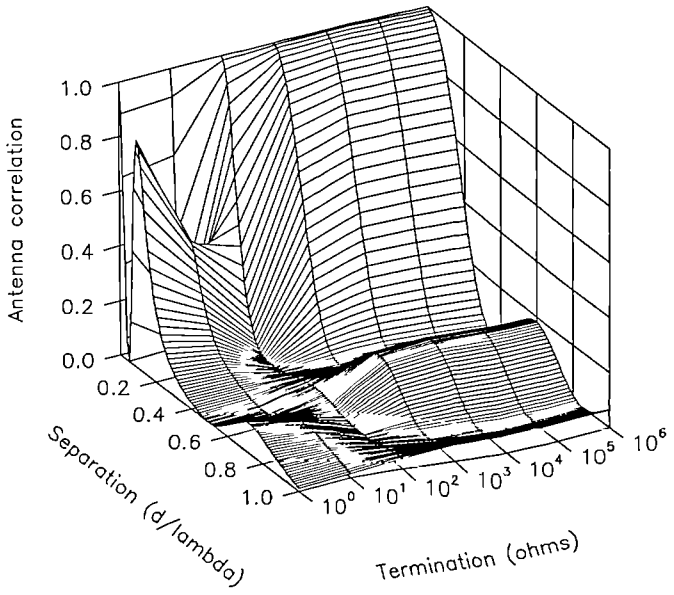

Figure 3-12b: As for Fig. 3-12a (surface plot).

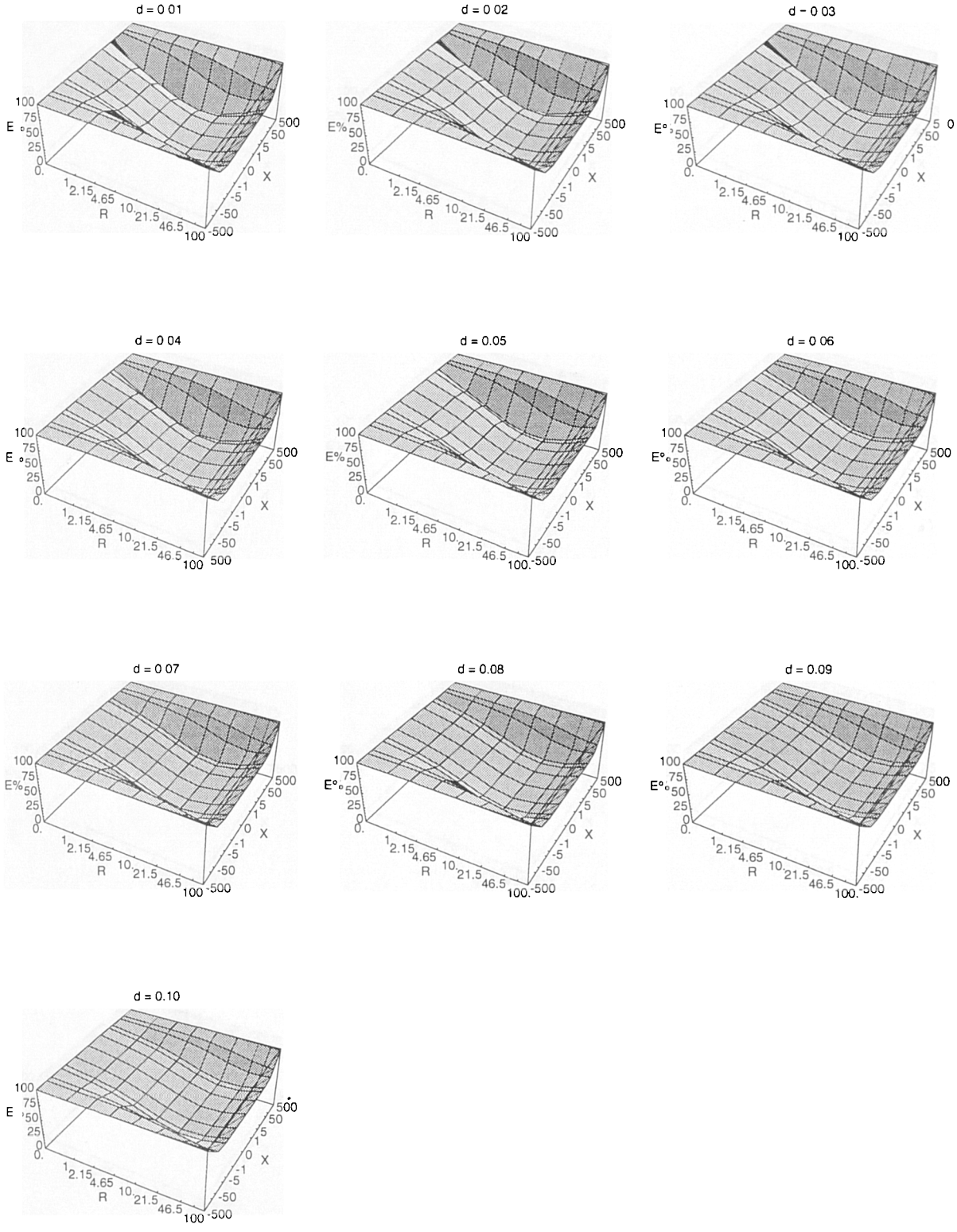

Figure 3-13: Radiation efficiency as a function of complex termination (R±jX) for antenna separations (d) in the range of 0.01 to 0.10λ.

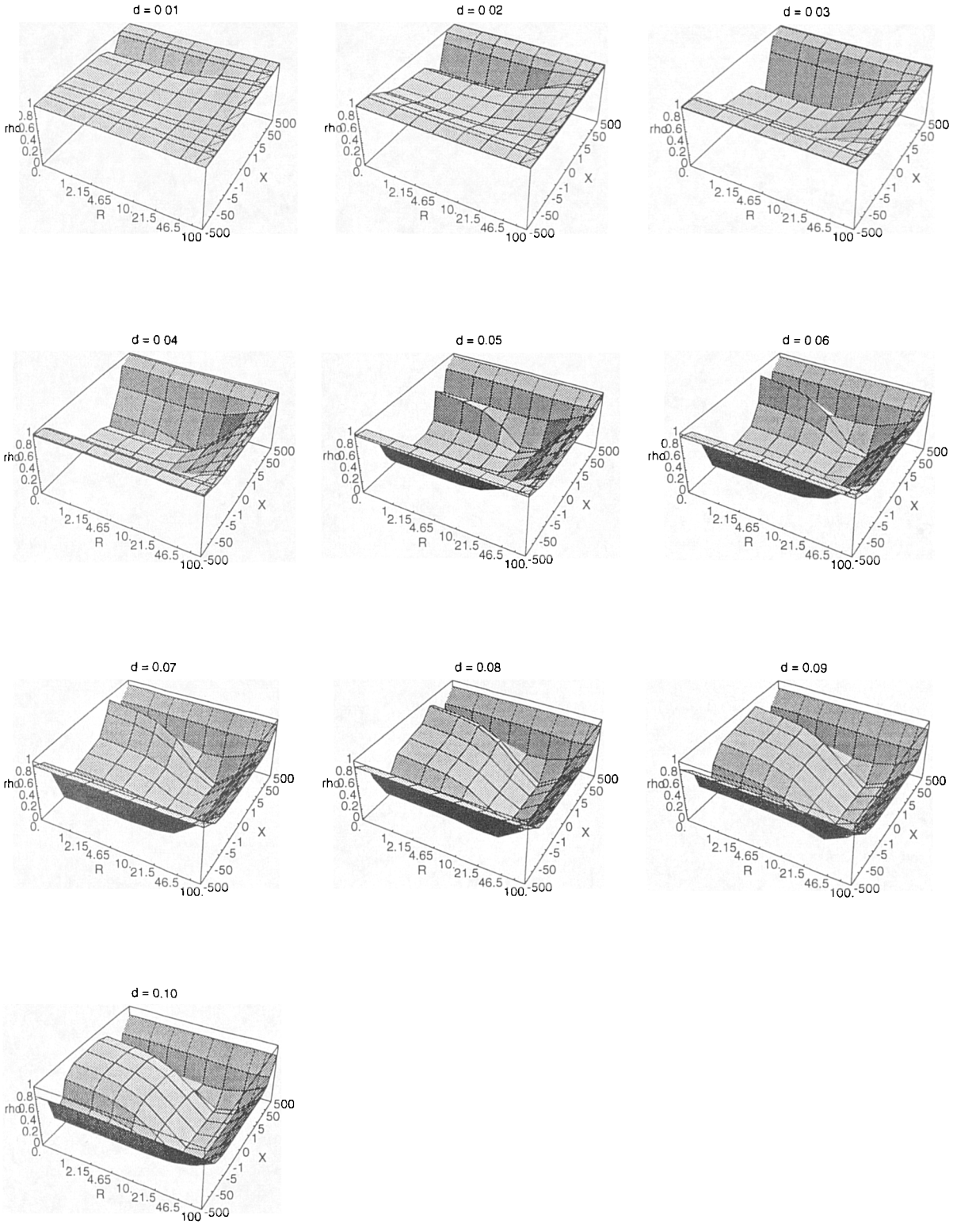

Figure 3 15: Antenna correlation as a function of complex termination (R±jX) for antenna separations (d) in the range of 0.01 to 0.10λ.

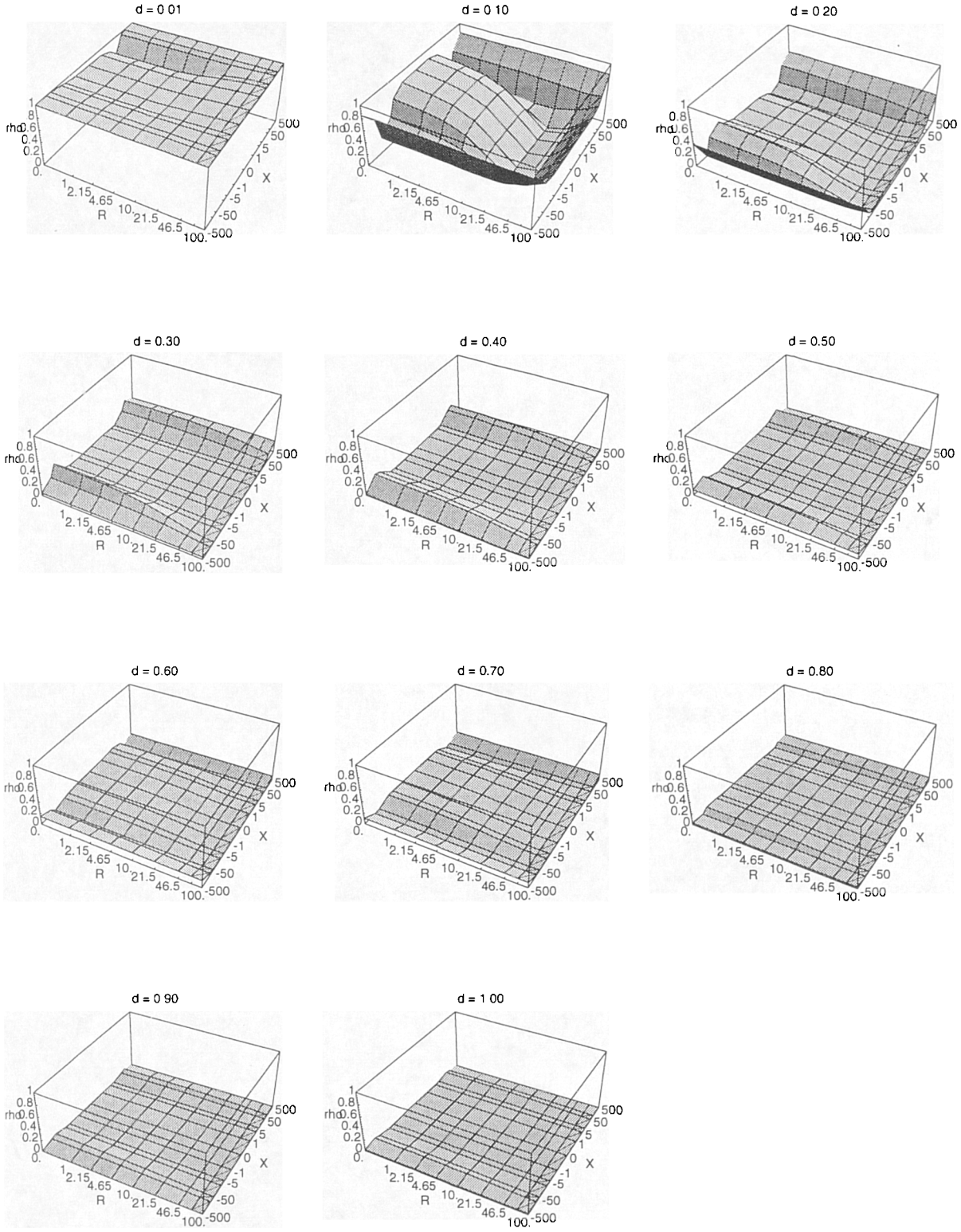

Figure 3-16: Antenna correlation as a function of complex termination (R±jX) for antenna separations (d) in the range of 0.01 to 1.00λ.

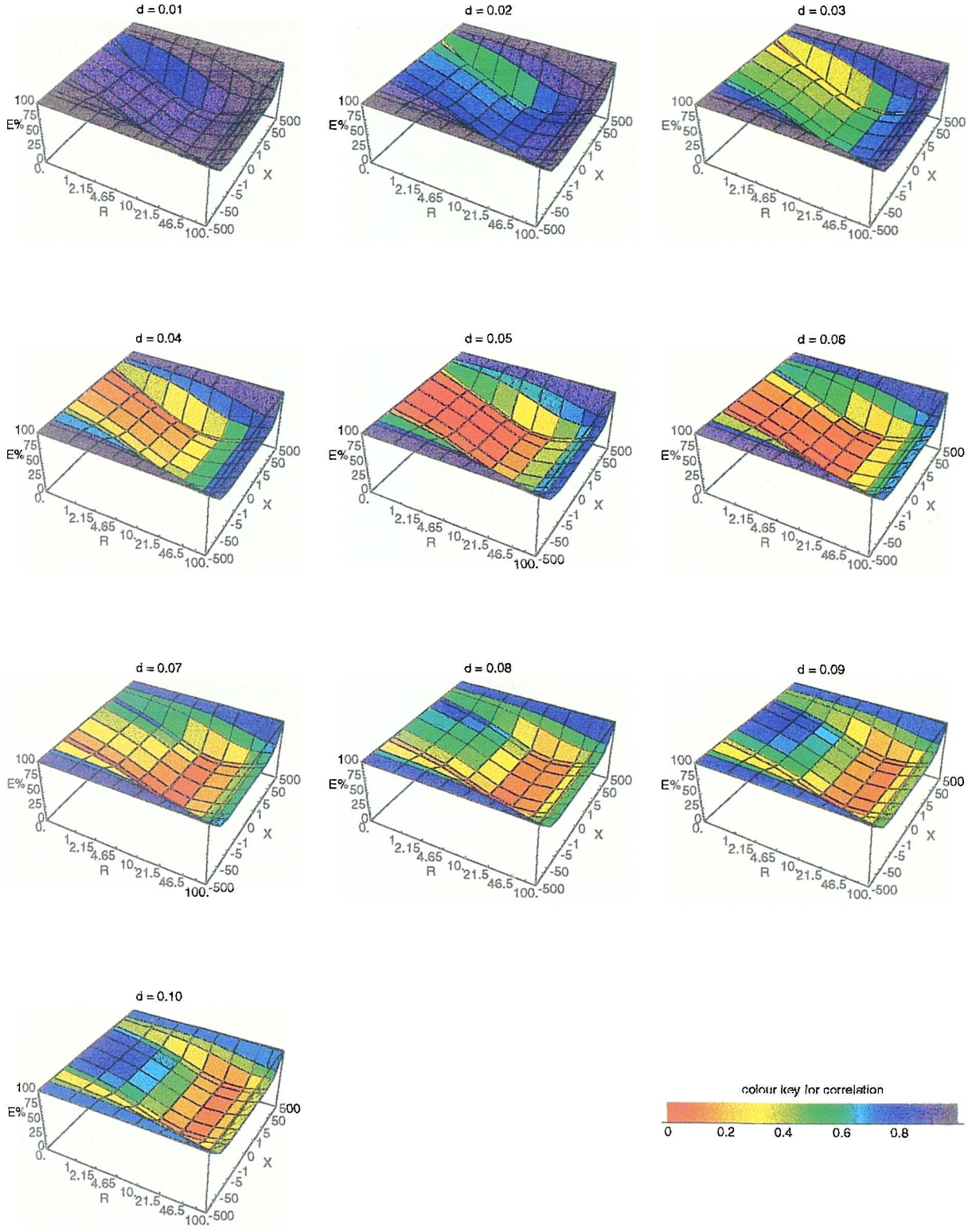

Figure 3-17: Radiation efficiency and antenna correlation as a function of complex termination (R±jX) for antenna separations (d) in the range of 0.01 to 0.10λ.

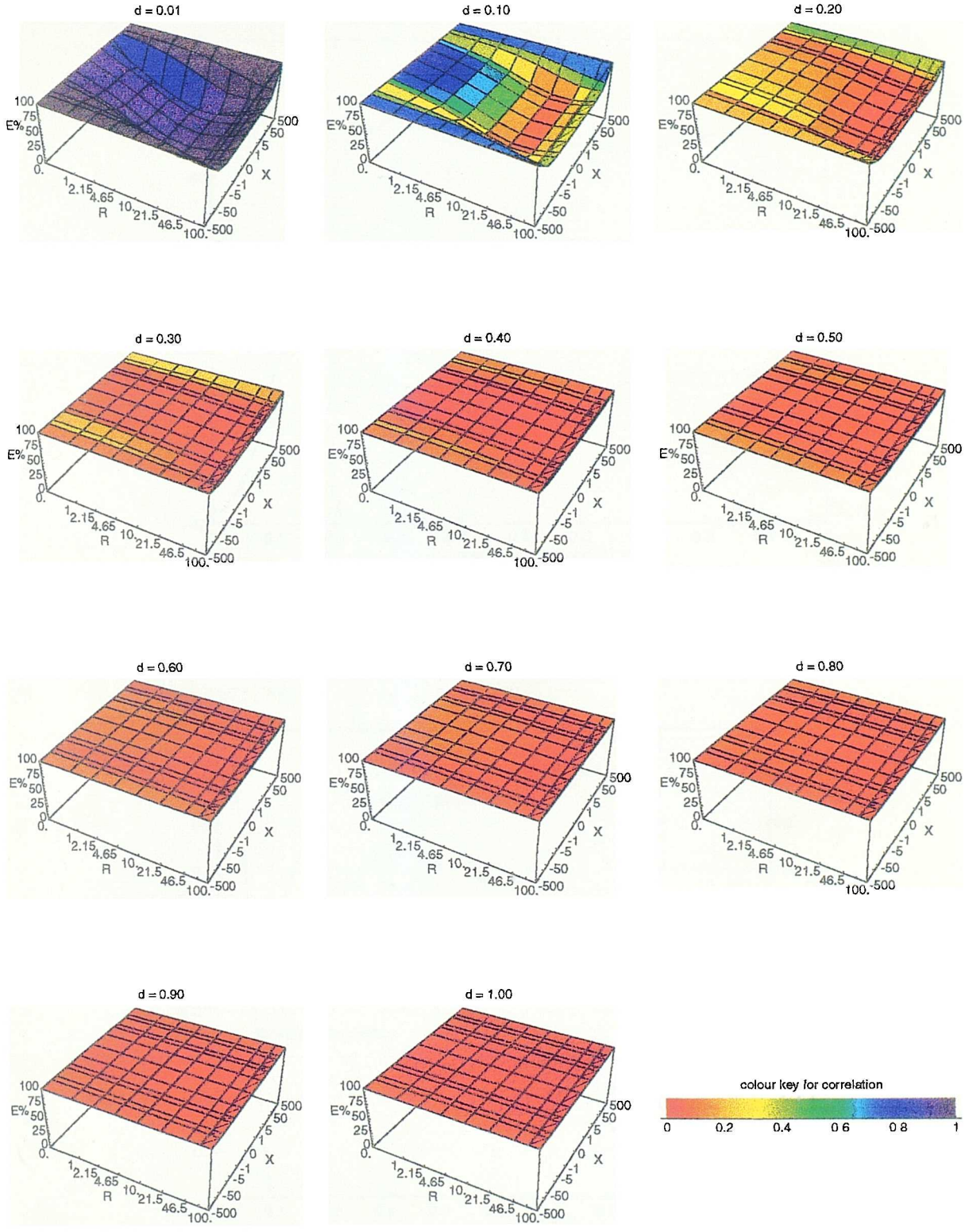

Figure 3-18: Radiation efficiency and antenna correlation as a function of complex termination (R±jX) for antenna separations (d) in the range of 0.01 to 1.00λ.

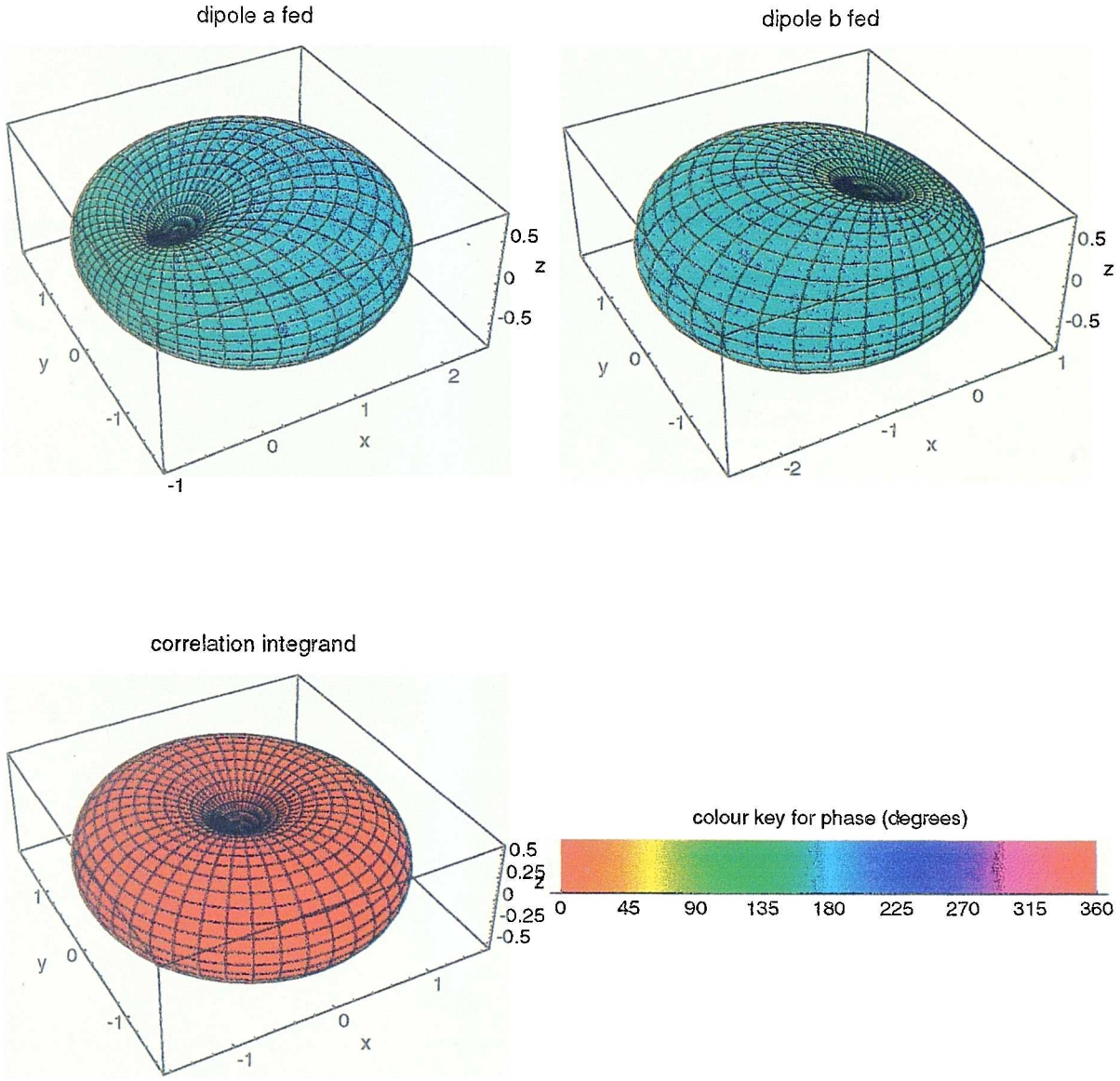

Figure 3-21: Antenna radiation patterns and antenna correlation integrand plot for d = 0.01λ and Z=0Ω.

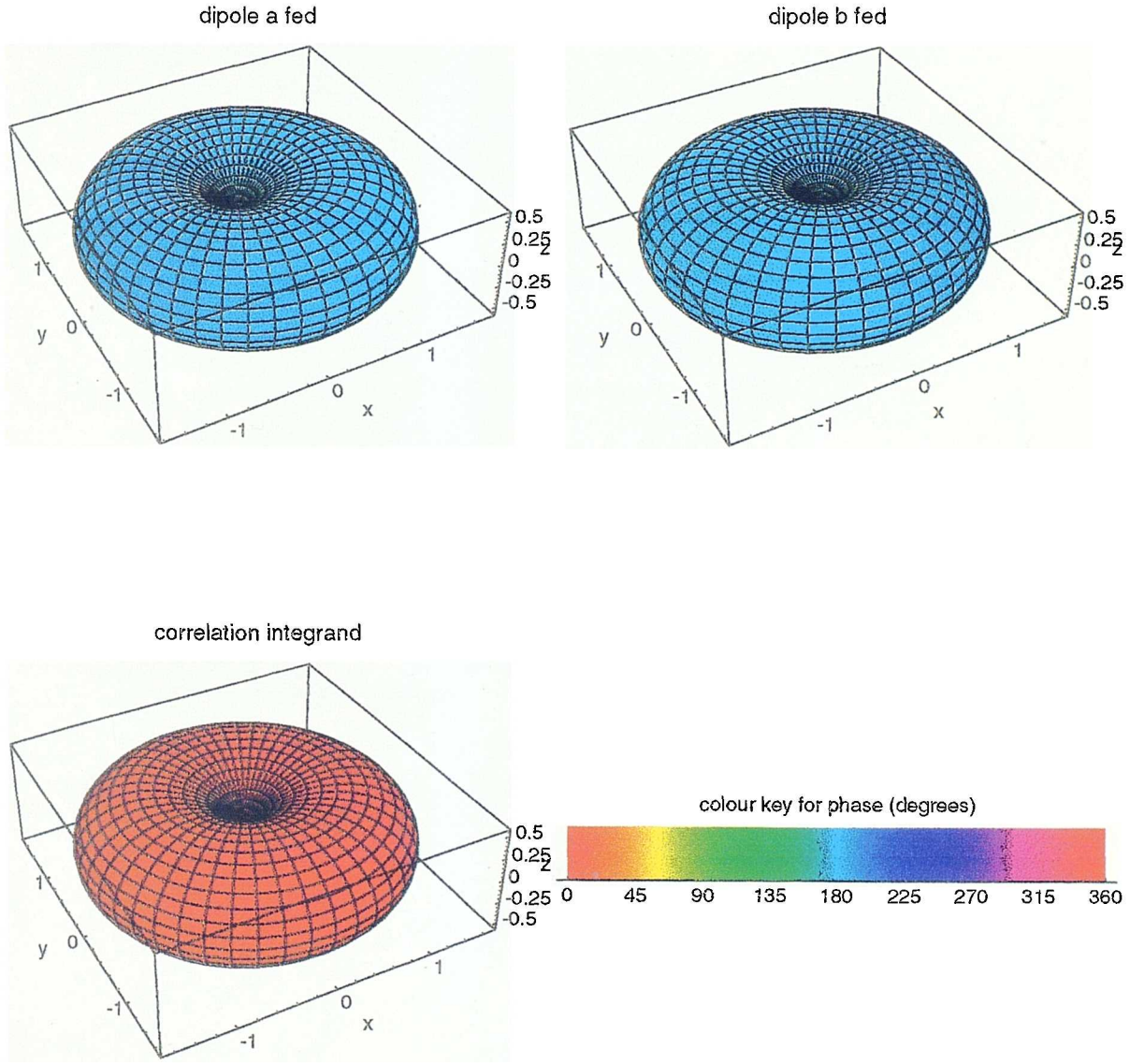

Figure 3-22: Antenna radiation patterns and antenna correlation integrand plot for d = 0.01λ and Z=100Ω.

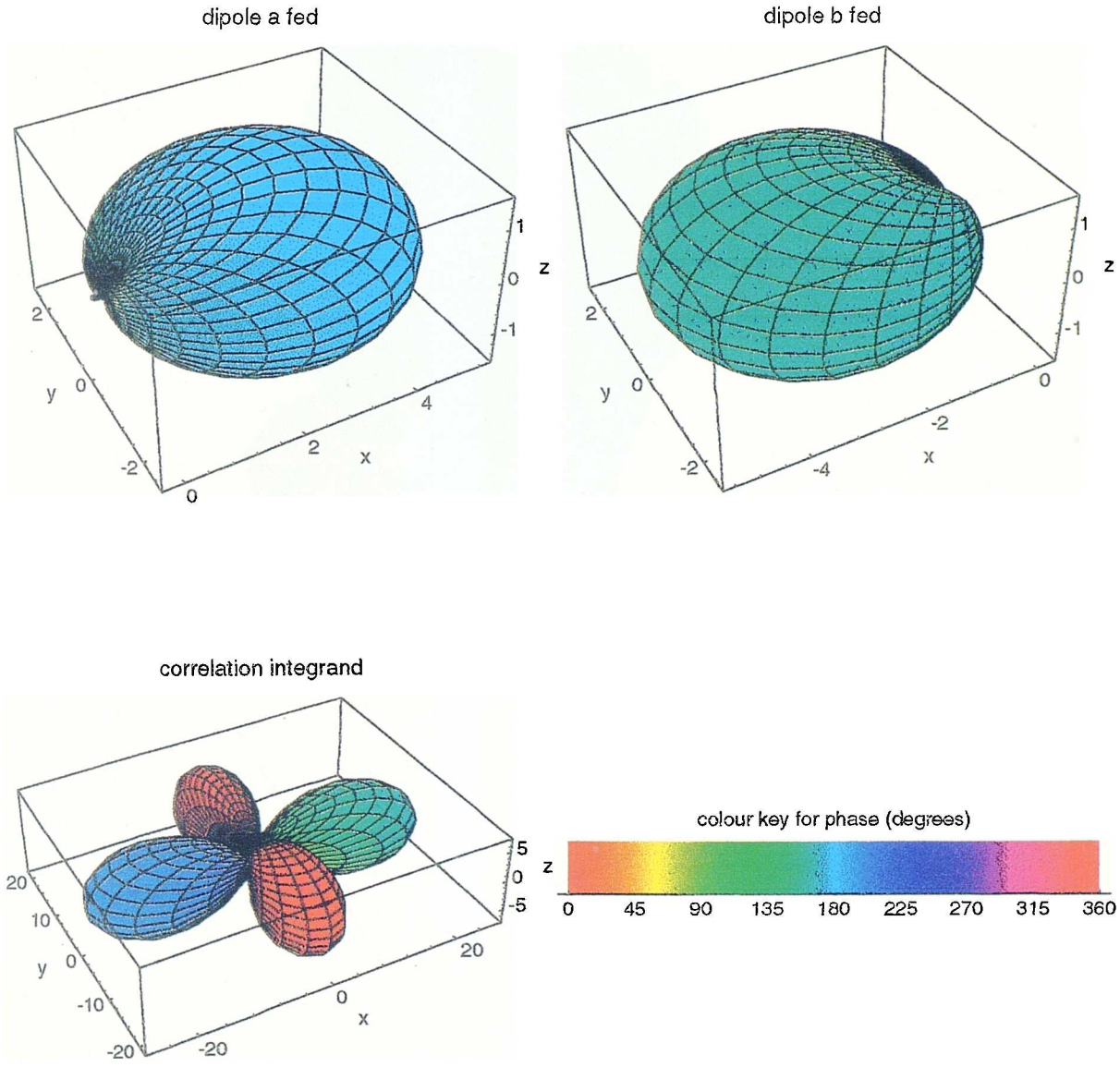

Figure 3-23: Antenna radiation patterns and antenna correlation integrand plot for d = 0.05λ and Z=0Ω.

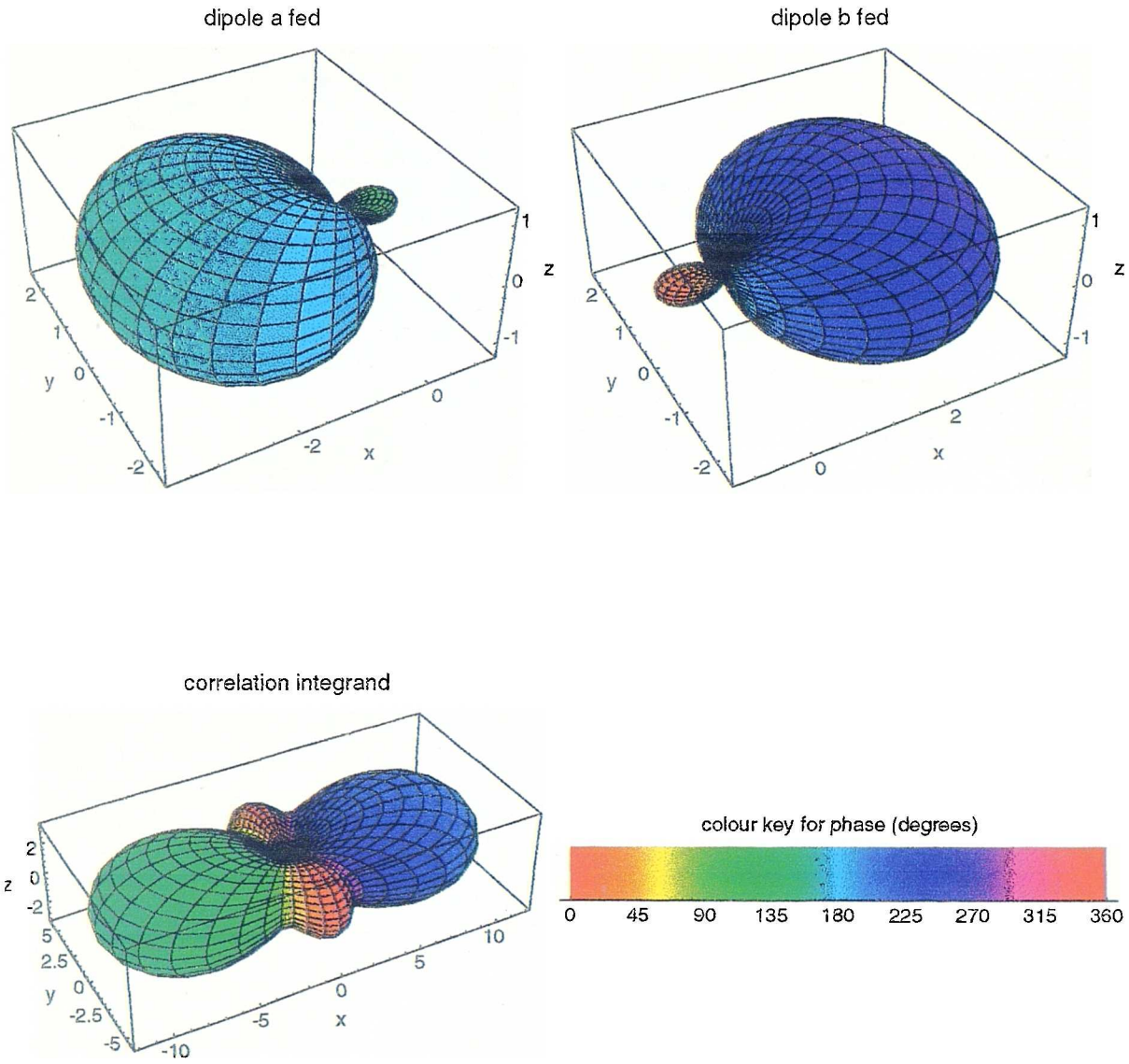

Figure 3-25: Antenna radiation patterns and antenna correlation integrand plot for d = 0.3λ and Z=0Ω.

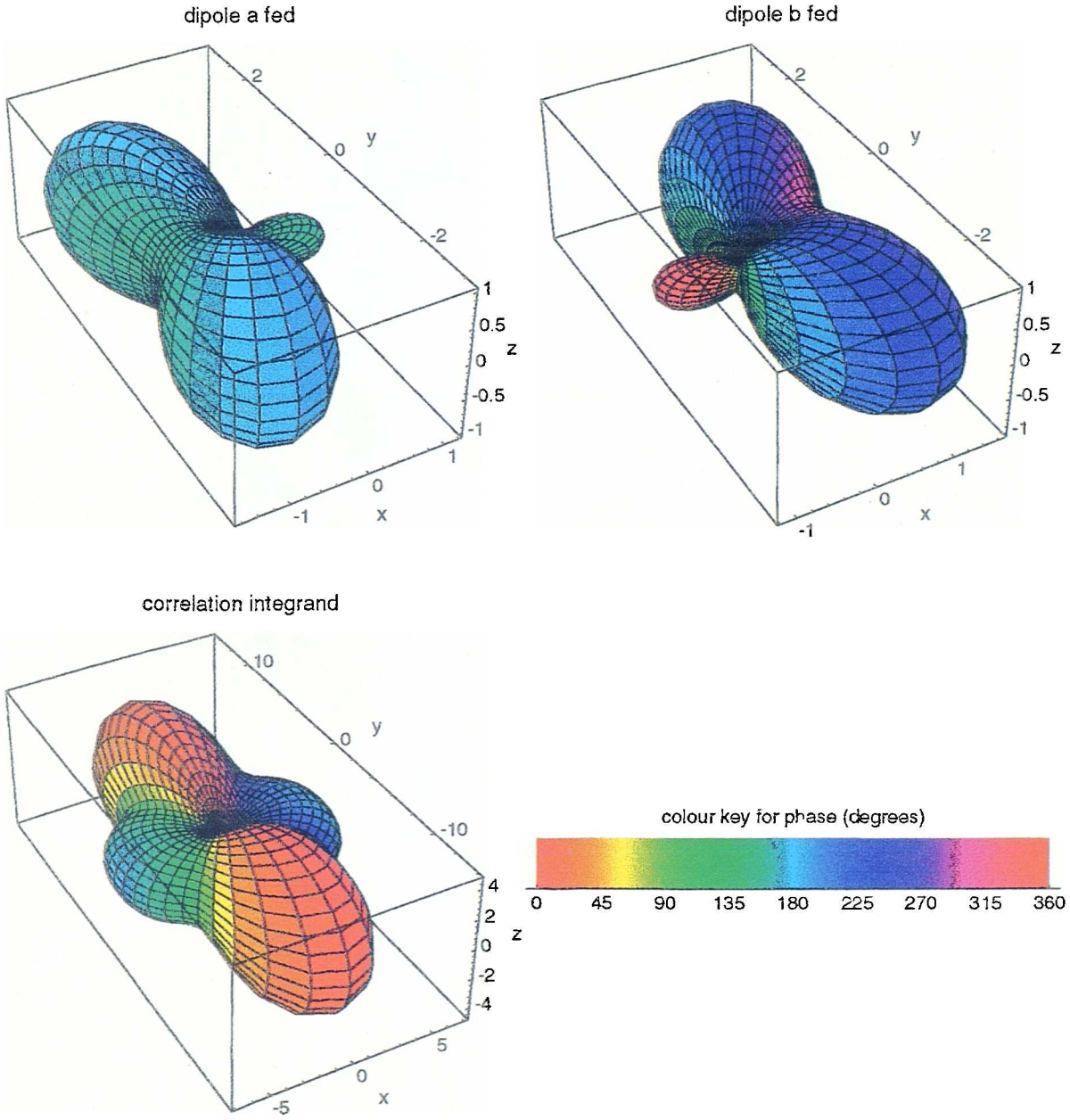

F'gure 3-26: Antenna rad ation patterns and antenna correlation integrand p ot for d = 0 5λ and Z=0Ω

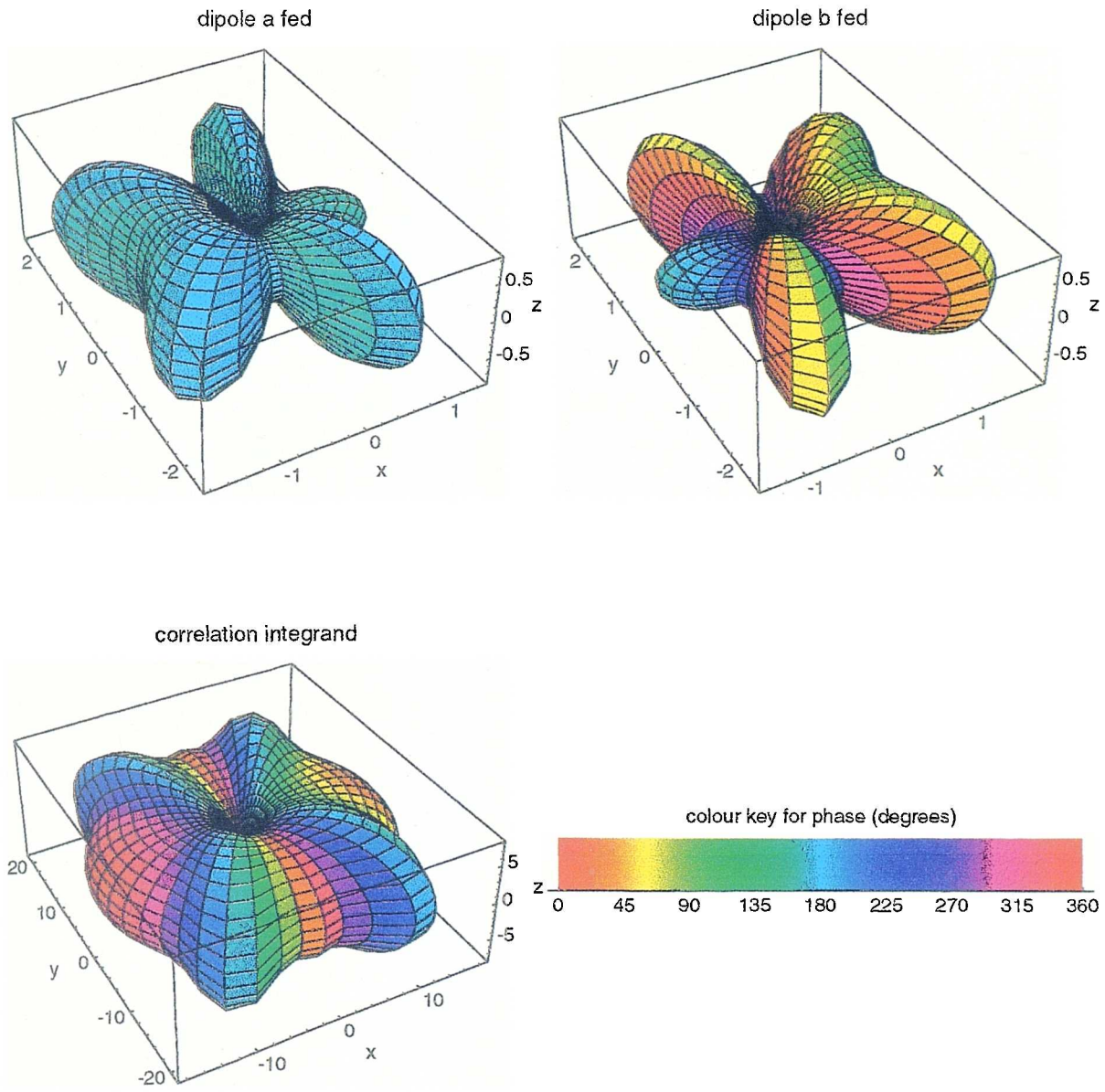

Figure 3-27: Antenna radiation patterns and antenna correlation integrand plot for d = 1.0λ and Z=0Ω.

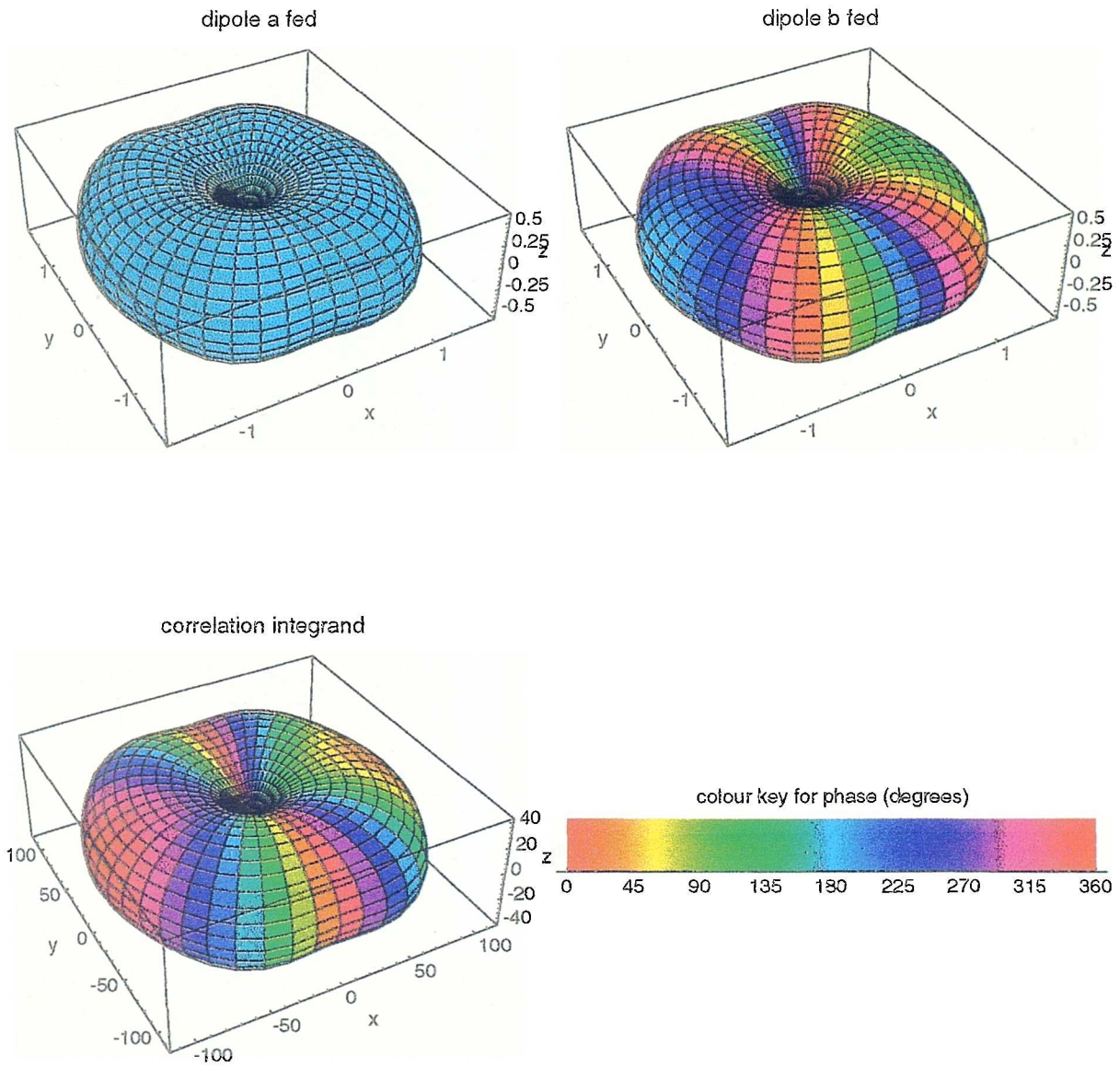

Figure 3-28: Antenna radiation patterns and antenna correlation integrand plot for d = 1.0λ and Z=(100+j500)Ω.

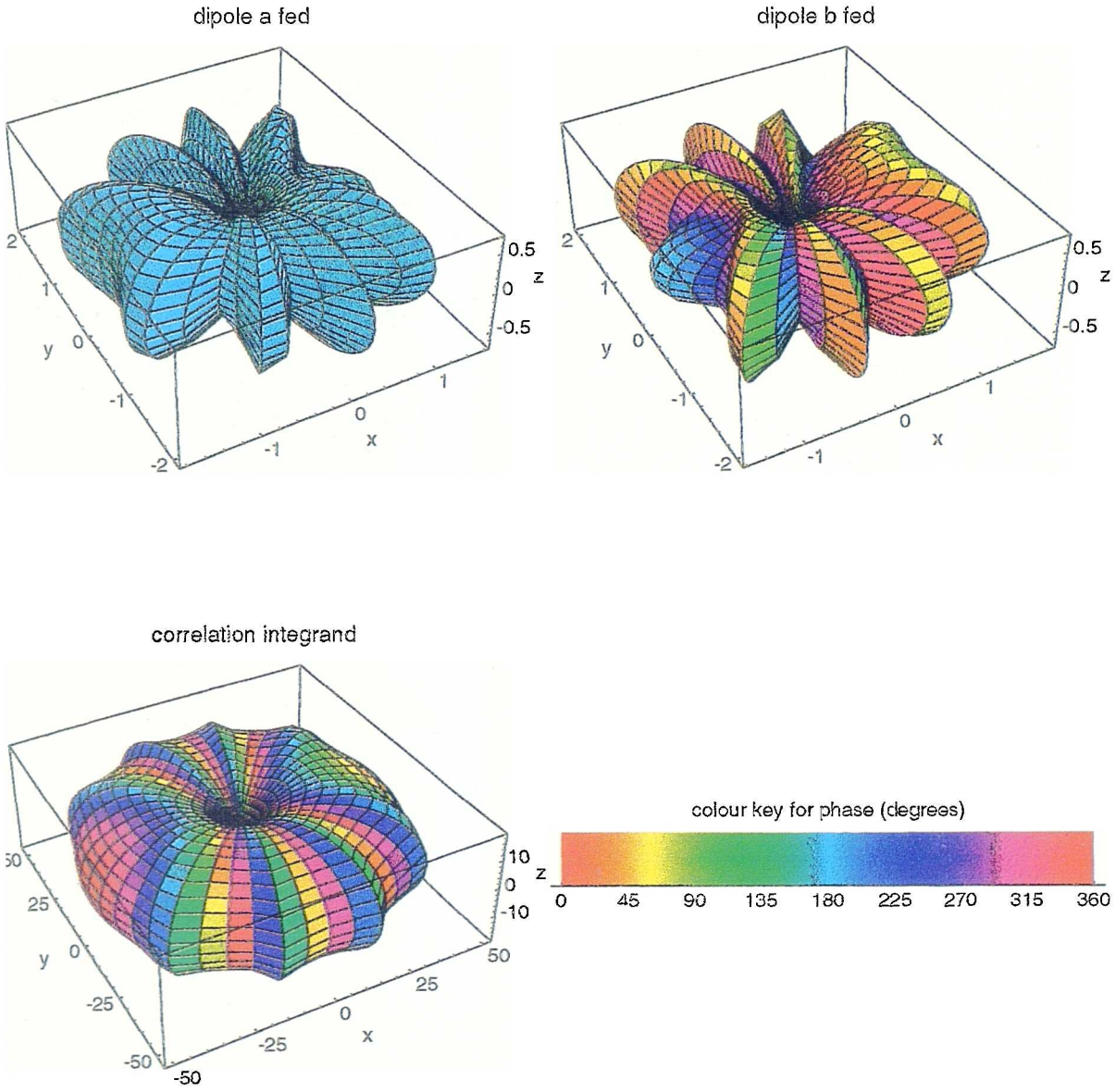

Figure 3-29 Antenna radiation patterns and antenna correlation integrand plot for d = 2.0λ and Z=0Ω.

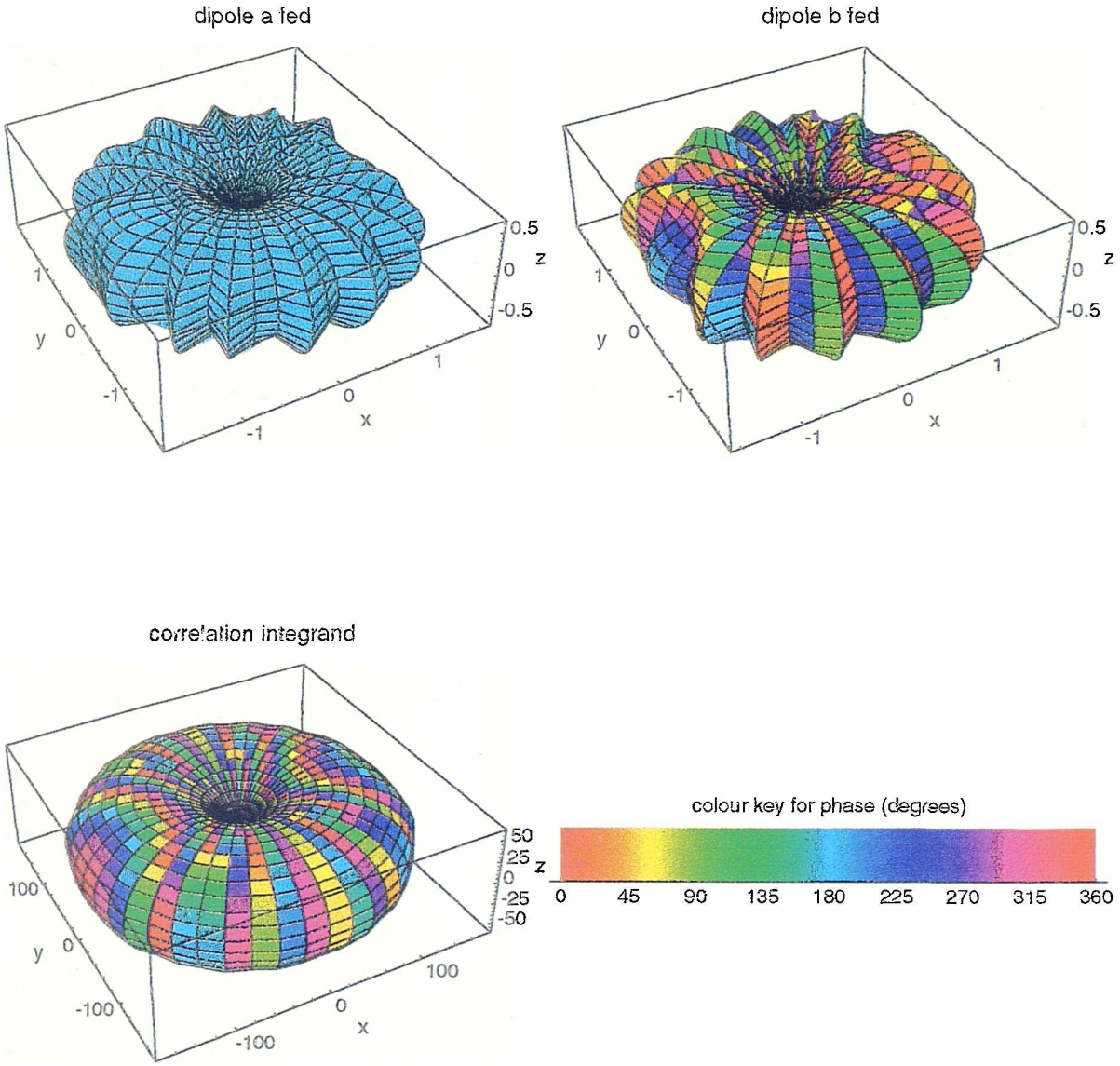

Figure 3-30: Antenna radiation patterns and antenna correlation integrand plot for d = 5.0λ and Z=0Ω.

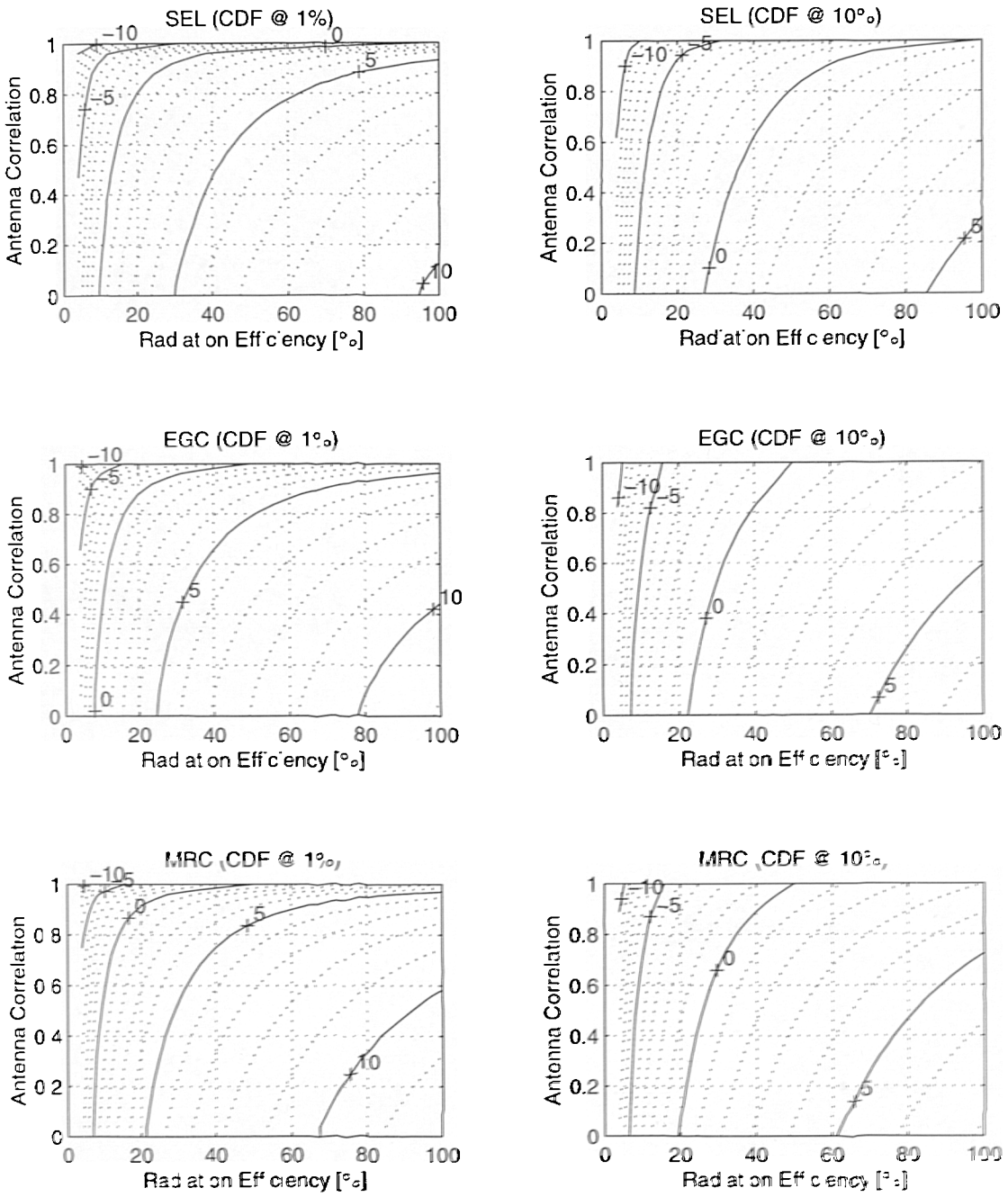

Figure 3-31: Contour plots of diversity gain (in dB) for selection diversity (SEL), equal gain combining (EGC) and maximal ratio combining (MRC) at the 1% and 10% cumulative distribution function levels

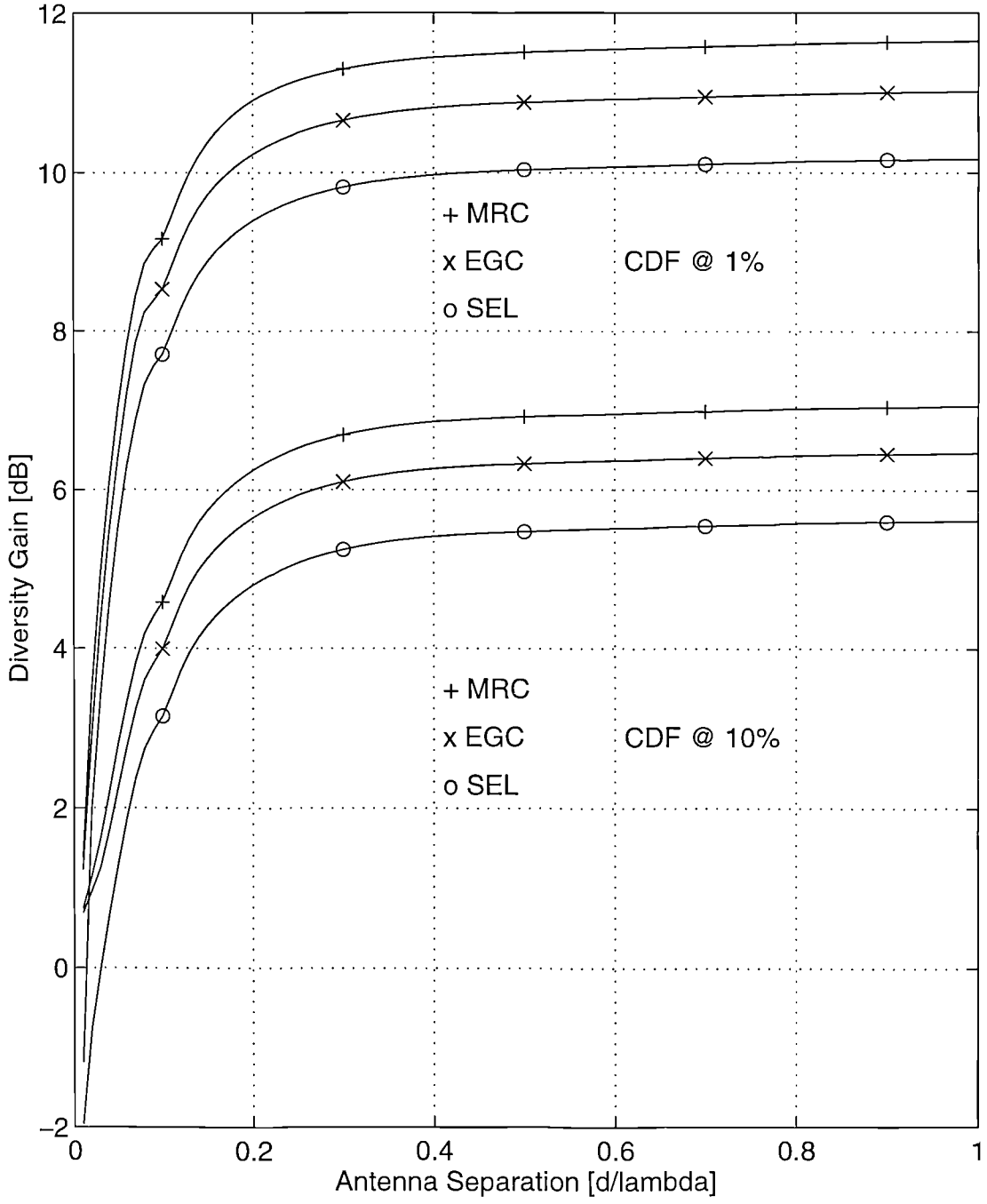

Figure 3-32: Diversity gain achievable using matched dipole terminations for selection diversity (SEL), equal gain combining (EGC) and maximal ratio combining (MRC) at the 1% and 10% cumulative distribution function levels.

4
Experimental Investigation Measurement Apparatus

4.1 Introduction

One of the methods that may be used to determine the complex cross-correlation between the signals produced by two receiving antennas and hence determine their correlation (that is the antenna correlation), is to transmit an unmodulated carrier wave from a base station location. The mobile equipment (Fig 4-1) is thus comprised of an experimental handset, a two-branch measuring receiver with complex or quadrature demodulation and a suitable data storage unit all of which are arranged to receive, measure and record the transmitted signal. The equipment is self contained, battery powered and fully portable. In the first section of this chapter, the requirements of this equipment are presented. The second section describes the construction and function of the various experimental handsets.

4.2 Antenna Correlation Measuring Receiver System

This section presents a simple antenna correlation measuring receiver system that is capable of measuring the complex cross-correlation of the signals produced by two receiving antennas connected to it. To measure complex correlation, information about the amplitude and phase of each signal is required. Synchronous phase measurement dictates that highly phase-stable oscillators and signal generators are used in both the transmitter and the receiver. The design presented here however, employs common first and second oscillators in a two-branch measuring receiver (Fig. 4-2). This method removes the necessity for expensive signal generators, as phase fluctuations (produced by either the transmitter or the shared receiver oscillators) are common to both branches and do not affect the complex correlation calculated between them.

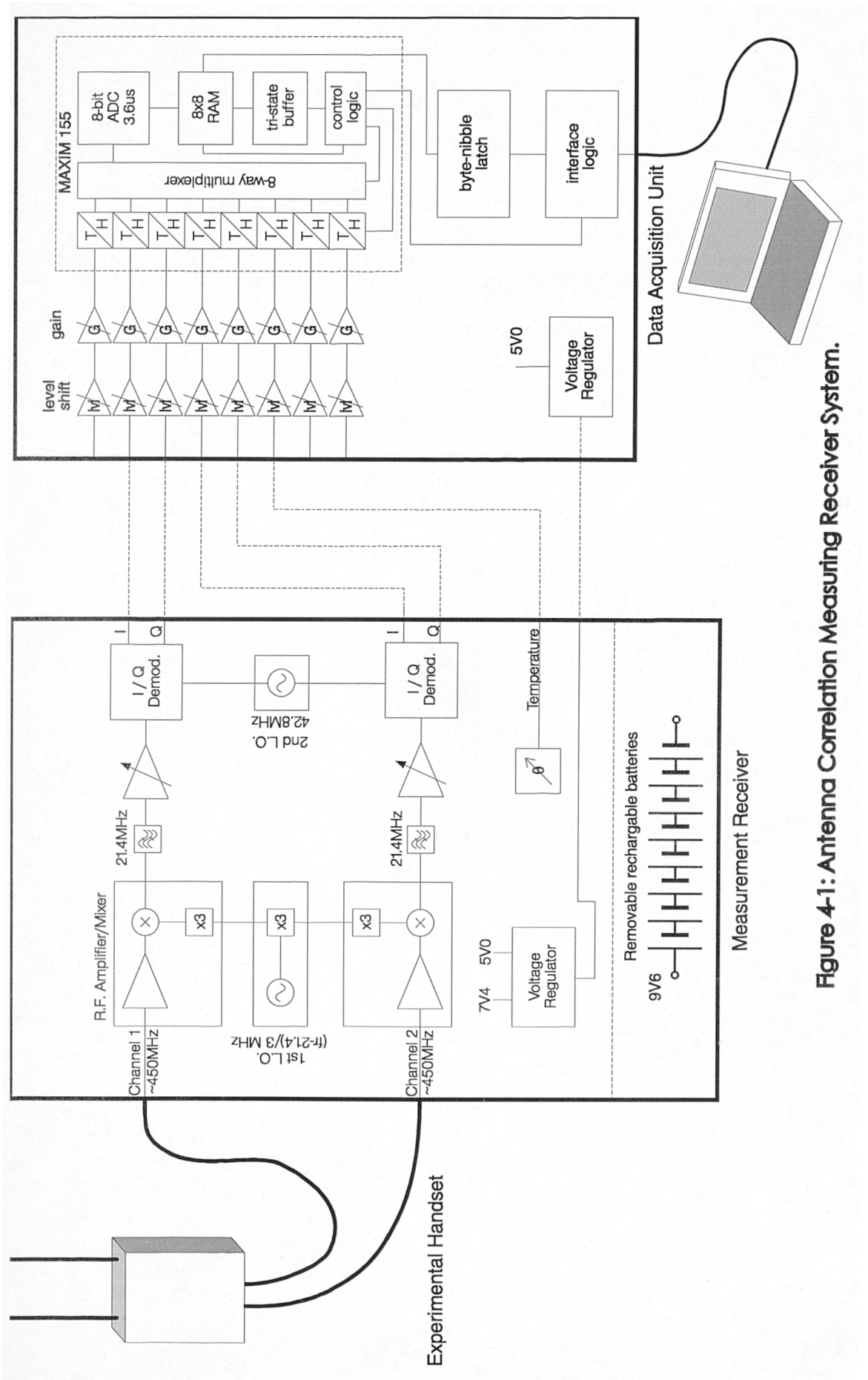

Figure 4-1: Antenna Correlation Measuring Receiver System.

4.2.1 Measuring Receiver

To determine the correlation between two complex signals, the ideal measuring receiver might possess the following: no branch-to-branch coupling; linear input power to output envelope conversion; constant relative phase difference between branches; identical branch characteristics; wide dynamic range; and high sensitivity. The effect of the departure from the ideal is illustrated for some of these conditions.

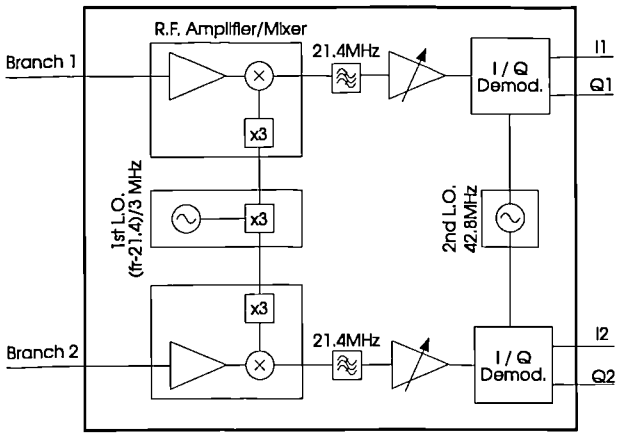

Figure 4-2: Antenna correlation measuring receiver block diagram.

4.2.1.1 Isolation between branches

Branch-to-branch coupling or branch isolation is defined here as the ratio of the power received in one branch to the power received in the other branch when it is connected to a matched load. The amount of coupling that can be tolerated between branches may be determined by analysis or simulation of a two-port network that models the coupling between branches. Signals of known correlation are connected to the input port of the network and the correlation of the output signals is calculated as a function of the branch coupling. The analytical method and simulation reveal that the input correlation has a much stronger effect on the output correlation than the branch coupling. Signal coupling levels of up to -20dB are tolerable for all input correlations.

4.2.1.2 Dynamic range

In a multipath propagation environment, fades in excess of 30dB below the mean signal level can be expected. This might suggest that a correlation measuring receiver should have a dynamic range to match. The vast majority of signal energy is however, concentrated about its mean and the correlation between two signal envelopes will therefore be more strongly affected by the variations about the mean rather than the fades. Furthermore, deep fades for

any signal envelope occur rarely and deep fades for both signal envelopes occur even less often. Simulations of reduced dynamic range receivers have shown that clipping levels of 5dB below the mean have little effect upon the change in correlation between the full range signal and the clipped signal. A wide dynamic range is therefore only necessary to ensure that the received signal envelope falls into the measuring range of the receiver.

4.2.1.3 Phase consistency and amplitude tracking

To determine the complex correlation between two strongly correlated complex envelopes, the phase performance of the receiver must be insensitive to the input power level. This requirement may be relaxed for lower levels of signal correlation as the inter-branch magnitude difference has a greater effect on the cross-correlation than the inter-branch phase difference (Fig. 4-3). Figure 4-4 shows the consistency of the inter-branch phase difference in the form of a probability distribution. The absolute value of phase difference is arbitrary. Observing the phase difference in this manner validates the architecture of the shared oscillator arrangement. The branch output amplitudes should also track the input power linearly and simultaneously. Amplitude tracking performance is easily checked by overplotting the amplitude cumulative distribution functions of each branch output. Ideally they should coincide. The maximum difference between the traces shown in Fig. 4-5 is <0.1dB and may thus be ignored.

4.2.1.4 Sensitivity

A measuring receiver must also be designed to operate above a minimum received power level. This is usually referred to as its sensitivity.

4.2.2 Measured Performance

Table 4-1 summarises the performance of the receiver measured at the operating frequency of 456.4875MHz.

Table 4-1: Antenna correlation measuring receiver performance.

Parameter	Value
Branch-to-branch isolation	≥33dB
Dynamic range	≥35dB for any operating range
Phase consistency	±3°
Amplitude tracking	<0.25dB for ≥90% of the time
Sensitivity	-115dBm

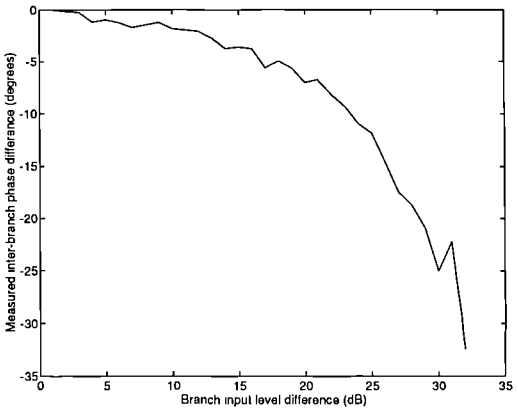

Figure 4-3: Measured inter-branch phase difference as function of unequal branch input levels.

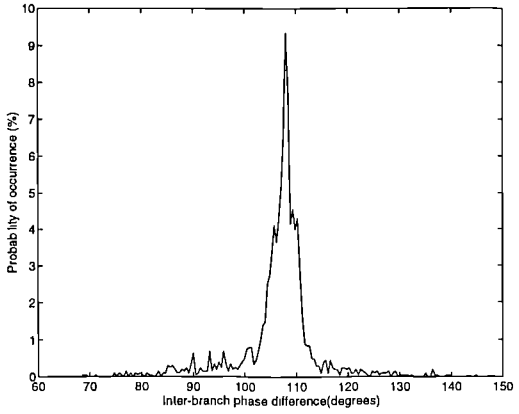

Figure 4-4: Sample probability distribution of inter-branch phase difference when both branches are fed from a common 99.5% amplitude modulated source.

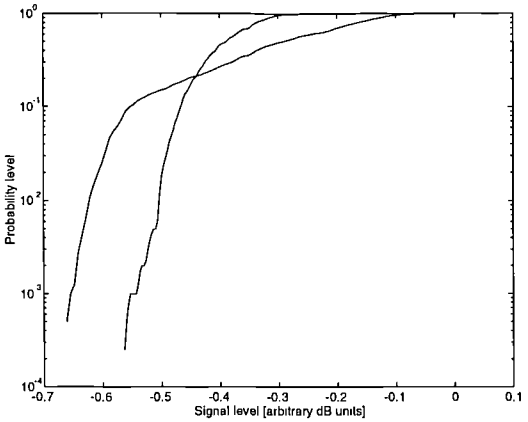

Figure 4-5: Sample cumulative distribution of output power levels when both branches are fed from a common unmodulated source.

4.2.3 Data Acquisition Unit

The data acquisition unit (DAU) can be realized through a four channel analogue-to-digital converter (ADC) suitably interfaced to a notebook-type personal computer. Many multi-channel ADC systems use a switched input that sequentially connects input channels and thus produces a cumulative sampling delay between channel samples. The sampling delay therefore imposes a restriction on the bandwidth of the signals that can be measured. In a two-branch quadrature receiver, the input channels to the DAU correspond to I_1, Q_1, I_2 and Q_2 where I_i and Q_i refer to the in-phase and quadrature components of the baseband signal of the i^{th} branch respectively. Whilst the bandwidth of these signals as a function of Doppler spread may be only several hertz for walking speeds, the temporal variation produced by the common oscillator scheme herein described may produce baseband signals with kilohertz bandwidths. However, the use of synchronised track and hold amplifiers for each input ensures that the sampling uncertainty created by shared oscillators is removed. Furthermore, the random phase of the receiver's local oscillators and that of the base station transmitter is common to each branch and does not therefore affect the calculation of the received signal complex correlation.

4.2.4 Summary

Some of the desirable performance parameters of an antenna correlation measuring receiver have been presented and a simplified receiver architecture has been introduced. The architecture used employs crystal oscillators that are common to both branches throughout the receive chain and thereby eliminates the need for expensive high stability sources.

4.3 Experimental Handsets

The experimental handsets described in this section were (unless stated otherwise) designed to resemble practical units and were therefore constrained in their physical size. A discussion of antenna design is considered beyond the scope of this thesis and the reader is therefore directed to one of the many excellent antenna texts; for example, Kraus [1] (where normal mode[1] helical antennas may be found on pp333-338, patch antennas on pp745-749, dipole antennas on pp200-234 and loop antennas on pp238-263).

[1]Normal mode helical antennas radiate maximum energy in a direction normal to the longitudinal axis of the antenna.

With the exception of experimental handset EH5, all of the normal mode helical antennas were constructed from 18SWG piano wire plated with 30micron copper. The helical antenna used in EH5 was made of 1.7mm beryllium copper wire. Both forms of helical antenna consisted of approximately 10 turns of wire with a nominal outside diameter of 9mm. The length of each helical antenna was trimmed to produce the lowest return loss when mounted on the relevant handset and held either next to the head or on the body in the required operating position.

The patch antennas used in experimental handsets EH2 and EH3 are electrically small and suffer from a fractional percentage VSWR bandwidth. Each patch antenna was however, tuned to the operating frequency using the PTFE loaded tuning device.

Another electrically small antenna is the loop antenna of experimental arrangement EH4. This was also tuned to resonance using capacitive loading in the form of a variable capacitor.

Table 4-2 lists the return loss, voltage standing-wave ratio and isolation between the antenna pairs used in each handset.

Table 4-2: Antenna driving point and isolation parameters measured at 456.4875MHz.

Experimental Handset	S11		S22		S12
	[dB]	[VSWR]	[dB]	[VSWR]	[dB]
EH1					
Position 0	-8.4	2.1:1	—	—	—
Position 1	-3.7	4.8:1	-3.7	4.7:1	-6.7
Position 2	-10.5	1.9:1	-11.7	1.7:1	-3.1
Position 3	-14.6	1.4:1	-15.5	1.4:1	-3.1
Position 4	-8.6	2.1:1	-10.7	1.8:1	-4.9
Position 5	-10.7	1.8:1	-8.1	2.3:1	-5.6
Position 6	-10.6	1.9:1	-7.8	2.4:1	-6.8
Position 7	-10.7	1.8:1	-8.4	2.2:1	-7.2
Position 8	-11.5	1.7:1	-8.2	2.3:1	-7.6
Position 9	-12.6	1.6:1	-9.7	2.0:1	-8.7
Position 10	-8.8	2.1:1	-19.0	1.4:1	-8.7
EH2 (S11 Helix, S22 Patch)	-16.8	1.3:1	-13.4	1.5:1	-13.5
EH3 (S11 Helix, S22 Patch)	-15.5	1.4:1	-9.0	2.1:1	-9.3
EH4 (S11 Dipole, S22 Loop)	-17.2	1.3:1	-18.7	1.3:1	-37.0
EH5 (S11 Straight branch, S22 Bent branch)	-9.1	2.1:1	-27.9	1.1:1	-3.1
EH6 (Port 1 Lapel unit, Port 2 Belt unit)	-9.4	1.9:1	-9.8	2.0:1	-93.4

4.3.1 Experimental Handset EH1

Experimental handset EH1 is shown in Fig. 4-6 with its lid removed. This handset was constructed specifically for the investigation of spatial antenna diversity. Helical antennas may be positioned in any of the ten equispaced holes along the top of the handset allowing antenna separations in the range of 10mm to 100mm. The maximum antenna separation is therefore in excess of the dimensions that may be accommodated on a regular sized hand-held radio and thus accounts for the unusual shape. The handset was constructed from 18SWG copper plate and has dimensions of: length 170mm; thickness 35mm; base width 70mm; and top width 130mm. A balun protrudes from the base of the unit.

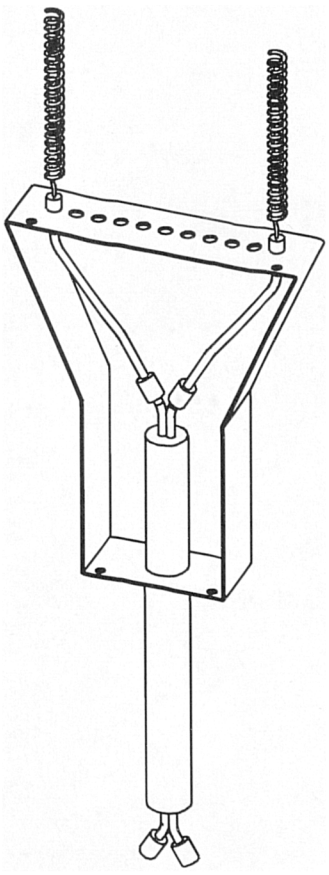

Figure 4-6: Experimental Handset EH1.

4.3.2 Experimental Handset EH2

Figures 4-7 and 4-8 show experimental handset EH3. The handset is constructed from 18SWG brass plate and comprises a single top mounted helical antenna and a side mounted horizontally orientated patch antenna. This antenna arrangement thus provides a combination of spatial, pattern and polarization diversity. The unit has dimensions of: length 170mm; thickness 35mm; and width 70mm. A balun projects from the bottom of the handset. The handset was held with the hand around the lower half of the unit with the patch antenna facing away from the experimenter's head as viewed in Fig. 4-7. An internal view showing the feed connections is given in Fig 4-8.

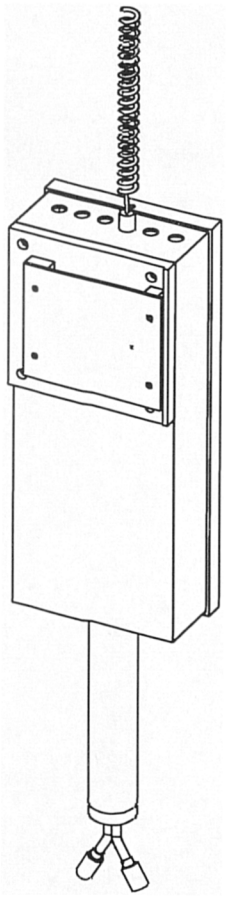

Figure 4-7: Experimental Handset EH2 (front view).

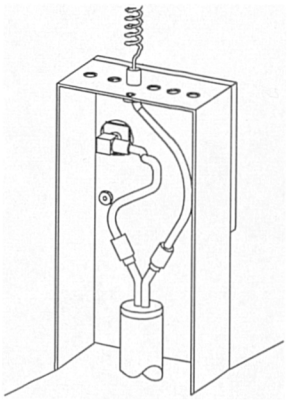

Figure 4-8: Experimental Handset EH2 (internal view showing feed arrangement).

4.3.3 Experimental Handset EH3

Figures 4-9 and 4-10 show experimental handset EH3. The handset is constructed from 18SWG brass plate and comprises a single top mounted helical antenna and a side mounted vertically orientated patch antenna. This antenna arrangement thus provides a combination of spatial and pattern diversity. The unit has dimensions of: length 170mm; thickness 35mm; and width 70mm. A balun projects from the bottom of the unit. The handset was held with the hand around the lower half of the unit with the patch antenna facing away from the experimenter's head as viewed in Fig. 4-9. An internal view showing the feed connections is given in Fig 4-10.

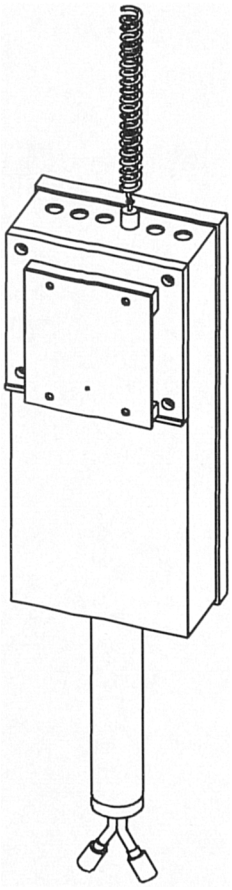

Figure 4-9: Experimental Handset EH3 (front view).

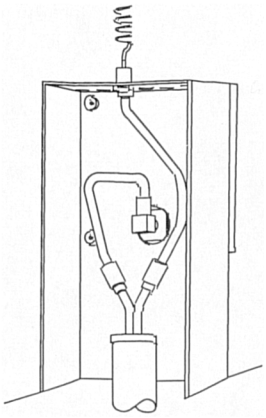

Figure 4-10: Experimental Handset EH3 (internal view showing feed arrangement).

4.3.4 Experimental Handset EH4

Experimental antenna configuration EH4 was constructed for cross-polar polarization ratio measurements and comprises a vertically oriented half-wave dipole and a horizontally oriented capacitively tuned loop antenna. The loop antenna is made from platinum plated copper (approximate diameter 53mm and height 5mm) and is arranged to be orthogonal and concentric to the brass dipole (approximate length 301mm and outside diameter 16mm). The lower arm of the dipole contains a balun whose coaxial feeder projects from one end. A non-metallic boom is provided to ensure that the antennas are held away from the experimenter's body at a distance of approximately 500mm (Fig. 4-11). Figure 4-12 shows a sectional view through the antenna feed arrangement where the dipole feed via the balun, the offset or shunt feed to the loop and the loop tuning capacitor are visible.

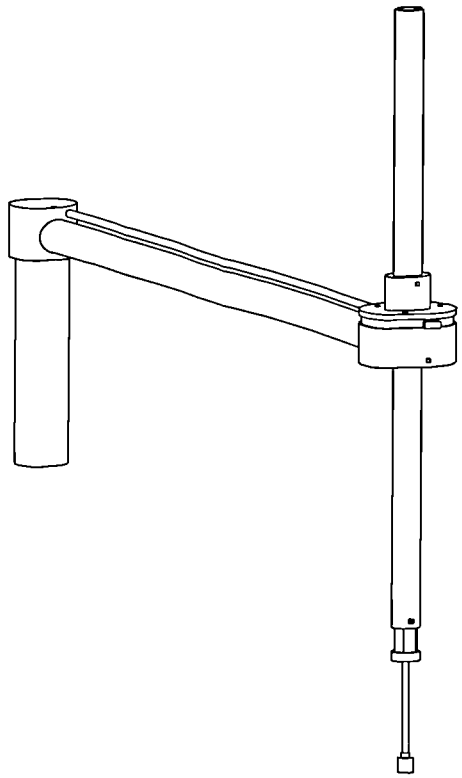

Figure 4-11: Experimental Handset EH4 (assembly drawing).

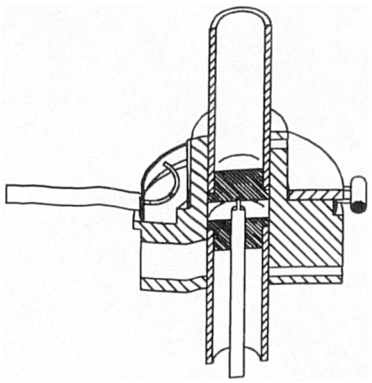

Figure 4-12: Experimental Handset EH4 (sectional view of feed arrangement).

4.3.5 Experimental Handset EH5

Experimental handset EH5[2] (Fig. 4-13) employs a single top mounted helical antenna with a split feed. The handset is constructed from Perspex and has dimensions of: length 170mm; thickness 36mm; and width 70mm. A balun is connected to each feed.

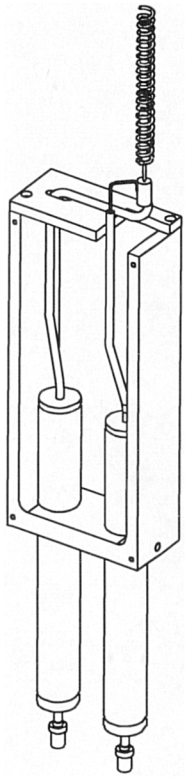

Figure 4-13: Experimental Handset EH5.

[2] At the time of writing, seven patent applications had been made for the design of this handset

4.3.6 Experimental Handset EH6

So-called two-piece handheld radios are popular with many private mobile radio users; for example, the police forces of the United Kingdom. This type of equipment usually comprises a belt-worn radio unit (containing the transceiver electronics and battery pack) and a lapel-worn user interface unit (consisting primarily of a microphone, loudspeaker, push-to-talk switch and channel selector) upon which a rubber encased helical antenna is mounted. It is conceivable that a second *diversity* antenna may be mounted to the belt-worn unit thus providing considerable antenna separation and pattern diversity through the user's body attenuating signals from one direction. This concept was executed in the construction of experimental handset EH6. The lapel unit measures: length 86mm; thickness 21mm; and width 51mm. The waist or belt unit measures: length 132mm; thickness 21mm; and width 51mm. Both units were made from 1.2mm phosphor bronze plate. To reduce the mass of the two units, ferrite beads were used in place of a balun. Figure 4-14 shows the two units with their lids removed.

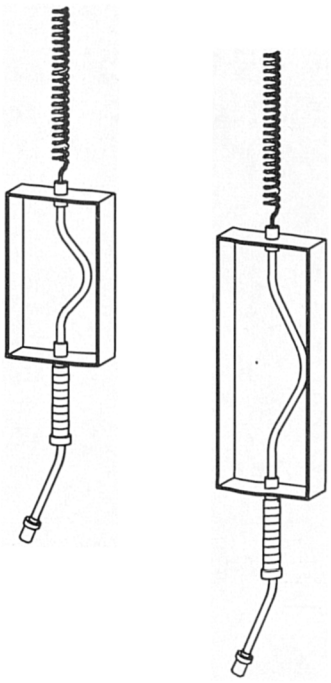

Figure 4-14: Experimental Handset EH6.

4.4 References

1. KRAUS, J.D., 1988, "Antennas", McGraw-Hill, Singapore (pages as listed in text)..

5
Experimental Investigation and Data Processing

5.1 Introduction

To investigate various antenna diversity systems and to evaluate the performance of certain candidate handset designs, a series of experimental measurements was performed using the equipment and experimental handsets described in Chapter 4. In this chapter, an explanation of the methodology employed and a discussion of the numerical processing applied to the measurement data is presented. An analysis of the results is given in Chapter 6.

5.2 Choice of Routes

Over relatively short distances (a few tens of wavelengths) the narrowband mobile radio propagation channel can best be described or categorized by the cumulative distribution function (CDF) of its fast fading component. In a multipath environment, where waves arrive at the receiver from many directions, the envelope of the fast fading component of the received signal is likely to follow the Rayleigh distribution. An alternative signal power distribution is named after Rice [1]. Rician distributed signals are typical of propagation scenarios where a line-of-sight path, or at least, a dominant specular component, exists between the receiver and transmitter. Routes were therefore chosen to produce signal CDF's that followed either the Rayleigh or Rician distributions. The location of the base station transmitter and the measurement routes are shown in Fig. 5-1.

5.2.1 Base Station Location

For all routes, the base station was located on the roof of the department of Electrical Engineering and Electronics building (A-block). Plate 5-1 shows a view of Mount Pleasant taken from this location.

5.2.2 Base Station Transmitter and Antenna

An unmodulated continuous wave (CW) signal of effective radiated power (ERP) 14W was radiated at a frequency of 456.4875MHz[1] using a vertically polarised four-element collinear array antenna at a height of approximately 35m above street level.

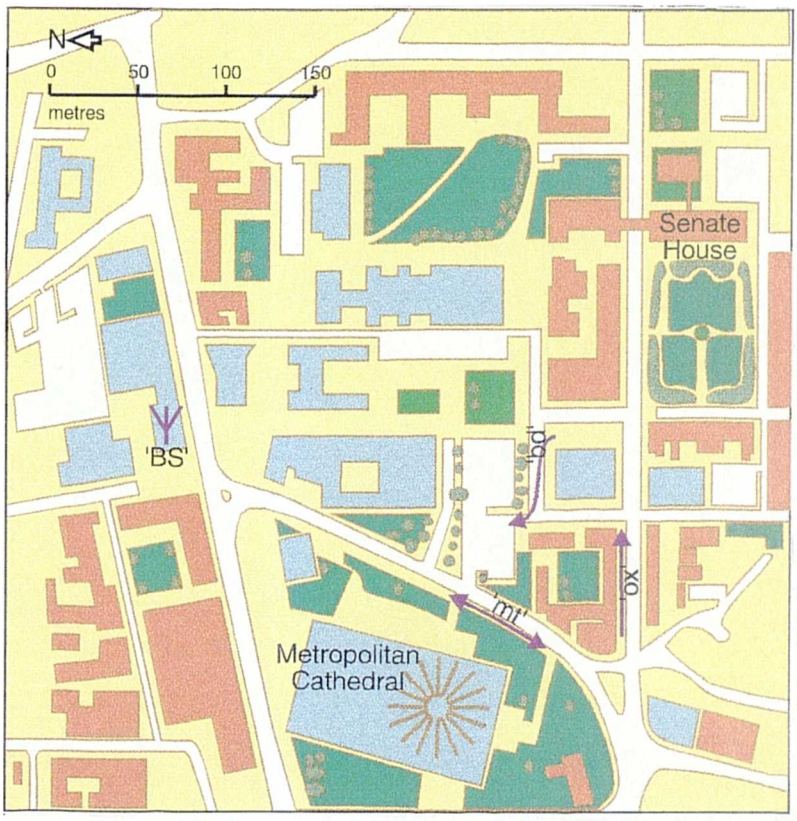

Figure 5-1: Section of the University of Liverpool precinct map to show the lo ation of the base station and the measurement routes. The routes and direction of travel are indicated by arrows.

5.2.3 Mount Pleasant

To obtain the Rician distributed signal, a section of Mount Pleasant was used (Plate 5 2) This LOS route follows a near radial path from the base station. Mount Pleasant is a reasonably busy through road that connects Brownlow Hill and Oxford Street. For the comparative set of experiments (Section 5.3.2), the direction of travel along the route was always away from the department. The abbreviation "mt" in Fig. 5–1 refers to this route.

[1]A Test and Development licence was issued by the Department of Trade and Industry's Radio-communications Agency with a frequency assignment of 456.4875MHz and a maximum ERP of 20W.

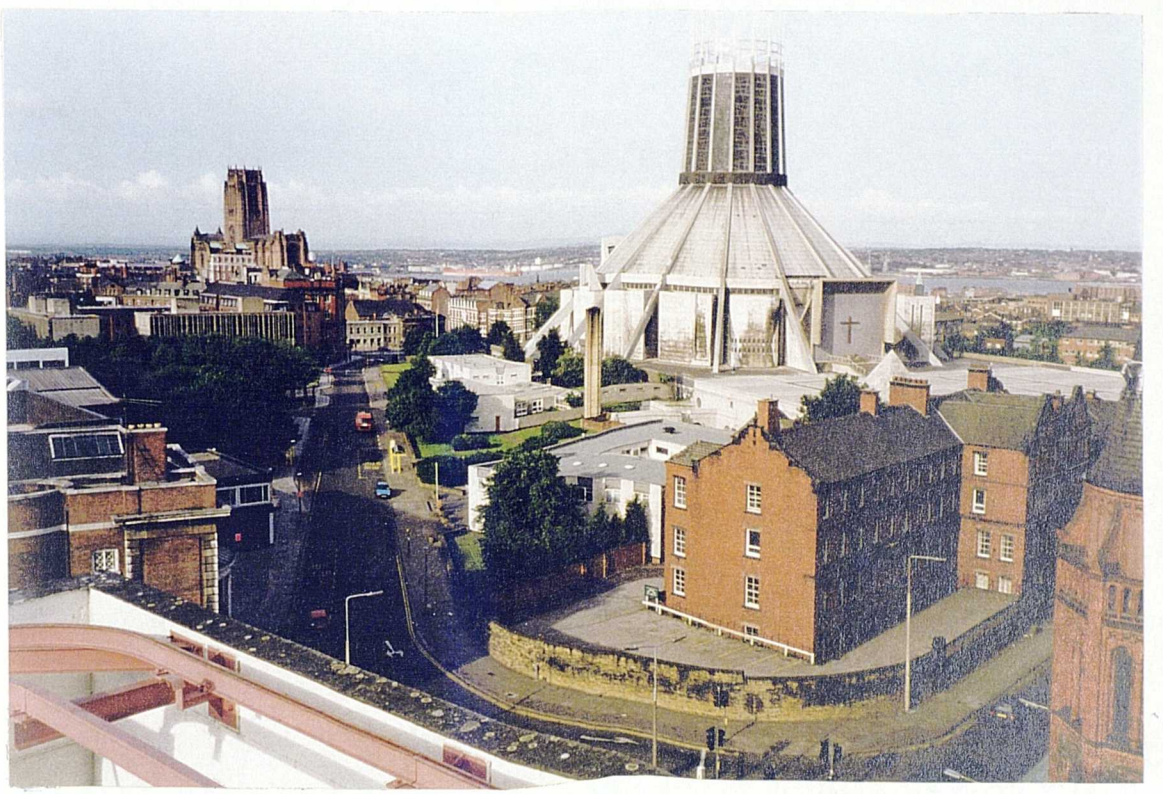

Plate 5-1: View of Mount Pleasant taken from the base station location.

Plate 5-2: Mount Pleasant measurement route. The author is shown with experimental handset EH4 performing cross-polar measurements at waist-height.

Plate 5-3: Oxford Street measurement route. The author is shown collecting with experimental handset EH2.

Plate 5-4: Bedford Street North measurement route. The author is shown collecting data with experimental handset EH3.

5.3 Measurement Procedure

The content of the experimental measurement programme may be divided into specific investigation areas, each with its own criterion. In this section, both the criteria investigated and the method of investigation are presented.

5.3.1 Common Method

Common to all experimental investigations was the method of data collection. For each handset-cum-antenna configuration, three walks were made over a similar section of the measurement route (allowing for vehicles, pedestrians and other obstructions). With the exception of experimental handsets EH4 and EH6, the handsets were held next to the head at an average angle of approximately 60° to the vertical [3]. During the walk, the position of the head was varied from side-to-side and up and down in order to simulate the way in which hand-held radios are often used [4]. Each walk was timed to ensure that the average speed was maintained constant to within 5%. A sampling rate of 100Hz (this satisfies the Nyquist sampling criterion for maximum Doppler frequency spreads produced by mobiles or local scatterers travelling in excess of 60mph) and a sample size of 6000 samples was used for each measurement. This combination of sampling frequency and sample size corresponds to approximately 60 metres or at least 121 fades.

In certain experiments, the mean signal level imbalance exceeded the dynamic measurement range of the receiver. Compensation of this imbalance was achieved by the insertion of calibrated attenuators into the appropriate antenna feed. The attenuation value used was recorded and entered into subsequent calculations.

5.3.2 Comparative Assessment

Diversity gain is a generally accepted term that represents the improvement in signal to noise ratio (SNR) between the output of a diversity combiner (Section 5.5.5) fed with more than one input (a multi-branch system) to the signal to noise ratio of a single branch system providing that the SNR of each system is measured at the same probability level [5]. In practical terms, the single branch SNR may be obtained from one of the inputs to an N-branch diversity combiner.

For the purposes of comparing the performance of various dual-antenna handsets, a pragmatic diversity gain measure is required. The so-called comparative antenna diversity gain[2] is thus defined here as the improvement in signal power produced by a pair of receiving antennas and diversity combiner to the signal power produced by a single reference antenna providing that the signal power of each system is measured at the same probability level. It is therefore essential to use the same reference signal when comparing the antenna diversity gain performances of various antenna handset arrangements.

Comparative assessment experiments were thus performed by first obtaining measurement data from the reference antenna handset, EH0, using the method described in the previous section. This procedure was then repeated for experimental handsets EH2, -3, -5 and -6. The measurement data was then applied to software implemented diversity combiners (Section 5.5.5) to yield a comparative diversity gain figure.

5.3.3 Spatial Diversity

Experimental handset EH1 (see Chapter 4) was designed for spatial diversity investigations. The construction of the handset enables the antennas to be separated by fixed distances. Data was thus collected using the experimental procedure described above for each of the ten available antenna separation positions. The comparative antenna diversity gain was calculated using the reference signal data obtained from experimental handset EH0.

5.3.4 Cross-polar Coupling Ratio Measurement

For each of the three measurement routes, the cross-polar coupling ratio (XPR) (Section 5.5.4) was determined from experiments performed using experimental handset EH4. Unlike the other experimental handsets, EH4 was designed specifically to measure the XPR and does not therefore resemble a typical hand-held radio handset. In use, EH4 was held at waist height (approximately 1.10m above the ground) for all routes and at head height (approximately 1.83m above the ground) for the Mount Pleasant route. In both cases, the antennas were positioned in front of the experimenter with the dipole aligned perpendicular to the ground.

[2]Unless stated otherwise, the term diversity gain used in this chapter implies comparative antenna diversity gain.

5.3.4.1 Antenna gain comparison

To calculate the XPR from measurement data, it is necessary to know the ratio of the mean effective gain (MEG [6]) of the antennas used for collecting that data. In the absence of a suitable antenna measurement facility (for example, a calibrated far-field antenna range) the MEG ratio of an antenna pair may be found by simultaneously exposing the antennas to fields that are uniformly distributed in space. This was achieved in practice by sweeping the antenna configuration of EH4 at various orientation angles over the surface of an imaginary sphere. A T-junction section of corridor was chosen on the ground floor of the department's B-block building where the polarization of field energy was expected to be uniformly distributed [7].

5.3.5 "Two-piece" Handset Unit

Experimental handset EH6, the two-piece handset unit, was used in a manner similar to the method described in Section 5.3.2 above with the exception that the handset was "worn". The method of "wearing" was adopted from the manufacturers recommended usage guide [8] with the lapel unit fastened to the experimenter's left jacket lapel and the belt unit hung from the back of the experimenter's trouser belt.

5.4 Measurement Parameters

The experimental measurement programme was designed to include experiments that would enable a number of antenna diversity system parameters to be computed from the directly measured received baseband signal. These parameters are described in the relevant section and include the following:

- P_{avg}, the branch mean signal level (Section 5.5.2)
- ρ_{12}, the complex signal correlation (Section 5.5.3)
- ρ_e, the envelope correlation (Section 5.5.3)
- XPR, the cross-polar coupling ratio (Section 5.5.4)
- G_{div}, diversity gain (Section 5.5.5)
- σ_{n-1}, the sample standard deviation (Section 5.5.7)

5.5 Data Analysis

An overview of the methods used to analyse the raw measurement data is presented in the following section.

5.5.1 Estimation of the Local Mean and Normalization

The envelope of the received signal is a combination of fast and slow fading components. Calculation of the cross-correlation[3] between the signals received by the two antennas requires that the slow fading component, often called the local mean, is removed. A moving average method may be used to estimate the local mean. The received signal $R(t)$ may be expressed as:

$$R(t) = r(t) \cdot m(t) \tag{51}$$

where $m^2(t)$ is the local mean power and $r(t)$ is a normalized received signal strength that varies quickly (that is, fast fading). In practice, a discrete time representation of $R(t)$ was formed from the time-sampled outputs of the receiver's quadrature demodulator:

$$R(t_n) = I(t_n) + jQ(t_n) \tag{52}$$

An estimate of the mean power, $m^2(t)$, at a time t_n, may be found from a series of N equi-spaced[4] samples using the moving average method presented by Feeney [10]:

$$\hat{m}^2(t_n) = \frac{1}{N} \sum_{m=\frac{-(N-1)}{2}}^{m=\frac{(N-1)}{2}} |R|^2(t_{n+m}) \tag{53}$$

where $\hat{m}^2(t_n)$ is the estimate of the local mean power.[5] The estimated fast fading component $\hat{r}(t_n)$ is given by:

[3] In this instance, cross-correlation includes both the complex correlation and the envelope correlation.

[4] Equidistant sampling may be realized in practice by ensuring that the mobile moves at a constant speed while regular samples are taken. Lee [9] presents a method for interpolating irregularly spaced samples using additional information from a tachograph.

[5] The hat symbol, $\hat{m}$, is used to represent an estimate of the variable m.

$$\hat{r}(t_n) = \frac{R(t_n)}{\sqrt{\hat{m}^2(t_n)}} \qquad (5\text{-}4)$$

The interval over which m^2 is estimated is $T = N / f_s$ where f_s is the sampling frequency. If T is incorrectly chosen then the local mean estimation will be poor: too short and the fast fading components remain; too long and the slow fading component is lost. Adachi and Feeney [11] investigated the effect of varying the normalized sample period $f_d T$ and reported that a value of $f_d T = 16$ yielded local mean estimates with an accuracy of between ±1dB and ±2dB.

It should be noted that the received signal, $R(t_n)$, and its normalized counterpart, $\hat{r}(t_n)$, are both complex voltage sequences.

5.5.2 Branch Mean Signal Level

Once the slow fading component is removed from the branch signal, the branch is said to be normalized and has a mean level of 0dB. The mean value of the recorded signal prior to normalization is also of importance and is calculated from the sample mean (eqn.(5-5)) of the recorded signal envelope. This value is combined with the receiver calibration data and any attenuation that may have been applied to the branch to yield an absolute mean value expressed in units of dBm.

$$\overline{R} = \frac{1}{n}\sum_{j=1}^{n} \left| R(t_n) \right| \qquad (5\text{-}5)$$

5.5.3 Cross-correlation

Having removed the slow fading component from each branch, the cross-correlation between branches can be calculated. Using the normalized complex data, $\hat{r}(t_n)$, both the complex cross-correlation and the envelope cross-correlation may be calculated. The normalized complex cross-correlation or complex correlation [12], ρ_{12}, is defined as:

$$\rho_{12} = \frac{\left\langle \left(\hat{r}_1 - \langle \hat{r}_1 \rangle\right)^* \left(\hat{r}_2 - \langle \hat{r}_2 \rangle\right) \right\rangle}{\sqrt{\left\langle \left| \hat{r}_1 - \langle \hat{r}_1 \rangle \right|^2 \right\rangle} \sqrt{\left\langle \left| \hat{r}_2 - \langle \hat{r}_2 \rangle \right|^2 \right\rangle}} \qquad (5\text{-}6)$$

where the angle brackets, $\langle \ldots \rangle$, are notation for expectation.

The cross-correlation of the envelope of $\hat{r}(t_n)$, that is the normalized envelope cross-correlation or envelope correlation [13], is defined as:

$$\rho_e = \frac{\overline{|\hat{r}_1||\hat{r}_2|} - \overline{|\hat{r}_1|}\,\overline{|\hat{r}_2|}}{\sqrt{\overline{|\hat{r}_1|^2} - \overline{|\hat{r}_1|}^2}\sqrt{\overline{|\hat{r}_2|^2} - \overline{|\hat{r}_2|}^2}} \qquad (5\text{-}7)$$

5.5.4 Cross-polar Coupling Ratio

The cross-polar coupling ratio (XPR) is defined here for received signals as the ratio of the average vertically polarized electric field energy to the average horizontally polarized electric field energy. Using the method outlined in Section 5.3.4, the XPR may be written in the form of a product of two terms as shown in eqn. (5–8).

$$XPR = \frac{\overline{P_{Dipole}}}{\overline{P_{Loop}}} \cdot \frac{MEG_{Loop}}{MEG_{Dipole}} \qquad (5\text{-}8)$$

5.5.5 Diversity Implementation

The various forms of selection and diversity combining, and the concept of diversity gain were described in Section 3.2.3 of Chapter 3. In this section, the continuous time equations of Section 3.2.3 (eqns. (3-5) to (3-7)) are expressed in discrete time. The following equations are applied to the received signal data prior to normalization.

Selection Diversity:

$$R_{sel}(t_n) = \begin{cases} |R_1(t_n)| & |R_1(t_n)| \geq |R_2(t_n)| \\ |R_2(t_n)| & |R_1(t_n)| < |R_2(t_n)| \end{cases} \qquad (5\,9)$$

Equal Gain Combining:

$$R_{egc}(t_n) = \frac{|R_1(t_n)| + |R_2(t_n)|}{\sqrt{2}} \qquad (5\,10)$$

Maximal Ratio Combining:

$$R_{mrc}(t_n) = \sqrt{\left|R_1(t_n)\right|^2 + \left|R_2(t_n)\right|^2} \qquad (5\text{-}11)$$

5.5.6 Diversity Gain Calculation

Equations (5–9) to (5–11) were implemented in software to enable off-line processing of the measurement data.. The newly formed diversity signals, R_{sel}, R_{egc} and R_{mrc} were then normalized using eqns. (5–3) and (5–4) to produce $\hat{r}_{sel}$, $\hat{r}_{egc}$ and $\hat{r}_{mrc}$. It should be noted that the diversity signals are real while the reference signal is complex. The discrete-time variable, t_n, which is implicit in all of these variables, has been omitted for clarity.

Using the "CDF intersect finder" technique introduced in Section 3.2.3.1.1 of Chapter 3, the signal level of the normalized reference signal and each of the normalized diversity signals was found at the 1% and 10% probability levels. This process may be written using the function H(Y) defined as:

$$H(F(x) = Y) = X|_{F(x)=Y} \qquad (5\ 12)$$

where the cumulative distribution of the random variable X is defined using the probability function:

$$F(x) = P(X \le x) \qquad (5\ 13)$$

If X is a discrete random variable, then F(x) is a step function. Smoothing, in the form of linear interpolation, was thus built into the CDF intersect find algorithm.

The normalized diversity signals and the normalized reference signal are combined with their respective absolute mean values (eqn.(5–5)) to yield the following diversity gain expressions:

Selection Diversity at the 1% and 10% Probability Levels:

$$G_{sel(1\%)_{dB}} = 20\log_{10}\left[H\left(\hat{r}_{sel}\cdot\frac{\overline{R}_{sel}}{\overline{R}_{ref}} = 1\%\right)\right] - 20\log_{10}\left[H\left(\left|\hat{r}_{ref}\right| = 1\%\right)\right] \qquad (5\ 14)$$

$$G_{sel(10\%)_{dB}} = 20\log_{10}\left[H\left(\hat{r}_{sel}\cdot\frac{\overline{R}_{sel}}{\overline{R}_{ref}}=10\%\right)\right]-20\log_{10}\left[H\left(\left|\hat{r}_{ref}\right|=10\%\right)\right] \quad (5\text{-}15)$$

Equal Gain Combining at the 1% and 10% Probability Levels:

$$G_{egc(1\%)_{dB}} = 20\log_{10}\left[H\left(\hat{r}_{egc}\cdot\frac{\overline{R}_{egc}}{\overline{R}_{ref}}=1\%\right)\right]-20\log_{10}\left[H\left(\left|\hat{r}_{ref}\right|=1\%\right)\right] \quad (5\text{-}16)$$

$$G_{egc(10\%)_{dB}} = 20\log_{10}\left[H\left(\hat{r}_{egc}\cdot\frac{\overline{R}_{egc}}{\overline{R}_{ref}}=10\%\right)\right]-20\log_{10}\left[H\left(\left|\hat{r}_{ref}\right|=10\%\right)\right] \quad (5\ 17)$$

Maximal Ratio Combining at the 1% and 10% Probability Levels:

$$G_{mrc(1\%)_{dB}} = 20\log_{10}\left[H\left(\hat{r}_{mrc}\cdot\frac{\overline{R}_{mrc}}{\overline{R}_{ref}}=1\%\right)\right]-20\log_{10}\left[H\left(\left|\hat{r}_{ref}\right|=1\%\right)\right] \quad (5\ 18)$$

$$G_{mrc(10\%)_{dB}} = 20\log_{10}\left[H\left(\hat{r}_{mrc}\cdot\frac{\overline{R}_{mrc}}{\overline{R}_{ref}}=10\%\right)\right]-20\log_{10}\left[H\left(\left|\hat{r}_{ref}\right|=10\%\right)\right] \quad (5\text{-}19)$$

In all the above computations of diversity gain, the signal received by a centrally mounted single helical antenna on experimental handset EH1, was used as the reference branch. This reference handset was earlier referred to as EH0 to avoid confusion with EH1.

5.5.7 Sample Standard Deviation

A tabular format is used in the next chapter to present the results. The rows of the tables are listed according to the measurement routes while the columns contain the result for each walk, the sample mean (or the average value) of the three walks, and the sample standard deviation of the three walks. The sample standard deviation is defined as:

$$\sigma_{n-1} = \sqrt{\frac{1}{n-1}\sum_{j=1}^{n}\left(x_j-\overline{x}\right)^2} \quad (5\ 20)$$

5.6 References

1. RICE, S.O., 1948, "Statistical Properties of a Sine Wave plus Random Noise", Bell Sys. Tech. J., Vol. 27, No.1, pp109-157.

2. CLARKE, R.H., 1968, "A Statistical Theory of Mobile-Radio Reception", Bell Sys. Tech. J., Vol. 47, No. 6, pp957-1000.

3. TSUNEKAWA, K., 1989, "Diversity Antennas for Portable Telephones", Proc. 39th IEEE Veh. Tech. Conf., San Francisco, USA, pp50-56.

4. HILL, C., and KNEISEL, T., 1991, "Portable Radio Antenna Performance in the 150, 450, 800, and 900 MHz Bands "Outside" and In-Vehicle", IEEE Trans. on Veh. Tech., Vol. VT-40, No. 4, pp750-756, 1991.

5. TURKMANI, A.M.D., AROWOJOLU, A.A., JEFFORD, P.A., and KELLETT, C.J., 1995, "An Experimental Evaluation of the Performance of Two-Branch Space and Polarization Diversity Schemes at 1800MHz", IEEE Trans. on Veh. Tech., Vol. VT-44, No. 2, pp318-326.

6. TAGA, T., 1990, "Analysis for Mean Effective Gain of Mobile Antennas in Land Mobile Radio Environments", IEEE Trans. on Veh. Tech., Vol. VT-39, No. 2, ppll7-131.

7. TAGA, T., TSUNODA. K, and IMAHORI, H., 1991, "Correlation Properties of Antenna Diversity in Indoor Mobile Communication Environments", Proc. 39th IEEE Veh Tech Conf., Vol. 2, pp446-451.

8. POPPLE, M., 1996, *Personal Correspondence*, Philips Telecom-PMR, Cambridge, UK.

9. LEE, W.C.-Y., 1982, "Mobile Communications Engineering", McGraw-Hill, New York, USA, pp16-20.

10. FEENEY, M.T., 1989, "The Complex Narrowband UHF Mobile Radio Channel", Ph.D. Thesis, University of Liverpool, UK, pp5.5-5.7.

11. ADACHI, F., FEENEY, M.T., WILLIAMSON, A.G., and PARSONS, J.D., 1986, "Cross correlation Between the Envelopes of 900MHz Signals Received at a Mobile Radio Base Station Site", IEE Proc. Pt. F., Vol. 133, No. 6, pp506-512.

12. PAPOULIS, A., 1981, "Probability Random Variables and Stochastic Processes", McGraw-Hill, New York, USA, pp206-231.

13. SCHWARTZ, M., BENNET, W.R., and STEIN, S., 1966, "Communication Systems and Techniques", McGraw-Hill, New York, USA, pp6-15.

6
Analysis of Results

6.1 Introduction

Using the processing methods described in the previous chapter, the results of the experimental investigation are now presented. In the first section of this chapter, the measurement routes are described in terms of: the cumulative distribution function (CDF) of the normalized received signal plotted on Rayleigh-scaled paper; the received signal mean power level; and the cross-polar coupling ratio (XPR). In the second section, the results, with the exception of EH4, are ordered by experimental handset. For each handset, the mean power level of the signal received by each antenna, and the cross-correlation of the signals received by the two antennas (see Section 5.5.4) is shown. This information is then effectively combined into a single relative figure of merit, the comparative antenna diversity gain (see Section 5.3.2).

Throughout this chapter, experimental handset EH1, fitted with a single centrally positioned helical antenna, is referred to as either experimental handset EH0 or the reference handset. This is to avoid confusion with experimental handset EH1 which was used for spatial diversity experiments. All comparative antenna diversity gain figures quoted in this chapter are thus relative to EH0 (see section 5.5.6).

6.2 Characterization of Routes

In the following sub-sections, the pertinent characteristics of the measurement routes are presented. The route names are abbreviated as shown in Table 6-1.

Table 6-1: Measurement route abbreviations.

Abbreviation	Measurement Route and Direction
mt or mt_f	Mount Pleasant away from the base station
mt_t	Mount Pleasant towards the base station
ox	Oxford Street towards Senate House
bd	Bedford Street North towards Metropolitan Cathedral

6.2.1 Cumulative Distribution of the Normalized Received Signal Envelope

A convenient visual representation of a signal's characteristics is a plot of its cumulative distribution function (CDF). Such plots are often made onto so-called 'Rayleigh' graph paper [1] whose axes are scaled so that the CDF of a Rayleigh distributed signal will appear as a straight line. This line shall be referred to as either the Rayleigh reference line or simply the Rayleigh-line when it represents the CDF of a signal with a Rayleigh distribution and a mean power of 0dB.

The CDF's of the normalized fast fading component (see Section 5.2.5) of the signals received using the reference handset are shown in Figs. 6-1 to 6-3. For the "ox" and "bd" measurement routes, the CDF's are similar to the Rayleigh-line for all walks. For the "mt" route however, due to its dominant line-of-sight (LOS) component, the CDF's show both a significant departure from the Rayleigh-line and greater variability between walks. This variability is caused by the variation in handset orientation and position relative to the measurement walk. In a truly scattered environment, where waves of all polarizations arrive from all directions with equal probability, such variations in handset position would have little effect upon the signal distribution. Classification of this type of signal distribution—other than to say it is non-Rayleigh—would require an alternative form of normalization.

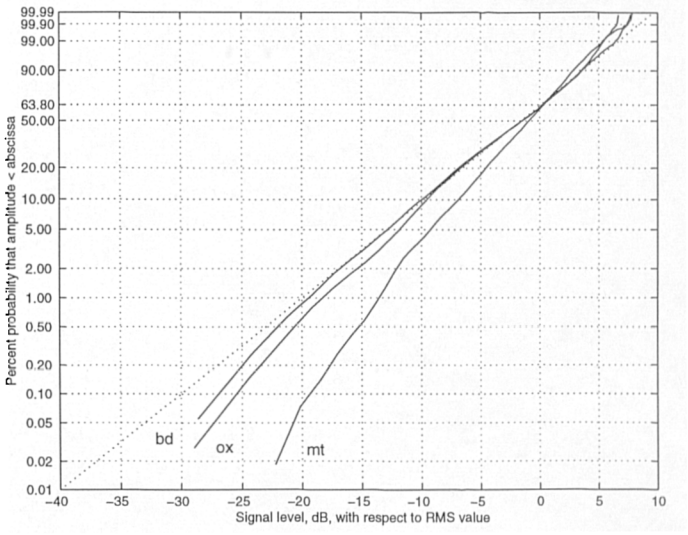

Figure 6-1: Sample cumulative distribution of the normalized reference signal amplitude for each measurement route (walk one). The dotted trace shows the CDF of a zero mean Rayleigh distributed signal for comparison.

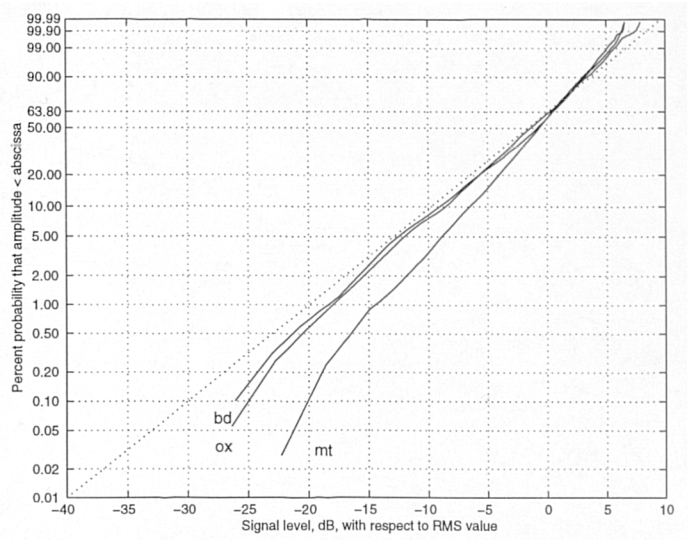

Figure 6-2: Sample cumulative distribution of the normalized reference signal amplitude for each measurement route (walk two). The dotted trace shows the CDF of a zero mean Rayleigh distributed signal for comparison.

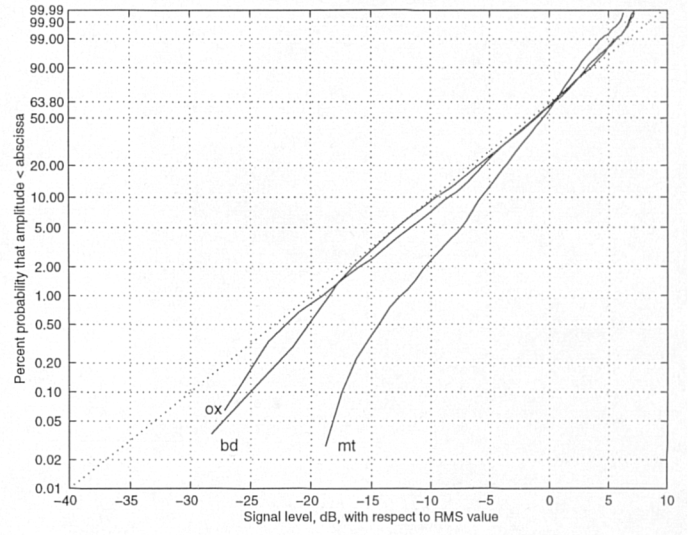

Figure 6-3: Sample cumulative distribution of the normalized reference signal amplitude for each measurement route (walk three). The dotted trace shows the CDF of a zero mean Rayleigh distributed signal for comparison.

6.2.2 Mean Signal Level

The experimental handsets described in Chapter 4 were developed in two batches over a period of approximately one year. Two groups of measurements were thus performed during the months of July 1995 and March 1996. For each set of experiments, receiver calibration data and route characterization information was obtained. Tables 6–2 and 6-3 compare the reference antenna mean signal levels (see Section 5.5.2) for the 1995 and 1996 sets of data. The tables show the mean power for each route and for each walk, the sample mean of the three walks, and the sample standard deviation.

The agreement between the two sets of data for the "mt" and "ox" routes is <0.4dB. This suggests that both the characteristics of the base station and the calibrated measuring receiver remained constant. The 1.4dB difference between the means of the "bd" sets of data may be due to a difference in foliage. Plate 5-4 in Chapter 5 was taken in July 1995 when the trees that line part of the "bd" route, were, in contrast to March 1996, in full leaf.

Table 6-2: Reference handset EH0 mean signal levels (July 1995 data set).

	Helical antenna mean power [dBm]				
route	walk-1	walk-2	walk-3	mean	σ_{n-1}
mt	-58.04	-59.55	-57.24	-58.28	1.17
ox	-75.41	-75.37	-75.24	-75.34	0.09
bd	-65.00	-65.07	-64.69	-64.92	0.20

Table 6-3: Reference handset EH0 mean signal levels (March 1996 data set).

	Helical antenna mean power [dBm]				
route	walk-1	walk-2	walk-3	mean	σ_{n-1}
mt	-57.49	-57.00	-61.30	-58.60	2.36
ox	-74.57	-75.02	-75.30	-74.96	0.37
bd	-62.66	-64.06	-63.88	-63.54	0.76

6.2.3 Cross-polar Coupling Ratio

A further parameter used to characterize the measurement routes was the cross-polar coupling ratio (XPR). Following the procedure outlined in Section 5.3.4 of Chapter 5, the XPR was found by first determining the gain ratio of the antennas that comprise EH4.

6.2.3.1 Antenna gain comparison

Experimental handset EH4 consists of a half-wave dipole antenna and an orthogonal loop antenna. The mean signal power received by each antenna in the "in-door" environment is tabulated below in Table 6-4.

Table 6-4: Branch mean signal levels for experimental handset EH4.

	Dipole antenna mean power [dBm]					Loop antenna mean power [dBm]				
route	walk-1	walk-2	walk-3	mean	σ_{n-1}	walk-1	walk-2	walk-3	mean	σ_{n-1}
in	-59.91	-58.70	-61.88	-60.17	1.61	-56.03	-57.37	-55.63	-56.34	0.91

Similarly, the mean signal powers received in the "out-door" environments are tabulated in Table 6-5. The abbreviations "mt_w" and "mt_h" denote Mount Pleasant measurements

performed at waist-height and head-head respectively (see Section 5.3.4 of Chapter 5). In both cases, the direction of travel was away from the base station. For the "ox" and "bd" routes, only waist height experiments were performed.

Table 6-5: Branch mean signal levels for experimental handset EH4.

	Dipole antenna mean power [dBm]					Loop antenna mean power [dBm]				
route	walk-1	walk-2	walk-3	mean	σ_{n-1}	walk-1	walk-2	walk-3	mean	σ_{n-1}
mt_w	-43.46	-43.36	-44.11	-43.65	0.41	-42.39	-46.74	-45.74	-44.96	2.28
mt_h	-42.27	-42.26	-41.89	-42.14	0.22	-50.49	-50.00	-49.52	-50.00	0.48
ox	-65.36	-66.20	-65.19	-65.58	0.54	-66.70	-66.19	-65.62	-66.17	0.54
bd	-52.20	-52.05	-52.39	-52.21	0.17	-57.80	-57.28	-57.25	-57.44	0.31

6.2.3.2 Cross-polar coupling ratio calculation

The XPR may now be calculated by extracting the mean values from Table 6-4 and Table 6-5 and substituting them into eqn. (5-8) from Chapter 5.

Table 6-6: Cross-polar coupling measured using experimental handset EH4.

	Antenna mean power			
route	Dipole [dBm]	Loop [dBm]	MEG ratio [dB]	XPR [dB]
mt_w	-43.65	-44.96	4.83	6.14
mt_h	-42.14	-50.00	4.83	12.69
ox	-65.58	-66.17	4.83	5.42
bd	-52.21	-57.44	4.83	10.06

The XPR figures in the above table show good agreement with those reported by Vaughan (see Table 2–1 of Chapter 2). It is interesting to note the variation between the "waist-height" and "head-height" XPR figures for the Mount Pleasant route. The figures suggest that there is a greater amount of horizontally polarized electric field energy at "waist-height" than at "head-height" for the "mt" route. Similar height variation experiments were not performed for the "ox" and "bd" routes.

6.2.3.3 Comparison of signal CDF's

Figures 6-4 to 6-6 show the CDF of the normalized fast fading component of the signals produced by the dipole and loop antenna of EH4 when used for both "waist-height" and "head-height" measurements along the Mount Pleasant measurement route. The CDF's of the normalized signals produced by the reference antenna, when held next to the head at a slant angle (Section 5.3.1, Chapter 5) in the same environment, are over-plotted for comparison.

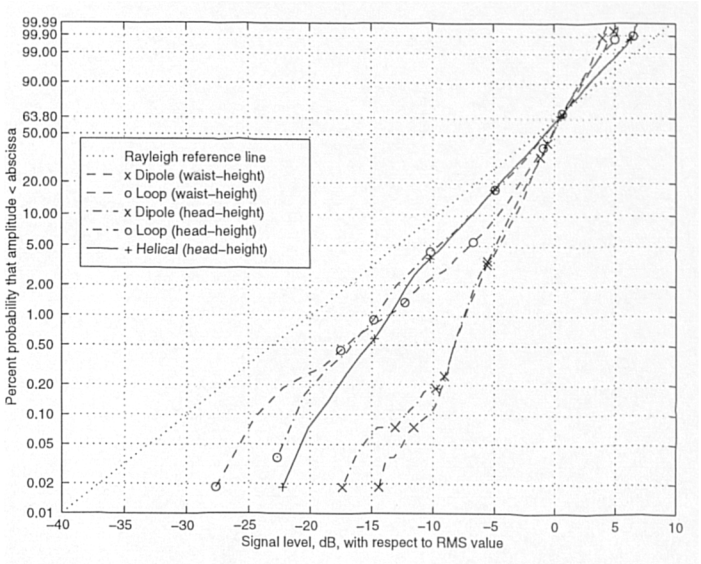

Figure 6-4: Comparison of the signal CDF's produced by the dipole and loop antennas of EH4, and the helical antenna of EH0. Walk one of three.

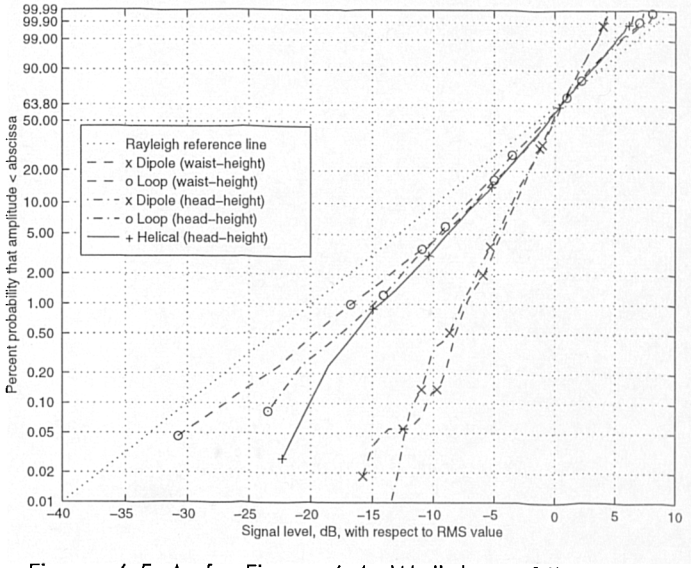

Figure 6-5: As for Figure 6-4. Walk two of three.

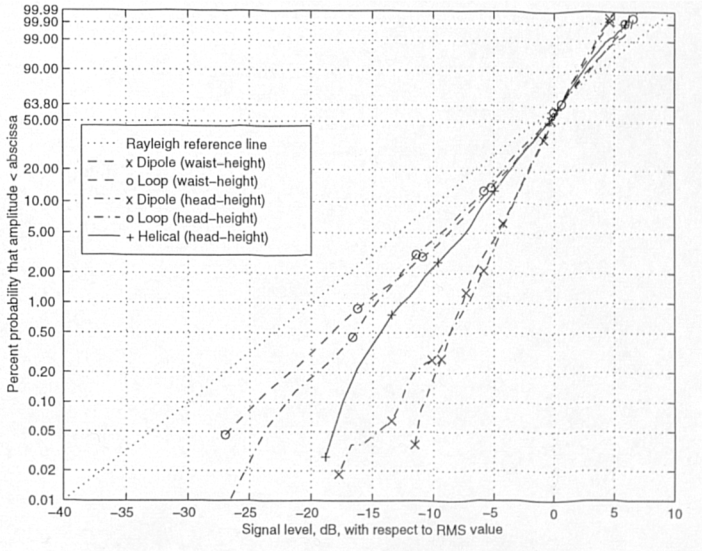

Figure 6-6: As for Figure 6-4. Walk three of three.

For all walks, the CDF of the signal produced by the vertically oriented dipole antenna, regardless of its height above the ground, shows a greater departure from the Rayleigh-line than the horizontally oriented loop antenna. This is because the cross-polar energy detected by the loop antenna is produced by the multi-path mechanisms of reflection and refraction (see Section 2.4.3 of Chapter 2), whereas the dipole receives a predominantly LOS wave. The CDF's of the normalized signals produced by the helical antenna mounted on EH0 lie somewhere in between the CDF's of the signals produced by the loop antenna and the dipole of EH4. This suggests that the helical antenna, due to the slant angle at which EH0 was held, detects a combination of vertically and horizontally polarized waves.

6.2.3.4 Signal correlation

Table 6-7 contains the values of cross-correlation calculated between the signals produced by the antennas of EH4. The signal measured at the terminals of the vertically oriented dipole is a representation of the E_z field component and that measured at the terminals of the loop antenna is a representation of the H_z field component. There is essentially zero correlation between the envelopes of these field components. This is also true for their complex correlation except in the LOS environment of Mount Pleasant. It should be remembered that the following approximation:

$$\rho_e \approx |\rho_{12}|^2 \qquad (61)$$

is valid when the signals are Rayleigh distributed [2]. The signals measured along the Mount Pleasant measurement route, as shown earlier in Figs. 6-1 to 6-3, are clearly non-Rayleigh distributed. This correlation parameter difference effect will be observed repeatedly throughout the results.

Table 6-7: Envelope and complex correlation for experimental handset EH4.

	ρ_e					$\lvert\rho_{12}\rvert^2$				
route	walk-1	walk-2	walk-3	mean	σ_{n-1}	walk-1	walk-2	walk-3	mean	σ_{n-1}
in	-0.052	-0.083	-0.023	-0.053	0.030	0.066	0.034	0.133	0.078	0.050
mt_w	0.010	0.007	0.006	0.008	0.002	0.643	0.356	0.511	0.503	0.144
mt_h	0.025	0.176	0.158	0.120	0.082	0.404	0.410	0.477	0.430	0 041
ox	0.121	0.028	-0.017	0.044	0.071	0.036	0.027	0.055	0.039	0 014
bd	0.020	0.045	0.071	0.045	0.025	0.040	0.069	0.077	0.062	0 020

6.3 Experimental Results

Before the detailed results of the experimental investigation are presented, it is appropriate to consider the performance of the helical antenna used in the reference handset.

6.3.1 Helical Antenna Gain Comparison

Table 6-6 should be read in conjunction with Table 6-2 to enable a gain comparison to be made between the dipole antenna of EH4 and the helical antenna of EH0. Using the antenna mean powers from the two tables, and assuming an alignment loss of 3dB and a gain of 2.15dBi for the dipole, the helical antenna of EH0, when held at a slant angle next to the user's head, has a gain in the range of -4.61dBi to -10.99dBi. This compares well with the work reported by Hill *et al* [3]. For their anechoic chamber antenna measurements at 450MHz, they report helical antenna gain figures between -4dBi and -15dBi.

6.3.2 Experimental Handset EH1

Experimental handset EH1 is described in Section 4.3.1 of Chapter 4. The handset was built to confirm the theoretical study presented in Chapter 3. Figure 6-7 compares mechanical length and electrical length at 456.4875MHz for free-space. The figure is useful for rapidly converting the abscissa values of Figs. 6-8 to 6-13 to their corresponding mechanical dimensions.

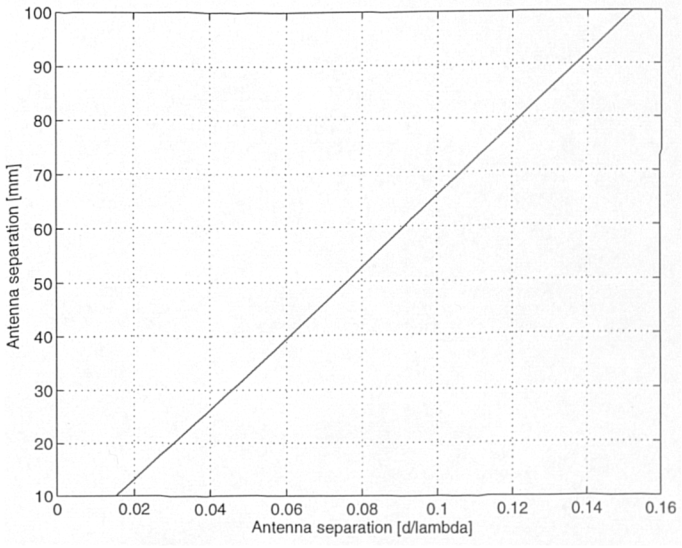

Figure 6-7: Electrical length to mechanical length conversion chart. Electrical lengths are measured at 456.4875MHz in free-space.

6.3.2.1 Correlation versus antenna separation

Figure 6-8 shows both the envelope correlation (ρ_e, denoted by rhoe), and the square of the magnitude of the complex correlation ($|\rho_{12}|^2$, denoted by rhoapx) plotted as a function of antenna separation. Clarke's field autocorrelation function and a theoretical trace (the 71Ω trace of Fig. 3-11, Chapter 3) are included for comparison.

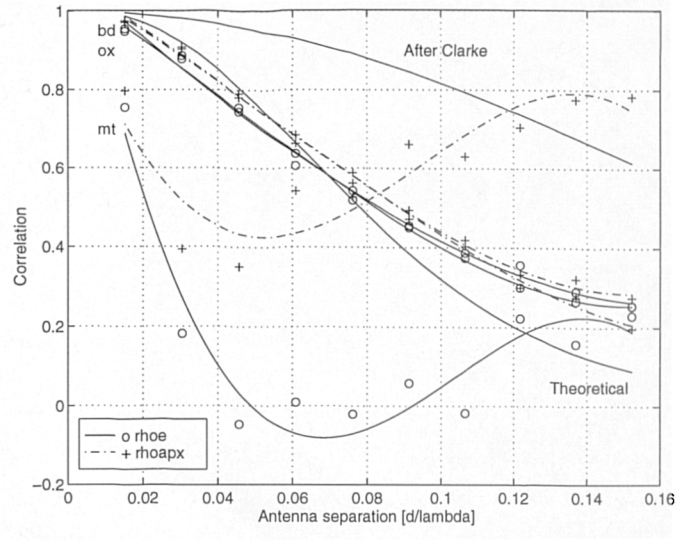

Figure 6-8: Correlation as a function of antenna separation. All walks have been averaged. Rhoe denotes envelope correlation and rhoapx denotes the square of the magnitude of the complex correlation. Clarke's field autocorrelation function and the theoretical curve (from Chapter 3) are plotted for comparison.

The two correlation traces for the "mt" measurement route show both significant departure from the traces for the other two routes and also greater difference between themselves. This, as reported earlier, is due to the non-Rayleigh signal statistics produced by the route.

For the "ox" and "bd" routes, the two correlation parameters are similar to one another as described by eqn. (6-1) and show lower levels of correlation than predicted by the field autocorrelation function. The values plotted are similar to Tsunekawa's results shown in Fig. 2-1 of Chapter 2. It is interesting to observe that the displacement of the measurement curves from the theoretical curve is in a direction towards the field autocorrelation function. This may be explained with reference to Figs. 3-5 to 3-10 of Chapter 3 that demonstrate the effect of varying the elevational and azimuthal distribution of the incoming waves. Similar effects are produced by the user's hand, head and body.

Another explanation for the difference between the curves may be found in a study of the antennas' directivity as a function of antenna separation. Whilst it is impossible to fully

describe the antennas' directivity without suitable antenna radiation patterns, it is possible to investigate their effective gain by examining the mean power they produce.

6.3.2.2 Mean power level and antenna gain comparison

Figure 6-9 presents the absolute mean power received by each of the two helical antennas used in EH1 and their average. Mean power level curves are shown for each measurement route as an average of the route's three walks. The handset was held with 'Antenna-A' preceding 'Antenna-B' in the forward direction of each walk.

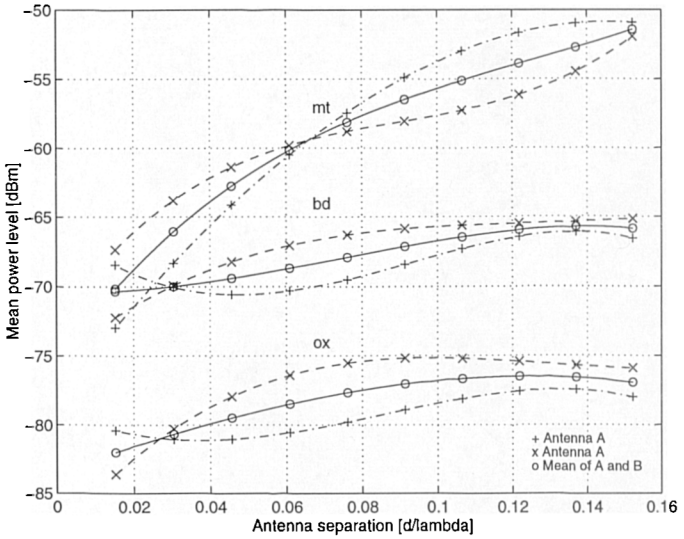

Figure 6-9: Antenna mean power as a function of antenna separation. All walks have been averaged.

The apparent reduction in effective antenna gain for both the "ox" and "bd" routes, which is not seen for the "mt" route, may be attributable to the operation of the helical antennas on the handset of EH1. Figure 4-6 of Chapter 4 shows an assembly drawing of EH1 with the lid removed. The body of the handset forms the lower arm of a dipole in which the helical antenna is the top arm. When the antennas are separated by distances greater than the base width of the body (70mm), the lower dipole arm is effectively "bent" out of line with the top arm due to the shape of the handset. This effect is most apparent when the handset is viewed from the side as shown in Fig. 4-6. The antenna currents flowing on the body of the handset under these conditions will affect the performance of the helical antenna and handset body as a dipole and hence reduce its gain. This effect will be less noticeable when the handset is viewed "edge-on" as happens for the "mt" route. Further experiments, beyond the scope of this immediate study, would be necessary to test this hypothesis.

6.3.2.3 Comparative antenna diversity gain

The comparative antenna diversity gains, plotted as a function of antenna separation, are shown in Figs. 6-10 to 6-12. In each figure, the diversity gain at the 1% and 10% probability level is shown as the average of the three walks for each measurement route. An additional theoretical trace, taken from the simulated diversity gain shown in Fig. 3-22 of Chapter 3 has been added to each figure for comparison.

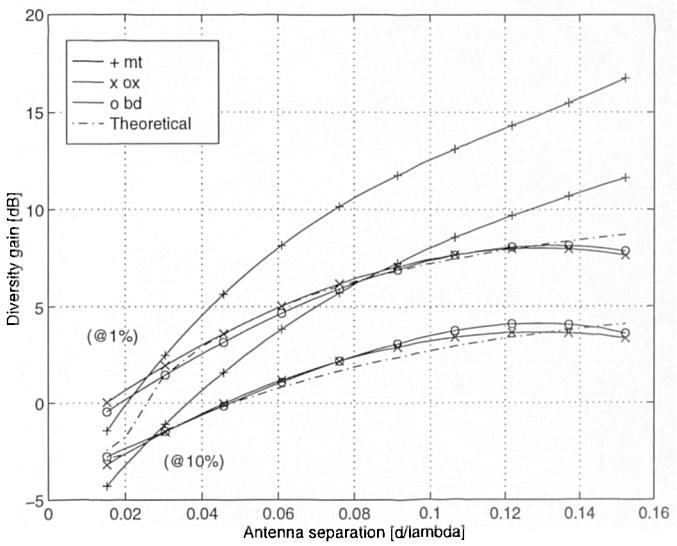

Figure 6-10: Diversity gain as a function of antenna separation for selection diversity. All walks have been averaged. A theoretical trace produced from simulations using dipole antennas, Rayleigh-fading data and similar signal selection techniques is included for comparison (see text).

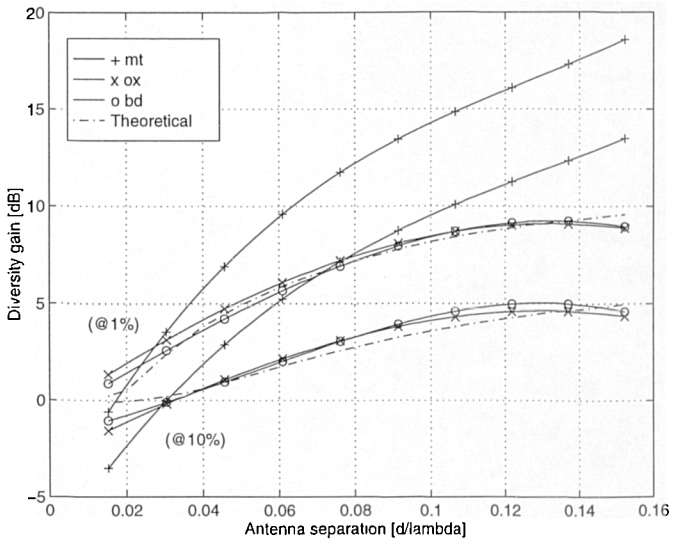

Figure 6-11: Diversity gain as a function of antenna separation for equal gain combining. All walks have been averaged. A theoretical trace produced from simulations using dipole antennas, Rayleigh-fading data and similar signal combining techniques is included for comparison (see text).

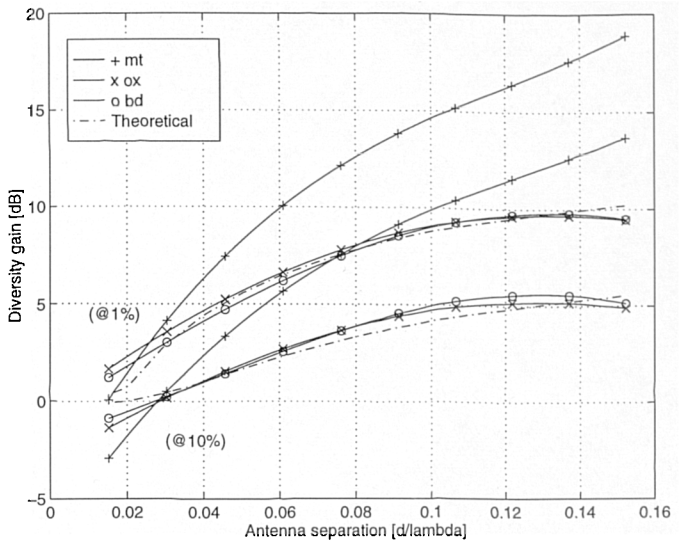

Figure 6-12: Diversity gain as a function of antenna separation for maximal ratio combining. All walks have been averaged. A theoretical trace produced from simulations using dipole antennas, Rayleigh-fading data and similar signal combining techniques is included for comparison (see text).

There is good agreement between the diversity gain computed from the measurement data for the "ox" and "bd" routes, and the curves produced using the simulation method described in Section 3.2.3.1 of Chapter 3. The reduction in diversity gain for antenna separations of $d>0.12\lambda$ is directly related to the reduction in effective antenna gain discussed earlier. This antenna gain effect, together with the non-Rayleigh signal distributions encountered in the "mt" route, are again evident in the diversity gain curves shown for this route.

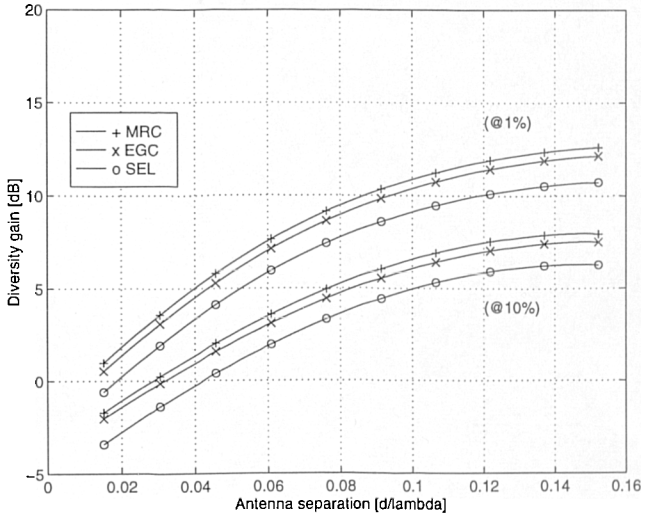

Figure 6-13: SEL, EGC and MRC diversity gain as a function of antenna separation. All routes and all walks have been averaged.

Figure 6-13 shows the diversity gain as a function of antenna separation at the 1% and 10% probability levels for the three methods of diversity selection or combining. The diversity

gain curves plotted are an average of all the walks and all of the routes. This "average of all averages" figure combines the very high diversity gain values of the "mt" route with the "ox" and "bd" values that reduce when the antenna separation is greater than 0.12λ.

6.3.2.4 Summary

For the "ox" and "bd" sets of measurement data, the computed values of signal correlation and diversity gain compare well with the values obtained from the simulation reported in Chapter 3. The similarity between the two signal correlation parameters for these measurement environments shows good agreement with eqn. (6-1).

In terms of both signal correlation and diversity gain, the "mt" measurement route data is in conflict with the results of Chapter 3. It should be remembered that the diversity gain calculation employed in the simulation method described in Chapter 3, assumed Rayleigh distributed fading data, dipole antennas in free-space and uniform wave arrival distributions. Further work is therefore needed to investigate the signal statistics experienced in the 'mt" LOS measurement environment.

6.3.3 Experimental Handsets EH2 and EH3

Experimental handsets EH2 and EH3 are described in Sections 4.3.2 and 4.3.3 of Chapter 4 A summary description is provided here for convenience. Both of the handsets comprise a top-mounted helical antenna and a side-mounted patch antenna. In EH2, the patch antenna is horizontally oriented whereas in EH3, the patch is vertically oriented.

The experimental results for the two handsets are tabulated in Tables 6-8 to 6-17. The tables are presented on consecutive pages to allow easier comparison between similar table entries. Tables 6-8 to 6-12 relate to EH2 and Tables 6-13 to 6-17 are associated with EH3. Each se of results contains the following: the signal correlation; the mean power produced by each antenna; and the computed diversity gains for the various methods of diversity combining. The table rows are ordered by measurement route, the columns by walk number, mean value and sample standard deviation.

Tables 6-8 to 6-12: Experimental Handset EH2

Table 6-8: Envelope and complex correlation for experimental handset EH2.

	ρ_e					$\lvert\rho_{12}\rvert^2$				
route	walk-1	walk-2	walk-3	mean	σ_{n-1}	walk-1	walk-2	walk-3	mean	σ_{n-1}
mt_f	-0.052	-0.337	-0.298	-0.229	0.155	0.150	0.030	0.209	0.130	0.091
mt_t	-0.102	-0.010	0.018	-0.031	0.063	0.401	0.420	0.569	0.463	0.092
ox	0.089	0.120	0.072	0.094	0.024	0.069	0.127	0.056	0.084	0.038
bd	0.271	0.267	0.190	0.243	0.046	0.155	0.155	0.153	0.154	0.001

Table 6-9: Branch mean signal levels for experimental handset EH2.

	Helical antenna mean power [dBm]					Patch antenna mean power [dBm]				
route	walk-1	walk-2	walk-3	mean	σ_{n-r}	walk-1	walk-2	walk-3	mean	σ_{n-r}
mt_f	-61.09	-63.87	-60.09	-61.68	1.96	-57.36	-56.77	-60.80	-58.31	2.18
mt_t	-54.09	-56.31	-54.72	-55.04	1.14	-56.84	-56.12	-56.70	-56.55	0.38
ox	-74.16	-74.69	-73.47	-74.11	0.61	-78.88	-78.00	-76.57	-77.82	1.16
bd	-64.32	-64.45	-64.60	-64.46	0.14	-69.08	-68.03	-67.64	-68.25	0.74

Table 6-10: SEL diversity gain for experimental handset EH2.

	Diversity gain for selection combining at the 1% probability level [dB]					Diversity gain for selection combining at the 10% probability level [dB]				
route	walk-1	walk-2	walk-3	mean	σ_{n-1}	walk-1	walk-2	walk-3	mean	σ_{n-1}
mt	13.03	13.92	12.32	13.09	0.80	9.55	9.68	8.07	9.10	0.89
ox	8.69	6.99	10.00	8.56	1.51	5.09	3.82	4.50	4.47	0.64
bd	7.88	7.59	7.56	7.68	0.17	3.54	3.85	4.17	3.85	0.32

Table 6-11: EGC diversity gain for experimental handset EH2

	Diversity gain for equal gain combining at the 1% probability level [dB]					Diversity gain for equal gain combining at the 10% probability level [dB]				
route	walk-1	walk-2	walk-3	mean	σ_{n-1}	walk-1	walk-2	walk-3	mean	σ_{n-1}
mt	13.46	14.95	13.36	13.92	0.89	10.93	10.83	8.97	10.24	1.11
ox	9.51	8.43	11.53	9.82	1.58	5.94	5.06	5.66	5.55	0.45
bd	8.86	8.34	8.36	8.52	0.30	4.62	4.84	5.31	4.92	0.36

Table 6-12: MRC diversity gain for experimental handset EH2.

	Diversity gain for maximal ratio combining at the 1% probability level [dB]					Diversity gain for maximal ratio combining at the 10% probability level [dB]				
route	walk-1	walk-2	walk-3	mean	σ_{n-1}	walk-1	walk-2	walk-3	mean	σ_{n-1}
mt	14.20	15.49	13.85	14.51	0.86	11.35	11.39	9.63	10.79	1.00
ox	10.15	8.74	11.84	10.25	1.55	6.55	5.50	6.19	6.08	0.53
bd	9.43	9.22	9.23	9.30	0.12	5.04	5.44	5.81	5.43	0.39

Tables 6-13 to 6-17: Experimental Handset EH3

Table 6-13: Envelope and complex correlation for experimental handset EH3.

	ρ_e					$\lvert\rho_{12}\rvert^2$				
route	walk-1	walk-2	walk-3	mean	σ_{n-1}	walk-1	walk-2	walk-3	mean	σ_{n-1}
mt_f	0.001	-0.076	-0.074	-0.050	0.044	0.143	0.187	0.266	0.198	0.062
mt_t	0.168	0.139	0.156	0.154	0.014	0.295	0.190	0.391	0.292	0.101
ox	-0.027	-0.028	-0.037	-0.031	0.006	0.042	0.046	0.027	0.038	0.010
bd	0.025	0.100	0.076	0.067	0.038	0.024	0.062	0.022	0.036	0.022

Table 6-14: Branch mean signal levels for experimental handset EH3.

	Helical antenna mean power [dBm]					Patch antenna mean power [dBm]				
route	walk-1	walk-2	walk-3	mean	σ_{n-1}	walk-1	walk-2	walk-3	mean	σ_{n-1}
mt_f	-59.56	-57.55	-57.59	-58.23	1.15	-63.91	-62.30	-64.02	-63.41	0.96
mt_t	-56.29	-56.43	-59.27	-57.33	1.68	-49.24	-48.48	-48.09	-48.60	0.58
ox	-75.42	-74.48	-74.48	-74.79	0.54	-76.11	-76.54	-76.34	-76.33	0.21
bd	-64.59	-64.77	-64.15	-64.50	0.32	-67.56	-66.29	-66.69	-66.85	0.65

Table 6-15: SEL diversity gain for experimental handset EH3.

	Diversity gain for selection combining at the 1% probability level [dB]					Diversity gain for selection combining at the 10% probability level [dB]				
route	walk-1	walk-2	walk-3	mean	σ_{n-1}	walk-1	walk-2	walk-3	mean	σ_{n-1}
mt	5.57	8.05	7.05	6.89	1.25	3.16	3.65	3.10	3.30	0.30
ox	9.95	10.74	11.29	10.66	0.68	5.71	5.59	5.11	5.47	0 32
bd	10.98	9.30	8.58	9.62	1.23	5.40	4.76	4.61	4.92	0.42

Table 6-16: EGC diversity gain for Experimental Handset EH3.

	Diversity gain for equal gain combining at the 1% probability level [dB]					Diversity gain for equal gain combining at the 10% probability level [dB]				
route	walk-1	walk-2	walk-3	mean	σ_{n-1}	walk-1	walk-2	walk-3	mean	σ_{n-1}
mt	6.77	9.32	8.09	8.06	1.27	4.18	4.75	4.23	4.39	0 32
ox	10.91	11.78	11.86	11.52	0.53	6.61	6.62	6.14	6 46	0 27
bd	12.16	9.89	9.41	10.49	1.47	6.63	5.76	5.54	5.97	0.58

Table 6-17: MRC combining diversity gain for experimental handset EH3.

	Diversity gain for maximal ratio combining at the 1% probability level [dB]					Diversity gain for maximal ratio combining at the 10% probability level [dB]				
route	walk-1	walk-2	walk-3	mean	σ_{n-1}	walk-1	walk-2	walk-3	mean	σ_{n-1}
mt	7.37	9.78	8.71	8.62	1.21	4.76	5.27	4.77	4.93	0.29
ox	11.54	12.22	12.55	12.10	0.52	7.12	7.18	6.65	6.98	0.29
bd	12.68	10.50	10.04	11.07	1.41	7.10	6.32	6.15	6.52	0.51

6.3.3.1 Signal correlation

For both handsets, the envelope correlation of the signals received in each measurement environment is low ($\rho_e \leq 0.243$). With the exception of the "mt" route, the similarity of the two correlation parameters for each walk is good and eqn. (6-1) is again confirmed.

6.3.3.2 Mean power level and antenna gain comparison

The mean powers produced by the helical antennas of EH2 and EH3 are similar to the mean powers produced by the helical antenna of the reference handset (Table 6-2 and 6-3). A comparison of the "mt_f" and "mt_t" routes (from and towards the transmitter respectively) indicate that the helical antenna of EH2 appears to be more affected by its orientation angle than the equivalent antenna of EH3. In the absence of suitable antenna radiation pattern information, an explanation of this effect would be conjectural and is thus avoided.

When comparing the effective gains of the two patch antennas, the values of XPR contained within Table 6-6 should be considered. For the "mt_f" route, the mean value of the horizontally polarized energy is approximately 13dB below the mean value of the vertically polarized energy. Experimental handsets EH2 and EH3 were held at a slant-angle, and as described in Section 6.2.3.3, their helical antennas in the "mt_f" environment therefore receive more horizontally polarized energy than vertically polarized energy The orthogonal-oriented patch antenna of EH2, because of the angle at which the handset is held, may thus be viewed as more vertically aligned than horizontally and is thus exposed to greater field energy than the helical antenna. This accounts for the +3.4dB effective gain increase between the helical and patch antennas of EH2 and the -5.2dB reduction seen for EH3.

6.3.3.3 Comparative antenna diversity gain

For the "mt" route, the comparative antenna diversity gain computed from the signals produced by the antennas of EH2 is greater than that for EH3. This is due to the effective gain difference between the patch antennas of the two handsets as discussed above.

The diversity gain for the "ox" route is approximately 1dB higher at the 1% probability level than for the "bd" route for both EH2 and EH3. Using the XPR figures of Table 6-6, this suggests that the handset antennas are exploiting the greater depolarization present in the "ox" route. This argument may be extended to explain the significantly lower levels of diversity gain seen for EH3 in the "mt" route.

6.3.4 Experimental Handset EH5

A description of the split feed experimental handset (EH5) was given in Section 4.3.5 of Chapter 4. This handset was designed to utilize the single helical antenna and each of its two feeds as individual diversity branches. The terminology of "straight branch" and "bent branch" appears in the following tables and refers to the mechanical arrangement of the semi-rigid coaxial feeds as illustrated in Fig. 4-13 of Chapter 4.

The effect of the user's hand upon the antenna currents flowing over the feeds was of particular practical and constructional interest. Two sets of experiments were thus performed: "hand-high" and "hand-low". In the first set of experiments, the hand was held around the top half of the handset and thus visibly obscured the antenna feeds. In the second set, the hand was held around the lower half of the handset and did not therefore obscure the antenna feeds. The results for the "hand-high" set of experiments are presented in Tables 6-18 to 6-22 and for the "hand-low" set, in Tables 6-23 to 6-27. Both sets of data are discussed together in the following sub-sections.

6.3.4.1 Signal correlation

For the "ox" and "bd" measurement routes, similarity between the envelope and complex correlation parameters is again observed. The envelopes of the signals for all routes are sufficiently decorrelated and may thus be used in a diversity receiver system. For different hand positions, the irregular variation in envelope correlation for the same route, suggests that the interaction of the user's hand and head is complex. In the absence of additional antenna characterization data, an explanation of these effects is impossible.

6.3.4.2 Mean power level and antenna gain comparison

With the hand in the "high" position, the mean power level produced by the "straight branch" is approximately 5.5dB to 9.8dB lower than when the hand is in the "low" position. This suggests that the "straight branch" feed connected to the helical antenna is acting as the lower arm of a dipole. Using the mean power levels for the helical antenna shown in Table 6-3 and the method described in Section 6.3.3.2, the effective gain of the "straight branch" with the hand in the "high" position is in the range of -14.8dBi to -19.2dBi. With the hand in the "low" position, the gain increases into the range of -6.0dBi to -9.7dBi.

For the "bent branch", the mean power level differs with the mean power of the "straight branch" by -6.6dB to 2.0dB with the hand in the "high" position and by -1.1dB to -7.8dB with the hand in the "low" position.

The complex variation of the mean power associated with each branch and hand position, suggests the existence of strong inter-operation between the two branches. This argument is supported by the poor branch-to-branch isolation of -3.1dB shown in Table 4-2 of Chapter 4.

6.3.4.3 Comparative antenna diversity gain

Of all the experimental handsets, the comparative antenna diversity gain figures for EH5 show the greatest amount of variation. The sample standard deviation figures of Tables 6-20 to 6-22 (for the "hand-high" position) and of Tables 6-25 to 6-27 (for the "hand-low' position) vary in the range of 0.6dB to 2.0dB and 0.8dB to 3.2dB respectively. Similar variations are not seen in either the mean power levels or the signal correlation parameters

With the hand in the "low" position, the mean power level produced by the "straight branch" is approximately 4dB greater than the reference branch for the "mt" route. This increase is reflected in the diversity gain figures for the same route.

The diversity gain figures, while appearing low compared to the other handsets are never below zero at the 1% probability level. This suggests that the concept of a split-feed antenna arrangement is practical and that with suitable improvement would yield an effective handset design.

Tables 6-18 to 6-22:Experimental Handset EH5 with Hand in 'High' Position

Table 6-18: Envelope and complex correlation for EH5 ('Hand High' Position).

	ρ_e					$\lvert\rho_{12}\rvert^2$				
route	walk-1	walk-2	walk-3	mean	σ_{n-1}	walk-1	walk-2	walk-3	mean	σ_{n-1}
mt_f	0.457	0.399	0.296	0.384	0.081	0.675	0.626	0.677	0.659	0.029
mt_t	0.143	0.303	0.136	0.194	0.095	0.379	0.561	0.810	0.583	0.216
ox	0.054	0.114	0.180	0.116	0.063	0.171	0.182	0.202	0.185	0.016
bd	0.624	0.414	0.422	0.487	0.119	0.615	0.449	0.477	0.514	0.089

Table 6-19: Branch mean signal levels for EH5 ('Hand-High' Position).

	'Straight branch' antenna mean power [dBm]					'Bent branch' antenna mean power [dBm]				
route	walk-1	walk-2	walk-3	mean	σ_{n-1}	walk-1	walk-2	walk-3	mean	σ_{n-1}
mt_f	-60.19	-62.81	-66.63	-63.21	3.24	-67.37	-71.29	-70.85	-69.84	2.15
mt_t	-61.02	-63.10	-64.95	-63.02	1.97	-63.85	-60.81	-58.89	-61.18	2.50
ox	-91.05	-88.13	-91.67	-90.28	1.89	-90.14	-89.68	-89.39	-89.74	0.38
bd	-72.62	-75.17	-76.35	-74.72	1.90	-72.71	-72.87	-72.74	-72.77	0.08

Table 6-20: SEL diversity gain for experimental handset EH5 ('Hand-High' Position).

	Diversity gain for selection combining at the 1% probability level [dB]					Diversity gain for selection combining at the 10% probability level [dB]				
route	walk-1	walk-2	walk-3	mean	σ_{n-1}	walk-1	walk-2	walk-3	mean	σ_{n-1}
mt	7.06	4.55	6.29	5.96	1.29	1.40	-0.62	1.74	0.84	1.27
ox	1.27	-1.35	2.52	0.81	1.97	-4.12	-4.60	-3.17	-3.96	0.73
bd	1.14	2.06	2.14	1.78	0.56	-3.67	-3.00	-3.22	-3.30	0 34

Table 6-21: EGC diversity gain for experimental handset EH5 ('Hand-High' Position)

	Diversity gain for equal gain combining at the 1% probability level [dB]					Diversity gain for equal gain combining at the 10% probability level [dB]				
route	walk-1	walk-2	walk-3	mean	σ_{n-1}	walk-1	walk-2	walk 3	mean	σ_{n}
mt	7.84	5.27	7.65	6.92	1.43	2.30	0.11	3.20	1.87	1.59
ox	2.44	-0.07	3.68	2.02	1.91	-2.99	-3.63	-2.13	-2.92	0.75
bd	1.85	2.94	2.92	2.57	0.62	-2.75	-2.24	-2.45	-2.48	0.26

Table 6-22: MRC diversity gain for experimental handset EH5 ('Hand-High' Position).

	Diversity gain for maximal ratio combining at the 1% probability level [dB]					Diversity gain for maximal ratio combining at the 10% probability level [dB]				
route	walk-1	walk-2	walk-3	mean	σ_{n-1}	walk-1	walk-2	walk-3	mean	σ_{n-1}
mt	8.59	6.02	8.10	7.57	1.37	2.83	0.77	3.59	2.39	1.46
ox	2.92	0.27	4.24	2.48	2.02	-2.49	-3.01	-1.61	-2.37	0.70
bd	2.53	3.46	3.51	3.17	0.55	-2.22	-1.67	-1.86	-1.91	0.28

Tables 6-23 to 6-27: Experimental Handset EH5 with Hand in 'Low' Position

Table 6-23: Envelope and complex correlation for EH5 ('Hand-Low' Position).

	ρ_e					$\lvert\rho_{12}\rvert^2$				
route	walk-1	walk-2	walk-3	mean	σ_{n-1}	walk-1	walk-2	walk-3	mean	σ_{n-1}
mt_f	0.443	0.493	0.094	0.343	0.218	0.752	0.879	0.781	0.804	0.066
mt_t	0.791	0.450	0.865	0.702	0.222	0.562	0.656	0.667	0.628	0.058
ox	0.329	0.421	0.316	0.355	0.057	0.311	0.368	0.329	0.336	0.029
bd	0.486	0.485	0.471	0.481	0.008	0.482	0.374	0.509	0.455	0.072

Table 6-24: Branch mean signal levels for EH5 ('Hand-Low' Position).

	'Straight branch' antenna mean power [dBm]					'Bent branch' antenna mean power [dBm]				
route	walk-1	walk-2	walk-3	mean	σ_{n-1}	walk-1	walk-2	walk-3	mean	σ_{n-1}
mt_f	-52.77	-54.27	-56.11	-54.38	1.67	-60.80	-60.87	-62.41	-61.36	0.91
mt_t	-55.88	-58.57	-57.13	-57.20	1.35	-63.67	-66.05	-65.29	-65.00	1.21
ox	-79.47	-81.42	-80.63	-80.51	0.98	-83.77	-84.81	-84.32	-84.30	0.52
bd	-67.91	-68.40	-67.48	-67.93	0.46	-68.50	-70.36	-68.24	-69.03	1.16

Table 6-25: SEL diversity gain for experimental handset EH5 ('Hand-Low' Position).

	Diversity gain for selection combining at the 1% probability level [dB]					Diversity gain for selection combining at the 10% probability level [dB]				
route	walk-1	walk-2	walk-3	mean	σ_{n-1}	walk-1	walk-2	walk-3	mean	σ_{n-1}
mt	13.81	9.68	14.09	12.53	2.47	8.53	6.14	9.40	8.02	1.69
ox	5.47	1.05	7.23	4.58	3.19	0.41	-2.57	0.78	-0.46	1 83
bd	3.50	5.24	4.87	4.54	0.91	-0.21	-0.54	0.52	-0.07	0.54

Table 6-26: EGC diversity gain for experimental handset EH5 ('Hand-Low' Position).

	Diversity gain for equal gain combining at the 1% probability level [dB]					Diversity gain for equal gain combining at the 10% probability level [dB]				
route	walk-1	walk-2	walk-3	mean	σ_{n-1}	walk-1	walk-2	walk-3	mean	σ_{n-1}
mt	14.63	11.28	15.48	13.79	2.22	8.81	7.05	10.20	8 68	1 58
ox	6.28	2.02	8.05	5.45	3.10	1.04	-1.60	1.64	0.36	1.72
bd	4.33	5.57	5.77	5.22	0.78	0.32	-0.05	1.65	0.64	0.89

Table 6-27: MRC diversity gain for experimental handset EH5 ('Hand Low' Position).

	Diversity gain for maximal ratio combining at the 1% probability level [dB]					Diversity gain for maximal ratio combining at the 10% probability level [dB]				
route	walk-1	walk-2	walk-3	mean	σ_{n-1}	walk-1	walk-2	walk-3	mean	σ_{n-1}
mt	15.32	11.74	15.83	14.30	2.23	9.53	7.55	10.72	9.27	1.60
ox	6.89	2.66	8.67	6.08	3.09	1.73	-1.11	2.26	0.96	1.81
bd	4.90	6.37	6.34	5.87	0.84	1.03	0.61	2.14	1.26	0.79

6.3.5 Experimental Handset EH6

The two-piece experimental handset (EH6) introduced in Section 4.3.6 of Chapter 4 comprises a belt-worn unit a lapel-worn unit. Each unit is fitted with a helical antenna

6.3.5.1 Signal correlation

For all the routes shown in Table 6-28, the correlation of the envelopes of the signals is very low ($\rho_e \leq 0.109$). This is to be expected for two reasons. Firstly, the two antennas are separated by a relatively large distance in the vertical plane ($\approx 1\lambda$). Secondly, the attenuation effect of the user's body, to waves arriving from certain directions, affects the wave arrival distribution seen by each antenna. This effectively creates a pair of directional antennas whose main lobes point in opposite directions.

6.3.5.2 Mean power level and antenna gain comparison

Comparing the mean power levels of Table 6-29 with the reference antenna mean power levels reported in Table 6-3, it may be stated that the lapel-worn helical antenna of EH6 exhibits similar effective antenna gains for the "ox" and "bd" routes. The belt-worn helical antenna also exhibits similar effective antenna gain for the "bd" route but approximately 3.6dB more for the "ox" route.

The aforementioned attenuation effect of the user's body is illustrated by comparing the mean power level difference of the signals produced by the belt-worn helical antenna and the lapel-worn helical antenna in the Mount Pleasant measurement environment. For walks in a direction away from the transmitter, the mean power level difference is 16.13dB Walks in the opposite direction, that is towards the transmitter, exhibit mean power level differences of 14.52dB. The body may therefore be considered to attenuate waves at 450MHz by approximately 15.3dB.

6.3.5.3 Comparative antenna diversity gain

Tables 6-30 to 6-32 contain the comparative antenna diversity gain figures for EH6. The combination of essentially zero signal correlation and signal mean power levels that are in some instances much greater than that of the reference antenna, yield very high diversity gain figures, sometimes in excess of the theoretical maximum values shown in Fig. 3-32 of Chapter 3.

Tables 6-28 to 6-32: Experimental Handset EH6

Table 6-28: Envelope and complex correlation for experimental handset EH6.

	ρ_e					$\lvert\rho_{12}\rvert^2$				
route	walk-1	walk-2	walk-3	mean	σ_{n-1}	walk-1	walk-2	walk-3	mean	σ_{n-1}
mt_f	0.144	-0.131	0.087	0.033	0.145	0.568	0.545	0.450	0.521	0.062
mt_t	0.104	0.096	0.126	0.109	0.015	0.380	0.357	0.410	0.383	0.027
ox	-0.006	0.101	0.170	0.089	0.089	0.017	0.013	0.011	0.014	0.003
bd	0.078	-0.042	-0.023	0.004	0.064	0.001	0.003	0.006	0.003	0.002

Table 6-29: Branch mean signal levels for experimental handset EH6.

	Lapel unit antenna mean power [dBm]					Belt unit antenna mean power [dBm]				
route	walk-1	walk-2	walk-3	mean	σ_{n-1}	walk-1	walk-2	walk-3	mean	σ_{n-1}
mt_f	-65.51	-65.86	-68.43	-66.60	1.60	-50.01	-50.10	-51.32	-50.47	0.73
mt_t	-46.54	-46.13	-46.76	-46.48	0.32	-59.69	-61.70	-61.61	-61.00	1.14
ox	-76.09	-75.76	-76.10	-75.98	0.19	-72.78	-71.69	-72.57	-72.35	0.58
bd	-63.40	-63.74	-62.90	-63.35	0.42	-62.90	-62.92	-62.65	-62.82	0 15

Table 6-30: SEL diversity gain for experimental handset EH6.

	Diversity gain for selection combining at the 1% probability level [dB]					Diversity gain for selection combining at the 10% probability level [dB]				
route	walk-1	walk-2	walk-3	mean	σ_{n-1}	walk-1	walk-2	walk-3	mean	σ_{n-1}
mt	18.73	17.30	19.79	18.61	1.25	11.97	10.95	14.12	12.35	1 62
ox	12.09	11.42	10.86	11.46	0.62	7.23	7.24	5 84	6.77	0.80
bd	11.52	10.16	11.86	11.18	0.90	7.67	7.51	7.91	7.70	0.20

Table 6-31: EGC diversity gain for experimental handset EH6.

	Diversity gain for equal gain combining at the 1% probability level [dB]					Diversity gain for equal gain combining at the 10% probability level [dB]				
route	walk-1	walk-2	walk-3	mean	σ_{n-1}	walk-1	walk-2	walk-3	mean	σ_{n-1}
mt	19.00	17.61	19.85	18.82	1.13	11.87	11.37	14.11	12.45	1 46
ox	12.40	12.26	11.74	12.14	0.35	8.12	7.79	6.60	7.50	0.80
bd	12.51	11.34	12.96	12.27	0.84	8.65	8.12	8.76	8.51	0.34

Table 6-32: MRC diversity gain for experimental handset EH6.

	Diversity gain for maximal ratio combining at the 1% probability level [dB]					Diversity gain for maximal ratio combining at the 10% probability level [dB]				
route	walk-1	walk-2	walk-3	mean	σ_{n-1}	walk-1	walk-2	walk-3	mean	σ
mt	19.93	18.70	21.01	19.88	1.15	12.90	12.28	15.20	13.46	1 54
ox	13.20	12.94	12.40	12.85	0.41	8.68	8.49	7.29	8.15	0.75
bd	13.25	11.75	13.54	12.85	0.96	9.26	8.73	9.38	9.13	0.35

6.4 Discussion

A varicty of antenna diversity experiments have been performed to dctermine the signal correlation, mean signal level and diversity gain that may be achieved using various combining techniques. Antennas mounted on a range of experimental handsets that employ either spatial, pattern or polarization diversity, or combinations of the three, were used.

For the spatial diversity experiments, it has been shown that significant diversity gains can be realized using closely spaced helical antennas at separations much less than those predicted using the established field autocorrelation model of Clarke [2]. Moreover, the experimental results show good agreement with both the antenna correlation and diversity gain predictions made using the antenna correlation analysis method described in Chapter 3.

The cross-polar coupling ratio for each measurement environment has been calculated. For "cluttered" environments with many close-in local scatterers, the XPR is observed to be approximately 7dB less than for the less crowded or "open" environments. The figures show good agreement with similar work reported by Vaughan (see Table 2-1 of Chapter 2).

It is evident from some of the peculiarities in the results that the interaction of the antenna, the handset, and the user's head, hand and body, is complex. In the absence of suitable antenna pattern information, conjectural explanations of such peculiarities have been avoided. The design of radio handsets and handset antennas for practical use would thus require a considerable investigation of these effects.

Using a method of comparison, the effective antenna gain was found to be in the range of -5dBi to -11dBi for the helical antennas, -5dBi to -15dBi for the patch antennas and -6dBi to -19dBi for the split-feed antennas. The antenna gain, in linear units, is the product of its directivity and radiation efficiency. Assuming an average directivity of 1.76dBi for all antennas, the radiation efficiency is in the range of 6-22% for the helical antennas, 2-22% for the patch antennas and 1-18% for the split-feed antennas.

The computed diversity gain figures produced by the various antenna arrangements may be used to objectively rank the handsets into a performance league table. Along with the objective measures, subjective grades may also be attributed to each design. An RF design robustness figure may therefore be used to describe the handset in terms of its radio frequency performance. This subjective parameter encompasses VSWR bandwidth, inter-antenna port isolation and the antenna's sensitivity to the user. A final practicality measure

describes the handset's operational effectiveness. This is perhaps the most subjective measure since consideration must be given to the handset's attractiveness to a potential user. The two-piece unit, EH6, may be quite acceptable as part of standard issue equipment for police officers but is hardly appropriate for a civilian mobile telephone user.

The objective and subjective measures are listed in Table 6-33. For each handset in the table, the performance measures are summed with equal weight to yield an overall performance rating.

Table 6-33: Experimental handset performance measures and rating.

Measure	Experimental handset star-rating.				
	EH1 Horizontal spatial	EH2 V. helical H. patch	EH3 V. helical V. patch	EH5 Split-feed antenna	EH6 Two-piece unit
Diversity performance	★/★★★	★★★	★★★★	★	★★★★★
RF design robustness	★★★★	★★★	★★★	★★	★★★★★
Operational usefulness	★★★	★★★★	★★★★	★★★★★	★★
Total score and position	8-10: 4th	10: 3rd	11: 2nd	8: 5th	12: 1st

The above table suggests that the two-piece unit of EH6 outperforms the other experimental handsets while the split-feed antenna design of EH5 performs worst of all. It is interesting to observe the trend illustrated in the table, namely the association of diversity performance with RF design robustness. This indicates that the single external antenna design of EH5 should match the performance of the two-piece unit upon appropriate optimization.

The work presented here has demonstrated that significant antenna diversity is achievable at 450MHz for hand-held mobile radio applications. Similar techniques may be used at higher frequencies.

6.5 References

1. BECKMAN, P., 1964, "Amplitude probability distribution of atmospheric radio noise", J. Res. Nat. Bur. Stand., Vol-68D, No. 6, pp723-36.

2. CLARKE, R.H., 1968, "A Statistical Theory of Mobile-Radio Reception", Bell Sys. Tech. J., Vol-47, pp957-1000.

3. HILL, C, and KNEISEL, T., 1991, "Portable Radio Antenna Performance in the 50, 450, 800, and 900 MHz Bands "Outside" and In-Vehicle", IEEE Trans. On Veh. Tech., Vol. VT-40, No. 4, pp750-756.

7
Conclusions

7.1 Preamble

A variety of approaches have been taken in the investigation of antenna diversity for hand-portable radio in this thesis. These have included: a literature search of approximately eighty relevant papers; over twelve thousand computer simulations of antenna diversity systems; and an experimental campaign containing 10km worth of measurement data collected *à pied.*

Throughout each chapter, points of discussion, summaries, and proposals for further work have been given where appropriate. This final chapter rephrases some of the previous conclusions and presents a second distillation of their essence. In addition, items worthy of continued study and new subject areas deserving attention are discussed.

7.2 Distillation

Chapter 1 introduced the contents of this thesis and described its structure. In Chapter 2, multipath propagation and fading were outlined prior to a more general discussion of the mathematical models available for their prediction. Antenna diversity was then introduced as a natural method for combating fading. Through the compilation of published experimental results, it was demonstrated that the classical field autocorrelation model, which has become established and accepted for use in base station antenna diversity calculations, is an inadequate tool for the prediction of the signal correlation associated with closely spaced antennas found in hand-held radio products. The requirement for an alternative modelling method was thus illustrated.

For reasons of clarity, the mathematical component of Chapter 3 was revealed separately in Appendix A whereupon the relationship between field, signal and antenna correlation was exposed. It was shown that under certain field phase conditions (typical of the mobile radio propagation channel), the correlation between two antenna far field radiation patterns is equal to the correlation between the deviations of the signal magnitudes from their means produced

at the terminals of the antennas. This mathematical device was applied to the so-called antenna correlation analysis method developed in Chapter 3.

A simplified parallel dipole configuration was employed in an investigation of antenna diversity in Chapter 3. It was shown that the antenna correlation is not only a function of the antenna separation but also of the angular distribution of the incoming plane waves and the impedances in which the antennas are terminated. For small horizontal antenna separations, lower levels of antenna correlation are predicted using the new analysis technique than with the established field autocorrelation model. This is due to the mutual coupling of the antennas affecting their combined radiation pattern and is achieved at the expense of reduced antenna radiation efficiency. The antenna correlation may be further reduced or optimized through the termination of the antennas in matched impedance loads.

Graphical visualization techniques were used to expose the radiation mechanisms affecting the antenna correlation. Three dimensional Cartesian figures combined with colour phase information were thus developed in the form of correlation integrand plots.

Using selection, equal gain and maximal ratio diversity combining systems, the improvements in mean signal level were computed from sequences of Rayleigh distributed fading data. The statistics of the data were controlled in relationship to the correlation and radiation efficiency of the closely spaced dipoles. Diversity gain surfaces were thus produced as a function of antenna separation.

In order to confirm some of the conclusions formed in Chapters 2 and 3, an experimental measurement campaign was designed. In association with such measurements, the requirements of an idealized antenna correlation measuring system were given in Chapter 4. In the same chapter, a two-branch quadrature demodulation receiver architecture was presented. The receiver employs inexpensive crystal controlled local oscillators and yet ensures phase tracking between the branches through oscillator commonality. In addition to the measurement system, a number of experimental handsets were designed to de ermine certain properties of the radio channel and to serve as product prototypes.

The details of the experimental campaign were given in Chapter 5. Line-of-sight, partial line of-sight and non-line-of-sight measurement routes were chosen within the precinct of The University of Liverpool to produce received signal distributions that were either Rayleigh like or non-Rayleigh-like. To enable a performance comparison to be made between handsets, an adaptation of the commonly accepted diversity gain measure was made. The o

called comparative antenna diversity gain relates the diversity gain of any particular handset to a common reference standard. In the context of this study, the signal produced by a single helical antenna mounted on a regular handset—a configuration currently used in many UHF hand-portable radio applications—was used as such a reference. Chapter 5 also detailed the data processing methods used for signal normalization, signal correlation and diversity gain calculation.

The results of the experimental campaign were analysed in Chapter 6. In the first section of the chapter, the theoretical work of Chapter 3 was compared with the measurement results for spatial diversity experiments. It was shown that the agreement between the two sets of data, in terms of both correlation and diversity gain, was excellent. This suggests that the antenna correlation analysis method is a powerful modelling tool for the prediction of the diversity gain achievable from any antenna configuration

In addition to the spatial diversity experiment, the results of investigations made using dipole-cum-loop antennas, helical and patch antennas, a split-feed antenna and a two-piece handset configuration were presented. The results for all the handsets were combined into a performance league table that includes both objective and subjective measures. Using a star-rating system, the league table succinctly illustrates the *pros and cons* of each design and thus shows that while the antenna diversity performance of certain designs is much less than that of others, the overall difference between scores is slight. This method of presentation allows both engineering and marketability comparisons to be made: the optimum handset-cum-antenna design being a compromise between the two.

7.3 Further work

Following on from some of the conclusions contained within the above distillation and from the individual chapters, it is appropriate to list items of future study or further work.

The cross-polar height dependency observed in the Mount Pleasant measurement route should be investigated further in both partial and non-line-of-sight environments. If greater wave depolarization is observed at waist height than at head height for all propagation environments, then the impact on handset antenna designs would be considerable.

In terms of both signal correlation and diversity gain calculation, the results obtained for experiments performed in the Mount Pleasant line-of-sight measurement route showed the

greatest level of sample variance. Moreover, the diversity gain figures were often several decibels in excess of those obtained for the other two routes. A detailed investigation of the signal statistics associated with this route would therefore be of benefit and would also serve as a starting point towards a study of signal correlation in non-Rayleigh distributed fields.

It is anticipated that many of the experimental results, for which satisfactory and non-conjectural explanations could not be found, may profit from a continued analysis in parallel with additional antenna far field information. The resources required for the production of such radiation patterns were not available during the course of this work.

The hand-portable radio is perhaps the most personalized piece of communication equipment in the world today. Its design cannot therefore be made in isolation of its application or deployment. The effects of the user on its performance (and vice versa for health and safety considerations) must therefore be recognised throughout its design process. The antenna correlation analysis method, as stated earlier, should thus be extended to incorporate models that include the effect of hand, head and body interactions.

A

Antenna Correlation and its Relationship to Field and Signal Correlation[1]

A.1 Introduction

The concept of correlation is relatively simple. The cross-correlation or normalized cross-covariance of two quantities a and b is defined as:

$$R_{ab} = \langle ab^* \rangle \qquad (A\text{-}1)$$

Where <...> denotes taking an average or expectation value. This quantity is often normalized to give:

$$\rho_{ab} = \frac{\langle ab^* \rangle}{\sqrt{\langle aa^* \rangle \langle bb^* \rangle}} \qquad (A\,2)$$

a and b may represent signal strengths, a stream of bits, field components, vector fields, antenna radiation patterns, envelopes of these quantities, or even the deviations of the means of these quantities. The averaging may be taken over time, a measurement path, or where appropriate, the stream of bits or the angles of the incident fields.

In fact their are so many choices for a and b and for the variable(s) to average over that there are a multitude of definitions of correlation, and discussions of "correlation" and antenna diversity are often confused. This appendix was written to alleviate some of the confusion. It provides an overview of many of the commonly used correlation definitions and points out their relations and similarities.

The formulas for antenna correlation are also generally poorly understood. While the antenna correlation formulas given in Section A-3 can be found throughout the literature, the

[1] This appendix first appeared in the report published by Leather and Massey [1].

author is unaware of any other publication that explains the mathematical relationship to the formulas for signal correlation. This relationship is explained in Sections A-8 and A-9.

A.2 Overview of Appendix's Contents

The appendix is arranged as follows:

- Section A.3 reviews the definition of antenna correlation.
- Section A.4 reviews the many definitions of field correlations.
- Section A.5 reviews the definitions of signal correlation and Section A.6 demonstrates some relations between the signal correlation definitions which are true when the signals are coming from antenna ports in multipath environments.
- Section A.7 contains a brief discussion of the relationship between field and signal correlation.
- The correlation of complex signals produced from two ports of an antenna arrangement can be derived in several ways. Two of these methods are described in Section A.8 and A.9:
  - Section A.8 gives a derivation which simplifies the expression for complex signal correlation in two steps. The first step assumes that the phases of the waves arriving from different directions are decorrelated. The second step uses the decorrelation between the polarizations of an incoming wave if the path is long enough.
  - Section A.9 gives a derivation which represents the incoming waves in terms of decorrelated real and imaginary components.

  Both of these derivations show that the antenna correlation defined in Section A.3 is proportional to the square of the magnitude of the signal correlation.
- The relationship between antenna correlation and complex signal correlation given in Sections A.8 and A.9 together with the relationships between signal correlations is sufficient to describe most forms of signal correlation in terms of the antenna correlation. However, the other forms of signal correlation could be expressed directly in terms of the antenna properties. Section A.10 looks at methods of expressing the

signal intensity correlation directly in terms of antenna parameters. The expressions are very complicated, and therefore rarely used.

- The main patterns of correlation definition and the relationships between them are summarized in Section A.11.

A.3 Antenna Correlation

The antenna correlation between two antenna configurations is defined as follows. Suppose that the electric field patterns of the two antennas are given by:

$$\mathbf{E}_1(\Omega) = E_{1\theta}(\Omega)\mathbf{a}_\theta(\Omega) + E_{1\phi}\mathbf{a}_\phi(\Omega) \qquad (A\,3)$$

$$\mathbf{E}_2(\Omega) = E_{2\theta}(\Omega)\mathbf{a}_\theta(\Omega) + E_{2\phi}\mathbf{a}_\phi(\Omega) \qquad (A\text{-}4)$$

where $\mathbf{a}_\theta$ and $\mathbf{a}_\phi$ are unit vectors associated with the Ω direction, E_{1_θ} and E_{1_ϕ} are the complex envelopes of the θ and ϕ components of the electric field pattern of the first antenna configuration, and E_{2_θ} and E_{2_ϕ} are the complex envelopes of the θ and ϕ components of the electric field pattern of the second antenna configuration and each pattern is with respect to the antenna configuration's origin.

Now let antenna configuration 1 be at the origin of an $\{r,\theta,\phi\} = \{r,\Omega\}$ spherical coordinat system, and let antenna configuration 2 be at a vector $\mathbf{d}$ in the coordinate system. The electric field pattern of configuration 1 is still given by eqn. (A-3), but the electric field pattern of configuration 2 is given by:

$$\tilde{\mathbf{E}}_2(\Omega) = \tilde{E}_{2\theta}(\Omega)\mathbf{a}_\theta(\Omega) + \tilde{E}_{2\phi}\mathbf{a}_\phi(\Omega) \qquad (A\,5)$$

where:

$$\tilde{\mathbf{E}}_{2\theta}(\Omega) = \tilde{E}_{2\theta}(\Omega)e^{-jk\mathbf{d}\bullet\mathbf{a}_r(\Omega)} \qquad (A\,6)$$

$$\tilde{\mathbf{E}}_{2\phi}(\Omega) = \tilde{E}_{2\phi}(\Omega)e^{-jk\mathbf{d}\bullet\mathbf{a}_r(\Omega)} \qquad (A\,7)$$

and $\mathbf{a}_r(\Omega)$ is the direction vector associated with Ω.

Let $P_\phi(\Omega)$ be the distribution with Ω of $\mathbf{a}_\phi$ polarized incoming waves. Let $P_\theta(\Omega)$ be the distribution with Ω of $\mathbf{a}_\theta$ polarized incoming waves. Then one can define the antenna correlation as:

$$\rho_a^2 = \frac{\left|\iint_\Omega \left(E_{1\theta}\tilde{E}_{2\theta}^* P_\theta + E_{1\phi}\tilde{E}_{2\phi}^* P_\phi\right) d\Omega\right|^2}{\iint_\Omega \left(E_{1\theta}E_{1\theta}^* P_\theta + E_{1\phi}E_{1\phi}^* P_\phi\right) d\Omega \iint_\Omega \left(\tilde{E}_{2\theta}\tilde{E}_{2\theta}^* P_\theta + \tilde{E}_{2\phi}\tilde{E}_{2\phi}^* P_\phi\right) d\Omega} \tag{A-8}$$

$$= \frac{\left|\iint_\Omega \left(E_{1\theta}E_{2\theta}^* P_\theta + E_{1\phi}E_{2\phi}^* P_\phi\right) e^{jk\mathbf{d}\bullet\mathbf{a}_r}\, d\Omega\right|^2}{\iint_\Omega \left(E_{1\theta}E_{1\theta}^* P_\theta + E_{1\phi}E_{1\phi}^* P_\phi\right) d\Omega \iint_\Omega \left(\tilde{E}_{2\theta}\tilde{E}_{2\theta}^* P_\theta + \tilde{E}_{2\phi}\tilde{E}_{2\phi}^* P_\phi\right) d\Omega} \tag{A-9}$$

Note that despite being called antenna correlation, this quantity is the *square* of the usual definition of correlation. The reason for using the square of the usual definition is explained in Section A.6.

The relationship between the above equations and the generalized definition eqn. (A-2) can be better seen if eqn. (A-8) is written as:

$$\rho_a^2 = \frac{\left\langle \mathbf{E}_1 \bullet (\tilde{\mathbf{E}}_2^* \mathbf{P})\right\rangle^2}{\left\langle \mathbf{E}_1 \bullet (\mathbf{E}_1^* \mathbf{P})\right\rangle \left\langle \tilde{\mathbf{E}}_2 \bullet (\tilde{\mathbf{E}}_2^* \mathbf{P})\right\rangle} = \frac{\left\langle \mathbf{E}_1\mathbf{p} \bullet (\tilde{\mathbf{E}}_2\mathbf{p})^*\right\rangle^2}{\left\langle \mathbf{E}_1\mathbf{p} \bullet (\mathbf{E}_1\mathbf{p})^*\right\rangle \left\langle \tilde{\mathbf{E}}_2\mathbf{p} \bullet (\tilde{\mathbf{E}}_2\mathbf{P})^*\right\rangle} \tag{A 10}$$

where $\mathbf{E}(\theta,\phi) = \{E_\theta, E_\phi\}$, $\mathbf{P}(\theta,\phi) = \{P_\theta, P_\phi\}$, $\mathbf{E}^*\mathbf{P} = \{E_\theta^* P_\theta, E_\phi^* P_\phi\}$, the averaging is done by integrating over the solid angle, and

$$\mathbf{p}(\Omega) = p_\theta(\Omega)\mathbf{a}_\theta(\Omega) + p_\phi(\Omega)\mathbf{a}_\phi(\Omega) \tag{A 11}$$

which represents the complex field components incident on the antenna.

There are a number of apparently alternative definitions of antenna correlation in the literature. In fact these are usually special cases of ρ_a^2, such as where the antennas are assumed to be co-polarized[2].

[2]See Massey [2] for examples.

A.4 Definitions of Field Correlation

There are a number of definitions of field correlation, many of which may be found in Clarke [3]. This section first reviews the definitions of correlation field components. Then the definitions of correlation between magnitudes of field components are reviewed. Finally a few of the most widely used relations between field correlations are discussed.

A.4.1 Correlations between Field Components

If $F=x+jy$ $(j=\sqrt{-1})$ is a field component, then there are the following definitions:

- ***The covariance of two fields***

$$R_F = \langle F_1^* F_2 \rangle \tag{A 12}$$

where $\langle \ldots \rangle$ denotes the average or expectation value.

- ***The normalized autocovariance function of the* x *and* y *random processes***

$$\rho = \frac{\langle x_1 x_2 \rangle}{\sqrt{\langle x_1^2 \rangle \langle x_2^2 \rangle}} = \frac{\langle y_1 y_2 \rangle}{\sqrt{\langle y_1^2 \rangle \langle y_2^2 \rangle}} \tag{A 13}$$

where $F_1=x_1+jy_1$ and $F_2=x_2+jy_2$.

- ***The normalized autocovariance function of two fields:***

$$\rho_F = \frac{\langle F_1^* F_2 \rangle}{\sqrt{\langle F_1^* F_1 \rangle \langle F_2^* F_2 \rangle}} \tag{A 14}$$

A.4.2 Correlations between Field Component Magnitudes

If $A=|F|=\sqrt{x^2+y^2}$, then there are the following definitions:

- ***The correlation of the magnitudes:***

$$R_A = \langle A_1 A_2 \rangle \tag{A 15}$$

- ***The correlation of the squared magnitudes:***

$$R_{A^2} = \left\langle A_1^2 A_2^2 \right\rangle \qquad \text{(A-16)}$$

- ***The normalized autocovariance function of the departure δA^2 of the squared magnitude A^2 from its mean:***

$$\rho_{\delta A^2} = \frac{\left\langle \left(A_1^2 - \overline{A}_1^2\right)\left(A_2^2 - \overline{A}_2^2\right)\right\rangle}{\sqrt{\left\langle \left(A_1^2 - \overline{A}_1^2\right)^2\right\rangle \left\langle \left(A_2^2 - \overline{A}_2^2\right)^2\right\rangle}} \qquad \text{(A-17)}$$

where $\overline{A}$ denotes the mean value of A.

- ***The normalized autocovariance function of the departure δA of the squared magnitude A from its mean:***

$$\rho_{\delta A} = \frac{\left\langle \left(A_1 - \overline{A}_1\right)\left(A_2 - \overline{A}_2\right)\right\rangle}{\sqrt{\left\langle \left(A_1 - \overline{A}_1\right)^2\right\rangle \left\langle \left(A_2 - \overline{A}_2\right)^2\right\rangle}} \qquad \text{(A 18)}$$

This is often expressed in the form:

$$\rho_{\delta A} = \frac{\left\langle A_1 A_2\right\rangle - \left\langle A_1\right\rangle\left\langle A_2\right\rangle}{\sqrt{\left\langle A_1^2\right\rangle - \left\langle A_1\right\rangle^2}\sqrt{\left\langle A_2^2\right\rangle - \left\langle A_2\right\rangle^2}}$$

$$= \frac{\overline{A_1 A_2} - \overline{A_1}\,\overline{A_2}}{\sqrt{\overline{A_1^2} - \overline{A_1}^2}\sqrt{\overline{A_2^2} - \overline{A_2}^2}} \qquad \text{(A-19)}$$

where again $\overline{}$ is an alternative way of denoting taking the average value. $\left(\overline{\ldots} = \langle \ldots \rangle\right)$

A.4.3 Relations between Field Correlation Definitions

For situations where:

$$\left\langle x_1 y_2\right\rangle = \left\langle x_2 y_1\right\rangle = 0 \qquad \text{(A 20)}$$

$$\left\langle x_1 x_2\right\rangle = \left\langle y_1 y_2\right\rangle \qquad \text{(A 21)}$$

Clarke [3] demonstrates a number of relations between his field correlation definitions. The most often quoted of these are the relations between ρ, $\rho_{\delta A}$ and $\rho_{\delta A^2}$:

$$\rho^2 \approx \rho_{\delta A} \approx \rho_{\delta A^2} \qquad \text{(A-22)}$$

One can also show that if eqns. (A-20) and (A-21) apply:

$$\rho_F \approx \rho \qquad \text{(A-23)}$$

$$R_{A^2} = 4\sigma^4 + R_F^2 \qquad \text{(A-24)}$$

where $\sigma = \langle x^2 \rangle = \langle y^2 \rangle$.

Equations (A-20) and (A-21) are true in many situations, and particularly when F_1 and F_2 represent the same field component displaced in time or space[3].

A.5 Signal Correlation Definitions

If V_1 and V_2 are the voltages detected at the two ports of the antenna configuration, then there are the following definitions:

- ***The (normalized) complex signal correlation***

$$\rho_{cs} = \frac{\langle V_1 V_2^* \rangle}{\sqrt{\langle |V_1|^2 \rangle \langle |V_2|^2 \rangle}} \qquad \text{(A 25)}$$

where $\langle \ldots \rangle$ is now a time averaging expectation value.

- ***The unnormalized signal amplitude correlation***

$$R_{As} = \langle |V_1||V_2| \rangle \qquad \text{(A 26)}$$

- ***The unnormalized signal intensity correlation***

$$R_{Is} = \langle |V_1|^2 |V_2|^2 \rangle \qquad \text{(A 27)}$$

[3]All of relations from eqns. (A-22) to (A-24) are derived by Clarke [3] using similar methods to those used in Section A.6.

- ***The normalized signal intensity correlation***

$$\rho_{Is} = \frac{\left\langle |V_1|^2 |V_2|^2 \right\rangle}{\sqrt{\left\langle |V_1|^4 \right\rangle \left\langle |V_2|^4 \right\rangle}} \qquad \text{(A-28)}$$

- ***The normalized correlation of the departures of the signal intensities from their means***

$$\rho_{\delta Is} = \frac{\left\langle \left(|V_1|^2 - \overline{|V_1|^2} \right) \left(|V_2|^2 - \overline{|V_2|^2} \right) \right\rangle}{\sqrt{\left\langle \left(|V_1|^2 - \overline{|V_1|^2} \right)^2 \right\rangle \left\langle \left(|V_2|^2 - \overline{|V_2|^2} \right)^2 \right\rangle}} \qquad \text{(A-29)}$$

- ***The normalized correlation of the departures of the signal magnitudes from their means***

$$\rho_{\delta |V|} = \frac{\left\langle \left(|V_1| - \overline{|V_1|} \right) \left(|V_2| - \overline{|V_2|} \right) \right\rangle}{\sqrt{\left\langle \left(|V_1| - \overline{|V_1|} \right)^2 \right\rangle \left\langle \left(|V_2| - \overline{|V_2|} \right)^2 \right\rangle}} \qquad \text{(A 30)}$$

Equations A-29 and A-30 are often referred to as the signal envelope correlations.

A.6 Signal Correlation Relations

Let

$$V_1 = x_{v1} + jy_{v1} \qquad \text{(A 31)}$$

$$V_2 = x_{v2} + jy_{v2} \qquad \text{(A 32)}$$

where x_{v1} and y_{v1} are the real and imaginary parts of V_1, and x_{v2} and y_{v2} are the real and imaginary parts of V_2. In the following derivations it will be assumed that:

1. x_{v1} , y_{v1} , x_{v2} and y_{v2} are zero-mean Gaussian random variables

$$\left\langle x_{v1} \right\rangle = \left\langle y_{v1} \right\rangle = \left\langle x_{v2} \right\rangle = \left\langle y_{v2} \right\rangle = 0 \qquad \text{(A-33)}$$

$$\left\langle x_{v1}^2 \right\rangle = \left\langle y_{v1}^2 \right\rangle = \sigma_{v1}^2 \qquad \text{(A 34)}$$

$$\left\langle x_{v2}^2 \right\rangle = \left\langle y_{v2}^2 \right\rangle = \sigma_{v2}^2 \qquad \text{(A 35)}$$

$$\langle x_{v1}x_{v2}\rangle = \langle y_{v1}y_{v2}\rangle \quad \text{(A-36)}$$

2. The real and imaginary components will be decorrelated:

$$\langle x_{v1}y_{v1}\rangle = \langle x_{v1}y_{v2}\rangle = \langle x_{v2}y_{v1}\rangle = \langle x_{v2}y_{v2}\rangle = 0 \quad \text{(A-37)}$$

This is true if V_1 and V_2 are Rayleigh distributed signals.

The normalized autocovariance function ρ_v of the x_v and y_v random processes can be defined in a manner analogous to that for ρ (eqn. (A-13)):

$$\rho_v = \frac{\langle x_{v1}x_{v2}\rangle}{\sqrt{\langle x_{v1}^2\rangle\langle x_{v2}^2\rangle}} = \frac{\langle y_{v1}y_{v2}\rangle}{\sqrt{\langle y_{v1}^2\rangle\langle y_{v2}^2\rangle}} \quad \text{(A-38)}$$

A.6.1 A Formula for ρ_{cs}

The numerator of eqn. (A-25) is:

$$\begin{aligned}\langle V_1V_2^*\rangle &= \langle (x_{v1}+jy_{v1})(x_{v2}+jy_{v2})\rangle \\ &= \langle x_{v1}x_{v2}+y_{v1}y_{v2}+j(x_{v2}y_{v1}-x_{v1}y_{v2})\rangle \\ &= 2\rho_v\sigma_{v1}\sigma_{v2}+j0\end{aligned} \quad \text{(A 39)}$$

Considering the denominator of eqn. (A-25):

$$\langle |V_1|^2\rangle = \langle x_{v1}^2+y_{v1}^2\rangle = 2\sigma_{v1}^2 \quad \text{(A-40)}$$

$$\langle |V_2|^2\rangle = \langle x_{v2}^2+y_{v2}^2\rangle = 2\sigma_{v2}^2 \quad \text{(A-41)}$$

Substituting into eqn. (A-25) gives:

$$\rho_{cs} = \frac{2\rho_v\sigma_{v1}\sigma_{v2}}{\sqrt{2\sigma_{v1}^2 2\sigma_{v2}^2}} = \rho_v \quad \text{(A-42)}$$

A.6.2 A Formula for R_{Is}

Substituting eqns. (A-31) and (A-32) into eqn. (A-27) gives:

$$\begin{aligned} R_{Is} &= \langle V_1 V_1^* V_2 V_2^* \rangle \\ &= \langle x_{v1}^2 x_{v2}^2 \rangle + \langle y_{v1}^2 y_{v2}^2 \rangle + \langle x_{v1}^2 y_{v2}^2 \rangle + \langle x_{v2}^2 x_{v1}^2 \rangle \end{aligned} \quad (A\text{-}43)$$

The terms on the right hand side of eqn. (A-43) may be evaluated by using the following formula—If x_1, x_2, x_3 and x_4 are real, zero-mean Gaussian random variables, then[4]:

$$\langle x_1 x_2 x_3 x_4 \rangle = \langle x_1 x_2 \rangle \langle x_3 x_4 \rangle + \langle x_1 x_3 \rangle \langle x_2 x_4 \rangle + \langle x_1 x_4 \rangle \langle x_2 x_3 \rangle \quad (A\text{-}44)$$

Using eqn. (A-44) together with eqns. (A-34) to (A-37) gives:

$$\langle x_{v1}^2 x_{v2}^2 \rangle = \langle y_{v1}^2 y_{v2}^2 \rangle = \sigma_{v1}^2 \sigma_{v2}^2 + 2\langle x_1 x_2 \rangle^2 \quad (A\text{-}45)$$

$$\langle x_{v1}^2 y_{v2}^2 \rangle = \langle x_{v2}^2 y_{v1}^2 \rangle = \sigma_{v1}^2 \sigma_{v2}^2 \quad (A\text{-}46)$$

Substituting these equations into eqn. (A-43) gives:

$$\begin{aligned} R_{Is} &= 4\sigma_{v1}^2 \sigma_{v2}^2 + 4\langle x_{v1} x_{v2} \rangle^2 \\ &= 4\sigma_{v1}^2 \sigma_{v2}^2 (1 + \rho_v^2) \end{aligned} \quad (A\ 47)$$

A.6.3 A Formula for ρ_{Is}

A formula for the numerator of eqn. (A-28) was derived in the last subsection. The denominator has expectation values of $|V_1|^4$ and $|V_2|^4$.

$$\langle |V_1|^4 \rangle = \langle (x_{v1}^2 + y_{v1}^2)^2 \rangle = \langle x_{v1}^4 + 2x_{v1}^2 y_{v1}^4 \rangle \quad (A\ 48)$$

The right hand side of eqn. (A-48) is evaluated using eqn. (A-44):

$$\langle x_{v1}^4 \rangle = 3\langle x_{v1}^2 \rangle \langle x_{v1}^2 \rangle = 3\sigma_{v1}^4 \quad (A\ 49)$$

$$\langle y_{v1}^4 \rangle = 3\langle y_{v1}^2 \rangle \langle y_{v1}^2 \rangle = 3\sigma_{v1}^4 \quad (A\ 50)$$

$$\langle x_{v1}^2 y_{v1}^2 \rangle = \langle x_{v1}^2 \rangle \langle y_{v1}^2 \rangle + 2(x_{v1} y_{v1})^2 = \langle x_{v1}^2 \rangle \langle y_{v1}^2 \rangle + 0 = \sigma_{v1}^4 \quad (A\ 51)$$

Substituting these relations into eqn. (A-48) gives:

[4]See Davenport *et al* [4].

$$\left\langle |V_1|^4 \right\rangle = 8\sigma_{v1}^2 \qquad \text{(A-52)}$$

The formula for $\langle |V_2|^4 \rangle$ is derived in a similar manner. Substituting this formula and eqns. (A-47) and (A-52) into eqn. (A-28) gives:

$$\begin{aligned} \rho_{Is} &= \frac{4\sigma_{v1}^2\sigma_{v2}^2(1+\rho_v^2)}{\sqrt{8\sigma_{v1}^4 2\sigma_{v2}^4}} \\ &= \frac{1+\rho_v^2}{2} \end{aligned} \qquad \text{(A-53)}$$

A.6.4 A Formula for $\rho_{\delta Is}$

First, consider the numerator of eqn. (A-29). Using eqns. (A-40), (A-41) and (A-47) gives:

$$\begin{aligned} \left\langle \left(|V_1|^2 - \overline{|V_1|^2} \right)\left(|V_2|^2 - \overline{|V_2|^2} \right) \right\rangle &= \left\langle |V_1|^2|V_2|^2 - 2\left(\sigma_{v1}^2|V_2|^2\right) + \sigma_{v2}^2|V_1|^2 + 4\sigma_{v1}^2\sigma_{v2}^2 \right\rangle \\ &= R_{Is} - 8\sigma_{v1}^2\sigma_{v2}^2 + 4\sigma_{v1}^2\sigma_{v2}^2 \\ &= 4\sigma_{v1}^2\sigma_{v2}^2\rho_v^2 \end{aligned} \qquad \text{(A 54)}$$

Now consider the denominator of eqn. (A-29):

$$\begin{aligned} \left\langle \left(|V_1|^2 - \overline{|V_1|^2} \right)^2 \right\rangle &= \left\langle |V_1|^4 - 4\sigma_{v1}^2|V_1|^2 + 4\sigma_{v1}^2 \right\rangle \\ &= \left\langle 8\sigma_{v1}^2 - 4\sigma_{v1}^2 2\sigma_{v1}^2 + 4\sigma_{v1}^4 \right\rangle \\ &= 4\sigma_{v1}^4 \end{aligned} \qquad \text{(A 55)}$$

By a similar argument:

$$\left\langle \left(|V_2|^2 - \overline{|V_2|^2} \right)^2 \right\rangle = 4\sigma_{v2}^4 \qquad \text{(A 56)}$$

Substituting eqns. (A-54), (A-55) and (A-56) into eqn (A-29) gives:

$$\rho_{\delta Is} = \frac{4\sigma_{v1}^2\sigma_{v2}^2\rho_v^2}{\sqrt{4\sigma_{v1}^4 4\sigma_{v2}^4}} = \rho_v^2 \qquad \text{(A 57)}$$

A.6.5 An Approximation for R_{As}

Clarke [3] and Lawson *et al* [5] state that:

$$R_{As} = \sigma_{v1}\sigma_{v2}\left(2E(\rho_v) - (1-\rho^2)K(\rho_v)\right) \qquad \text{(A-58)}$$

where K and E are the complex elliptic integrals of the first and second kind. In series form

$$R_{As} = \frac{\pi}{2}\sigma_{v1}\sigma_{v2}\left(1+\frac{\rho_v^2}{4}+\frac{\rho_v^4}{64}+\ldots\right) \qquad \text{(A 59)}$$

so that to a good approximation, neglecting powers of ρ_v higher than the second:

$$R_{As} \approx \frac{\pi}{2}\sigma_{v1}\sigma_{v2}\left(1+\frac{\rho_v^2}{4}\right) \qquad \text{(A 60)}$$

A.6.6 An Approximation for $\rho_{\delta|V|}$

As V_1 and V_2 are Gaussian functions with probability functions:

$$P(V) = \frac{1}{\sqrt{2\pi\sigma_v^2}}\exp\left(-\frac{x^2}{2\sigma_v^2}\right) \qquad \text{(A-61)}$$

then $|V_1|$ and $|V_2|$ have Rayleigh distribution functions [6,7]:

$$P(|V|) = \frac{V}{\sigma_v^2}\exp\left(-\frac{V^2}{2\sigma_v^2}\right) \qquad \text{(A 62)}$$

Evaluating $\overline{|V|}$ using this probability function gives:

$$\left\langle\overline{|V|}\right\rangle = \int_0^\infty VP(V)dV = \sqrt{\frac{\pi}{2}}\sigma_v \qquad \text{(A 63)}$$

Substituting eqns. (A-63) and (A-60) in the numerator of eqn. (A-30) gives:

$$\begin{aligned}\left\langle \left(|V_1| - \overline{|V_1|}\right)\left(|V_2| - \overline{|V_2|}\right)\right\rangle &= \left\langle |V_1||V_2| - \sqrt{\frac{\pi}{2}}\sigma_{v1}|V_2| - \sqrt{\frac{\pi}{2}}\sigma_{v2}|V_1| + \frac{\pi}{2}\sigma_{v1}\sigma_{v2}\right\rangle \\ &\approx \frac{\pi}{2}\sigma_{v1}\sigma_{v2}\left(1+\frac{\rho_v^2}{4}\right) - \frac{\pi}{2}\sigma_{v1}\sigma_{v2} - \frac{\pi}{2}\sigma_{v2}\sigma_{v1} + \frac{\pi}{2}\sigma_{v1}\sigma_{v2} \\ &= \frac{\pi}{8}\sigma_{v1}\sigma_{v2}\rho_v^2 \end{aligned} \quad \text{(A-64)}$$

In the denominator:

$$\begin{aligned}\left\langle \left(|V_1| - \overline{|V_1|}\right)^2\right\rangle^2 &= \left\langle |V_1|^2 - 2\sqrt{\frac{\pi}{2}}\sigma_{v1}|V_1|\right\rangle + \frac{\pi}{2}\sigma_{v1}^2 \\ &= 2\sigma_{v1}^2 - \pi\sigma_{v1}^2 + \frac{\pi}{2}\sigma_{v1}^2 \\ &= \left(2-\frac{\pi}{2}\right)\sigma_{v1}^2 \end{aligned} \quad \text{(A 65)}$$

$\left\langle \left(|V_2| - \overline{|V_2|}\right)\right\rangle$ gives a similar expression with the appropriate subscripts modified. Substituting these relations and eqn. (A-64) into eqn. (A-30) gives:

$$\rho_{\delta|V|} \approx \frac{\pi}{16-4\pi}\rho_v^2 \cong 0.9149\rho_v^2 \quad \text{(A 66)}$$

The coefficient is sufficiently near 1 to be able to say that:

$$\rho_{\delta|V|} \approx \rho_v^2 \quad \text{(A 67)}$$

A.7 Relationships between Field and Signal Correlation

The definitions of correlation for fields (Section A.4) are very similar to the definitions for signals (Section A.5). Therefore it could be expected that if two antennas detected two fields, then the (normalized) correlation between the signals would be the same as the (normalized) correlation between the fields, i.e. $\rho_{cs} = \rho_F$, $\rho_{\delta|V|} = \rho_{\delta A}$, $\rho_{\delta|V|} = \rho_{\delta A^2}$.

Unfortunately only the smallest field probing antennas detect distinct field components, and these antennas are two inefficient for normal transceiver applications. Practical antennas detect combinations of field components and these combinations are detected over an extended region of space. Therefore the signal correlation between practical antennas must be calculated taking this into account. The relation for the complex signal correlations between practical antennas is derived in the following two sections.

A.8 Complex Signal Correlation 1

The performance of an antenna diversity is largely determined by the correlation between the signals received by the two antennas.

In this section, the complex signal correlation between the signals received by two antennas arrangements is derived this gives a relation between complex signal correlation and antenna correlation. The derivation proceeds in the following way:

1. The antenna arrangements are thought of as being in a region where they are bombarded by plane waves. The complex signal correlation between the voltages at the antenna connectors is expressed in terms of the antenna arrangement's radiation patterns and the incoming planes received by the two antennas. (Equations (A-68) to (A-73).)

2. The phase variations of the plane waves imply that for a significantly long path of integration, the integrands in the expression for signal correlation involving integrations over two sets of angles (one set of angles for each of the antenna arrangements) simplify to integrations over one set of angles. (Equations (A 74) to (A-79).)

3. If the antenna arrangements are moved through different regions, then the phase relationships between cross-polarized incoming plane waves varies. Therefore the expectation values for cross-polar products is 0, and the expression for ρ_s simplifies to the square root of the expression for the antenna correlation, introduced in Section A.3.

A.8.1 Complex signal correlation expressed in terms of antenna field patterns and incoming plane waves

The complex signal correlation can be defined as:

$$\rho_{cs} = \frac{\langle V_1 V_2^* \rangle}{\sqrt{\langle |V_1|^2 \rangle \langle |V_2|^2 \rangle}} \qquad (A\ 68)$$

where V_1 and V_2 are the voltages detected at the two antenna configuration ports, and $\langle \ldots \rangle$ is now a time average expectation value.

$$V_1 = c_1 \iint_{\Omega} \left(E_{1\theta p\theta} + E_{1\phi p\phi} \right) d\Omega \qquad (A\ 69)$$

$$V_2 = c_2 \iint_{\Omega} \left(\tilde{E}_{2\theta p\theta} + \tilde{E}_{2\phi p\phi} \right) d\Omega \qquad (A\text{-}70)$$

where c_1 and c_2 are constants dependent on the port impedances, and the phase of p_θ and p are functions of the position of the antenna arrangements:

$$p_\theta(\Omega) = |p_\theta| e^{j(c_{p\theta} + k\mathbf{a}_r \bullet \mathbf{q})} \qquad (A\ 71)$$

$$p_\phi(\Omega) = |p_\phi| e^{j(c_{p\phi} + k\mathbf{a}_r \bullet \mathbf{q})} \qquad (A\ 72)$$

where $c_{p\theta}(\Omega)$ and $c_{p\phi}(\Omega)$ are the relative phase constants of the incoming waves, k is the wave-number, $\mathbf{a}_r$ is the direction vector associated with Ω, and $\mathbf{q}$ is the position vector of the local origin of the antenna arrangements.

Substituting eqns. (A-69) and (A-70) into eqn. (A-68) gives:

$$\rho_{cs} = \frac{\left\langle \left(c_1 \iint_{\Omega} \left(E_{1\theta p\theta} + E_{1\phi p\phi} \right) d\Omega \right) \left(c_2 \iint_{\Omega} \left(\tilde{E}_{2\theta p\theta} + \tilde{E}_{2\phi p\phi} \right) d\Omega \right)^* \right\rangle}{\sqrt{\left\langle \left| c_1 \iint_{\Omega} \left(E_{1\theta p\theta} + E_{1\phi p\phi} \right) d\Omega \right|^2 \right\rangle \left\langle \left| c_2 \iint_{\Omega} \left(\tilde{E}_{2\theta p\theta} + \tilde{E}_{2\phi p\phi} \right) d\Omega \right|^2 \right\rangle}} \qquad (A\ 73)$$

A.8.2 ρ_{cs} Simplifications for Averaging Across a Region

Consider the numerator of this expression:

$$\left\langle \left(c_1 \iint_\Omega \left(E_{1\theta p\theta} + E_{1\phi p\phi}\right) d\Omega\right)\left(c_2 \iint_\Omega \left(\tilde{E}_{2\theta p\theta} + \tilde{E}_{2\phi p\phi}\right) d\Omega\right)^* \right\rangle =$$

$$c_1 c_2^* \left\langle \iint_{\Omega'} \left(\iint_\Omega \begin{bmatrix} \left(E_{1\theta}(\Omega) p_\theta(\Omega)\right) + \left(E_{1\phi}(\Omega) p_\phi(\Omega)\right) \\ \left(\tilde{E}_{2\phi}(\Omega') p_\phi(\Omega')\right) + \left(\tilde{E}_{2\theta}(\Omega') p_\theta^*(\Omega')\right)^* \end{bmatrix} d\Omega \right) d\Omega' \right\rangle \qquad \text{(A-74)}$$

The products in the integrand have factors of the form $p_i(\Omega)p_j(\Omega')$, where $i, j = \theta, \phi$. Substituting in eqns. (A-71) and (A-72) shows that these factors are of the form:

$$p_i(\Omega) p_j(\Omega') = \left|p_i\right| \left|p_j\right| e^{j(c_{pi}(\Omega) + c_{pj}(\Omega'))} e^{jk(\mathbf{a}_r(\Omega) + \mathbf{a}_r(\Omega'))\bullet \mathbf{q}} \qquad \text{(A-75)}$$

If $\Omega \neq \Omega'$, then the phase of the last factor in eqn. (A-75) varies with $\mathbf{q}$. Thus over a sufficiently long its expectation value is 0. Therefore, for a sufficiently long path:

$$\left\langle p_\theta(\Omega) p_\theta^*(\Omega)\right\rangle \approx \left\langle p_\theta(\Omega) p_\phi^*(\Omega')\right\rangle \approx \left\langle p_\phi(\Omega) p_\theta^*(\Omega')\right\rangle \approx \left\langle p_\phi(\Omega) p_\phi^*(\Omega')\right\rangle \approx 0 \qquad \Omega \neq \Omega' \qquad \text{(A 76)}$$

Therefore in the limit of a sufficiently long path:

$$\left\langle \left(c_1 \iint_\Omega \left(E_{1\theta p\theta} + E_{1\phi p\phi}\right) d\Omega\right)\left(c_2 \iint_\Omega \left(\tilde{E}_{2\theta p\theta} + \tilde{E}_{2\phi p\phi}\right) d\Omega\right)^* \right\rangle \rightarrow$$

$$\left\langle c_1 c_2^* c_3 \iint_\Omega \begin{bmatrix} \left(E_{1\theta}(\Omega) p_\theta(\Omega)\right) + \left(E_{1\phi}(\Omega) p_\phi(\Omega)\right) \\ \left(\tilde{E}_{2\phi}(\Omega) p_\phi(\Omega)\right) + \left(\tilde{E}_{2\theta}(\Omega) p_\theta^*(\Omega)\right)^* \end{bmatrix} d\Omega \right\rangle \qquad \text{(A 77)}$$

where the factor c_3 is a function of the path length.

This expression can be written in a more compact form using eqns. (A-3), (A-5) and (A 11):

$$\left\langle \left(c_1 \iint_\Omega \left(E_{1\theta p\theta} + E_{1\phi p\phi}\right) d\Omega\right)\left(c_2 \iint_\Omega \left(\tilde{E}_{2\theta p\theta} + \tilde{E}_{2\phi p\phi}\right) d\Omega\right)^* \right\rangle =$$

$$\left\langle (c_1 \iint_\Omega \mathbf{E}_1 \bullet \mathbf{p}\, d\Omega)(c_2 \iint_\Omega \tilde{\mathbf{E}}_2 \bullet \mathbf{p}\, d\Omega)^* \right\rangle \rightarrow$$

$$\left\langle c_1 c_2^* c_3 \iint_\Omega \left[(\mathbf{E}_1 \bullet \mathbf{p})(\tilde{\mathbf{E}}_2 \bullet \mathbf{p})^*\right] d\Omega \right\rangle \qquad \text{(A 78)}$$

Similar simplifications can be applied to the denominator of eqn. (A-73) to give:

$$\rho_{cs} = \frac{c_1 c_2^* \left\langle \iint_\Omega \left[(\mathbf{E}_1 \bullet \mathbf{p})(\tilde{\mathbf{E}}_2 \bullet \mathbf{p})^* \right] d\Omega \right\rangle}{|c_1||c_2| \sqrt{\left\langle \iint_\Omega |\mathbf{E}_1 \bullet \mathbf{p}|^2 d\Omega \right\rangle \left\langle \iint_\Omega |\tilde{\mathbf{E}}_2 \bullet \mathbf{p}|^2 d\Omega \right\rangle}} \qquad \text{(A-79)}$$

A.8.3 ρ_{cs} Simplifications for Averaging Across Several Regions

Within a single region the relative phases of the incoming plane waves are fixed. However, when several regions are considered, the phase constants of the plane waves vary randomly from region to region. Therefore, when the expectation values of the factors in the integrands of eqn. (A-79) involving the products

$$p_\theta(\Omega) p_\phi^*(\Omega), \quad p_\phi(\Omega) p_\theta^*(\Omega) \qquad \text{(A 80)}$$

are evaluated over many regions, they have expectation values of 0. Substituting this simplification into eqn. (A-79) gives:

$$\rho_{cs} = \frac{c_1 c_2^* \left\langle \iint_\Omega (\mathbf{E}_1 \mathbf{p}) \bullet (\tilde{\mathbf{E}}_2 \mathbf{p}) d\Omega \right\rangle}{|c_1||c_2| \sqrt{\left\langle \iint_\Omega (\mathbf{E}_1 \mathbf{p})(\mathbf{E}_1 \mathbf{p})^* d\Omega \right\rangle \left\langle \iint_\Omega (\tilde{\mathbf{E}}_2 \mathbf{p})(\tilde{\mathbf{E}}_2 \mathbf{p})^* d\Omega \right\rangle}} \qquad \text{(A 81)}$$

$$= \frac{c_1 c_2^* \left\langle \iint_\Omega \mathbf{E}_1 \bullet (\tilde{\mathbf{E}}_2^* \mathbf{P}) d\Omega \right\rangle}{|c_1||c_2| \sqrt{\left\langle \iint_\Omega \mathbf{E}_1 \bullet (\mathbf{E}_1^* \mathbf{P}) d\Omega \right\rangle \left\langle \iint_\Omega \tilde{\mathbf{E}}_2 \bullet (\tilde{\mathbf{E}}_2^* \mathbf{P}) d\Omega \right\rangle}} \qquad \text{(A 82)}$$

where $\mathbf{P}(\Omega) = \{P_\theta(\Omega), P_\phi(\Omega)\} = \{|p_\theta|^2, |p_\phi|^2\}$ represents the power distribution of the incoming waves.

A.9 Complex Signal Correlation 2

This section gives an alternative derivation for ρ_{cs} to that described in the previous section. While the starting point is again eqns. (A-68), (A-69) and (A-70), now p_θ and p_ϕ are written as:

$$p_\theta(\Omega) = x_\theta(\Omega) + jy_\theta(\Omega) \quad \text{(A-83)}$$

$$p_\phi(\Omega) = x_\phi(\Omega) + jy_\phi(\Omega) \quad \text{(A 84)}$$

where x_θ and y_ϕ are the real and imaginary parts of p_θ, and x_ϕ and y_ϕ are the real and imaginary parts of p_ϕ. Due to the decorrelation and random phase of the incoming waves:

$$\langle x_\theta x_\phi \rangle = \langle y_\theta y_\phi \rangle = \langle x_\theta y_\theta \rangle = \langle x_\theta y_\theta \rangle \equiv 0 \quad \text{(A-85)}$$

$$\begin{aligned} \langle x_\theta(\Omega) x_\theta(\Omega') \rangle &= \langle y_\theta(\Omega) y_\theta(\Omega') \rangle = \\ \langle x_\phi(\Omega) x_\phi(\Omega') \rangle &= \langle y_\phi(\Omega) y_\phi(\Omega') \rangle \equiv 0, \qquad \Omega \neq \Omega' \end{aligned} \quad \text{(A-86)}$$

$$\langle (x_\theta(\Omega))^2 \rangle = \langle (y_\theta(\Omega))^2 \rangle = \sigma_\theta^2(\Omega) \quad \text{(A-87)}$$

$$\langle (x_\phi(\Omega))^2 \rangle = \langle (y_\phi(\Omega))^2 \rangle = \sigma_\phi^2(\Omega) \quad \text{(A-88)}$$

With these conditions:

$$\langle p_\theta(\Omega) p_\theta^*(\Omega') \rangle = \langle p_\theta(\Omega) p_\phi^*(\Omega') \rangle = \langle p_\phi(\Omega) p_\theta^*(\Omega') \rangle = \langle p_\phi(\Omega) p_\phi^*(\Omega') \rangle \equiv 0 \quad \text{(A 89)}$$
$$\Omega \neq \Omega'$$

$$\langle p_\theta(\Omega) p_\theta^*(\Omega) \rangle = \langle x_\theta^2(\Omega) y_\theta^2(\Omega) \rangle = 2\sigma_\theta^2(\Omega) \quad \text{(A 90)}$$

$$\langle p_\phi(\Omega) p_\phi^*(\Omega) \rangle = \langle x_\phi^2(\Omega) y_\phi^2(\Omega) \rangle = 2\sigma_\phi^2(\Omega) \quad \text{(A-91)}$$

Substituting eqns. (A-89), (A-90) and (A-91) into eqn. (A-73) gives eqn. (A-82), where:

$$\mathbf{P}(\Omega) = \{P_\theta(\Omega), P_\phi(\Omega)\} = \{|p_\theta|^2, |p_\phi|^2\} - \{2\sigma_\theta^2, 2\sigma_\phi^2\} \quad \text{(A 92)}$$

A.10 Signal Intensity Correlations

The correlation between signal intensities can be defined as:

$$\rho_{ls} = \frac{\left\langle |V_1|^2 |V_2|^2 \right\rangle}{\sqrt{\left\langle |V_1|^4 \right\rangle \left\langle |V_2|^4 \right\rangle}} \qquad (A\ 93)$$

Substituting in eqns. (A-69) and (A-70) gives:

$$\rho_{ls} = \frac{\left\langle \iint_\Omega \mathbf{E}_1 \bullet \mathbf{p}\, d\Omega \iint_\Omega \mathbf{E}_1^* \bullet \mathbf{p}^* d\Omega \iint_\Omega \tilde{\mathbf{E}}_2 \bullet \mathbf{p}\, d\Omega \iint_\Omega \tilde{\mathbf{E}}_2^* \bullet \mathbf{p}\, d\Omega \right\rangle}{\sqrt{\left\langle \left| \iint_\Omega \mathbf{E}_1 \bullet \mathbf{p}\, d\Omega \right|^4 \right\rangle \left\langle \left| \iint_\Omega \tilde{\mathbf{E}}_2 \bullet \mathbf{p}\, d\Omega \right|^4 \right\rangle}} \qquad (A\text{-}94)$$

Applying the simplifications of eqn. (A-76) to the numerator of eqn. (A-94) gives:

$$\begin{aligned}
&\left\langle \iint_\Omega \mathbf{E}_1 \bullet \mathbf{p} d\Omega \iint_\Omega \mathbf{E}_1^* \bullet \mathbf{p}^* d\Omega \iint_\Omega \tilde{\mathbf{E}}_2 \bullet \mathbf{p} d\Omega \iint_\Omega \tilde{\mathbf{E}}_2^* \bullet \mathbf{p}^* d\Omega \right\rangle = \\
&c_3^2 \left\langle \iint_\Omega (\mathbf{E}_1 \bullet \mathbf{p})(\mathbf{E}_1 \bullet \mathbf{p})^* d\Omega \iint_\Omega (\tilde{\mathbf{E}}_2 \bullet \mathbf{p})(\tilde{\mathbf{E}}_2 \bullet \mathbf{p})^* d\Omega \right\rangle = \\
&c_3^3 \left\langle \iint_\Omega (\mathbf{E}_1 \bullet \mathbf{p})(\mathbf{E}_1 \bullet \mathbf{p})^* (\tilde{\mathbf{E}}_2 \bullet \mathbf{p})(\tilde{\mathbf{E}}_2 \bullet \mathbf{p})^* d\Omega \right\rangle = \\
&c_3^3 \iint_\Omega \left\langle \begin{matrix} (E_{1\theta} p_\theta + E_{1\phi} p_\phi) & (E_{1\theta} p_\theta + E_{1\phi} p_\phi)^* \\ (\tilde{E}_{2\theta} p_\theta + \tilde{E}_{2\phi} p_\phi) & (\tilde{E}_{2\theta} p_\theta + \tilde{E}_{2\phi} p_\phi)^* \end{matrix} \right\rangle d\Omega
\end{aligned} \qquad (A\text{-}95)$$

This can be further simplified if x_θ, y_θ, x_ϕ and y_ϕ have Gaussian distributions about 0. For if x_1, x_2, x_3 and x_4 are real zero-mean Gaussian random variables [4]:

$$\langle x_1 x_2 x_3 x_4 \rangle = \langle x_1 x_2 \rangle \langle x_3 x_4 \rangle + \langle x_1 x_3 \rangle \langle x_2 x_4 \rangle + \langle x_1 x_4 \rangle \langle x_2 x_3 \rangle \qquad (A\ 96)$$

Using eqn. (A-96) and eqn. (A-58) gives:

$$\begin{aligned}
\left\langle p_\theta p_\theta^* p_\theta p_\theta^* \right\rangle &= \left\langle x_\theta^4 + 2x_\theta^2 y_\theta^2 + y_\theta^4 \right\rangle \\
&= \left\langle 3\sigma_\theta^4 + 2\sigma_\theta^4 + 3\sigma_\theta^4 \right\rangle = 8\sigma_\theta^4
\end{aligned} \qquad (A\ 97)$$

Applying eqn. (A-96) and eqn. (A-85) to the other terms in eqn. (A-95) gives:

$$\left\langle p_\phi p_\phi^* p_\phi p_\phi^* \right\rangle = 8\sigma_\phi^4 \qquad (A\ 98)$$

$$\left\langle p_\phi p_\theta^* p_\phi p_\phi^* \right\rangle = 0 \qquad (A\ 99)$$

$$\left\langle p_\theta p_\phi^* p_\theta p_\theta^* \right\rangle = 0 \qquad \text{(A-100)}$$

$$\left\langle p_\theta p_\theta^* p_\phi p_\phi^* \right\rangle = 0 \qquad \text{(A-101)}$$

$$\left\langle p_\theta p_\theta^* p_\phi p_\phi^* \right\rangle = 4\sigma_\theta^2 \sigma_\phi^2 \qquad \text{(A-102)}$$

Substituting relations (A-97) to (A-102) into eqn. (A-95) gives:

$$\left\langle \iint_\Omega \mathbf{E}_1 \bullet \mathbf{p}\, d\Omega \iint_\Omega \mathbf{E}_1^* \bullet \mathbf{p}^* d\Omega \iint_\Omega \tilde{\mathbf{E}}_2 \bullet \mathbf{p}\, d\Omega \iint_\Omega \tilde{\mathbf{E}}_2^* \bullet \mathbf{p}^* d\Omega \right\rangle =$$
$$c_3^3 \iint_\Omega \left[\begin{array}{c} E_{1\theta} E_{1\theta}^* \tilde{E}_{2\theta} \tilde{E}_{2\theta}^* 8\sigma_\theta^4 + E_{1\phi} E_{1\phi}^* \tilde{E}_{2\phi} \tilde{E}_{2\phi}^* 8\sigma_\phi^4 \\ + \left(\begin{array}{c} E_{1\theta} E_{1\theta}^* \tilde{E}_{2\phi} \tilde{E}_{2\phi}^* + E_{1\phi} E_{1\theta}^* \tilde{E}_{2\theta} \tilde{E}_{2\phi}^* \\ + E_{1\theta} E_{1\phi}^* \tilde{E}_{2\phi} \tilde{E}_{2\theta}^* + E_{1\phi} E_{1\phi}^* \tilde{E}_{2\theta} \tilde{E}_{2\theta}^* \end{array} \right) 4\sigma_\theta^2 \sigma_\phi^2 \end{array} \right] d\Omega \qquad \text{(A-103)}$$

The parts of the denominator of eqn. (A-94) is simplified in a similar way to give:

$$\left\langle \left| \iint_\Omega \mathbf{E}_1 \bullet \mathbf{p}\, d\Omega \right|^4 \right\rangle = 8c_3^3 \iint_\Omega \left[\left| E_{1\theta} \right|^4 \sigma_\theta^4 + \left| E_{1\phi} \right|^4 \sigma_\phi^4 + 2 \left| E_{1\theta} E_{1\phi} \right|^2 \sigma_\theta^2 \sigma_\phi^2 \right] d\Omega \qquad \text{(A-104)}$$

$$\left\langle \left| \iint_\Omega \mathbf{E}_2 \bullet \mathbf{p}\, d\Omega \right|^4 \right\rangle = 8c_3^3 \iint_\Omega \left[\left| E_{2\theta} \right|^4 \sigma_\theta^4 + \left| E_{2\phi} \right|^4 \sigma_\phi^4 + 2 \left| E_{2\theta} E_{2\phi} \right|^2 \sigma_\theta^2 \sigma_\phi^2 \right] d\Omega \qquad \text{(A-105)}$$

Substituting eqns. (A-103), (A-104) and (A-105) into eqn. (A94) gives:

$$\rho_{Is} = \frac{\iint_\Omega \left[\begin{array}{c} E_{1\theta} E_{1\theta}^* \tilde{E}_{2\theta} \tilde{E}_{2\theta}^* 2\sigma_\theta^4 + E_{1\phi} E_{1\phi}^* \tilde{E}_{2\phi} \tilde{E}_{2\phi}^* 2\sigma_\phi^4 \\ + \left(\begin{array}{c} E_{1\theta} E_{1\theta}^* \tilde{E}_{2\phi} \tilde{E}_{2\phi}^* + E_{1\phi} E_{1\theta}^* \tilde{E}_{2\theta} \tilde{E}_{2\phi}^* \\ + E_{1\theta} E_{1\phi}^* \tilde{E}_{2\phi} \tilde{E}_{2\theta}^* + E_{1\phi} E_{1\phi}^* \tilde{E}_{2\theta} \tilde{E}_{2\theta}^* \end{array} \right) \sigma_\theta^2 \sigma_\phi^2 \end{array} \right]}{2 \sqrt{\iint_\Omega \left[\begin{array}{c} \left| E_{1\theta} \right|^4 \sigma_\theta^4 + \left| E_{1\phi} \right|^4 \sigma_\phi^4 \\ + 2 \left| E_{1\theta} E_{1\phi} \right|^2 \sigma_\theta^2 \sigma_\phi^2 \end{array} \right] d\Omega \iint_\Omega \left[\begin{array}{c} \left| E_{2\theta} \right|^4 \sigma_\theta^4 + \left| E_{2\phi} \right|^4 \sigma_\phi^4 \\ + 2 \left| E_{2\theta} E_{2\phi} \right|^2 \sigma_\theta^2 \sigma_\phi^2 \end{array} \right] d\Omega}} \qquad \text{(A 106)}$$

This formula is much more complicated than eqn. (A-81). The formulas for ρ_{sI} and ρ_{sIV} are even more complicated. Therefore ρ_{Is}, ρ_{sIs} and ρ_{sIV} are almost never computed directly from the antenna patterns. Instead ρ_{cs} is computed, and the other signal correlations are determined using the relations between the signal correlations which were demonstrated in Section A.6.

A.11 Summary of Main Correlation Definitions and Relations

There are four main ways of defining (normalized) signal correlation:

1. The complex signal correlation ρ_{cs}
2. The correlation between signal intensities ρ_{Is}
3. The correlation between the deviations of the signal intensities from their norms $\rho_{\delta I}$
4. The correlation between the deviations of the signal magnitudes from their norms $\rho_{\delta V}$

When the signals are Rayleigh distributed[5], the signal correlations are related by:

$$\rho_v = |\rho_{cs}| \qquad (A\text{-}107)$$

$$\rho_v^2 = \rho_{\delta Is} \cong \rho_{\delta V|} \qquad (A\ 108)$$

$$\rho_{Is} = \frac{1+\rho_v^2}{2} \qquad (A\ 109)$$

This is usually true when the signals are being received by a mobile receiver. The signal correlations can be predicted from the antennas' properties by computing the antenna correlation ρ_a^2, which for Rayleigh distributed fields is equal to ρ_v^2.

There are a number of definitions of the correlations between field components. Some of these are described in Section A.4. While they are often referred to in the academic literature on propagation statistics, they are rarely used in computing the signal correlations between receiver branches. This is because all practical antennas detect combinations of field components.

[5]That is, the real and imaginary components are uncorrelated and have Gaussian distributions about 0.

A.12 References

1. LEATHER, P.S.H., and MASSEY, P.J., 1996, "Antenna Diversity from Two Closely Spaced Dipoles", Report No. RP3492, Philips Research Laboratories, Redhill, UK.

2. MASSEY, P.J., 1992, "Future Antennas For Handheld Phones, Radios, and Pagers", Report No. 3436, Philips Research Laboratories, Redhill, UK, p31.

3. CLARKE, R.H., 1968, "A Statistical Theory of Mobile-Radio Reception", Bell Sys. Tech. J., Vol. 47, No. 6, pp957-1000.

4. DAVENPORT, W.B., and ROOT, W.L., 1958,"An Introduction to the Theory of Random Signals and Noise", McGraw-Hill, New York, USA, p168.

5. LAWSON, J.L., and UHLENBECK, G.E., 1950, "Threshold Signals", MIT Radiation Laboratory Series, Vol. 24, McGraw-Hill, New York, USA.

6. JAKES, W.C., 1974, "Microwave Mobile Communications", IEEE Inc. (1993) New York, USA, pp16-17.

7. RICE, S.O, 1944, "Mathematical Analysis of Random Noise", Bell Sys. Tech. J., Vol. 23, pp282-332.